HYDROGEOLOGIC STUDY OF CASTLE VALLEY, GRAND COUNTY, UTAH

by Erin Brinkman, Greg Gavin, Trevor H. Schlossnagle, and Janae Wallace

SPECIAL STUDY 176
UTAH GEOLOGICAL SURVEY
UTAH DEPARTMENT OF NATURAL RESOURCES
2025

Blank pages are intentional for printing purposes.

HYDROGEOLOGIC STUDY OF CASTLE VALLEY, GRAND COUNTY, UTAH

by
Erin Brinkman, Greg Gavin, Trevor H. Schlossnagle, and Janae Wallace

Cover photo: *View to the northwest of Castle Valley highlighting the vertical Wingate sandstone cliffs of Adobe Mesa, Castleton Tower, The Rectory, Sister Superior, and Parriott Mesa. Photo by Erin Brinkman.*

Suggested citation:
Brinkman, E., Gavin, G., Schlossnagle, T.H., and Wallace, J., 2025, Hydrogeologic study of Castle Valley, Grand County, Utah: Utah Geological Survey Special Study 176, 56 p., 2 appendices, https://doi.org/10.34191/SS-176.

SPECIAL STUDY 176
UTAH GEOLOGICAL SURVEY
UTAH DEPARTMENT OF NATURAL RESOURCES
2025

STATE OF UTAH
Spencer J. Cox, Governor

DEPARTMENT OF NATURAL RESOURCES
Joel Ferry, Executive Director

UTAH GEOLOGICAL SURVEY
Darlene Batatian

PUBLICATIONS
contact
Natural Resources Map & Bookstore
1594 W. North Temple
Salt Lake City, UT 84116
telephone: 801-537-3320
toll-free: 1-888-UTAH MAP
website: utahmapstore.com
email: geostore@utah.gov

UTAH GEOLOGICAL SURVEY
contact
1594 W. North Temple, Suite 3110
Salt Lake City, UT 84116
telephone: 801-537-3300
website: geology.utah.gov

CONTENTS

FIGURES

TABLES

HYDROGEOLOGIC STUDY OF CASTLE VALLEY, GRAND COUNTY, UTAH

by Erin Brinkman, Greg Gavin, Trevor H. Schlossnagle, and Janae Wallace

ABSTRACT

Castle Valley, located in Grand County, Utah, is a northwest-trending valley on the Colorado Plateau. This study characterizes the groundwater and surface water system, addresses long-standing water quality issues, and provides an updated water budget in this area. New data and analyses were collected in 2023 and 2024, including water-level measurements, an updated potentiometric surface map, and water-level trend analysis. The study also includes three cross sections of the subsurface based on well lithologic logs, a map of transmissivity of the valley-fill and bedrock aquifers, streamflow and seepage measurements and analysis. In addition, it presents a comprehensive analysis of general chemistry and stable isotope signatures of groundwater and surface water, a groundwater recharge-age analysis using radiogenic isotope data, a sulfate isotope analysis used to determine sources of high sulfate concentrations in the study area. Finally, the study provides a water budget for the study area and valley-fill aquifer derived from a Soil-Water-Balance model.

Our major findings show that water-level trends in the valley-fill aquifer are stable, with little to no long-term decline. Transmissivity of the valley-fill aquifer exceeds that of bedrock aquifers in the study area, with geometric means of 379 and 119 ft^2/day, respectively. Castle Creek is a net gaining stream, based on seepage measurements and stable isotope data, and is the primary pathway for groundwater discharge from the valley-fill aquifer. Water quality issues, including high total-dissolved-solids (TDS) and sulfate concentrations located on the valley margins match the sulfate isotope signature of evaporite deposits, indicating the evaporite-rich Paradox Formation is the primary source of these problems. Radiogenic isotope data suggest that valley-fill groundwater consists primarily of recently recharged water, except where influenced by older flow through adjacent bedrock on valley margins. Recharge to the valley-fill aquifer occurs primarily through direct infiltration of precipitation (2700 acre-feet/yr) and from mountain-block recharge (1240 acre-feet/yr). Snow water equivalent at the Lasal Mountain SNOTEL site shows a decreasing trend of 0.15 inches per year from 1980 through 2024, suggesting a gradual decline in mountain snowpack that may influence streamflow. Groundwater discharge from the valley-fill aquifer is primarily from stream gain (3788 acre-feet/yr) and well water withdrawal (741 acre-feet/yr).

Despite current water stability in Castle Valley, potential development and shifting precipitation patterns pose a risk of increased demand on water resources, particularly the valley-fill aquifer. The strong interconnection between surface water and groundwater highlights the need of integrated water management, as changes to one component directly influence the other. Integrated water management is critical given the potential for long-term precipitation declines, increased groundwater withdrawals, and continued irrigation diversions from Castle Creek, all of which threaten the valley-fill aquifer's stability. Groundwater age estimates (25 to 33 years) suggest the aquifer may potentially begin to experience the effects of long-term declines observed in streamflow records, which began in 1993. Even with current stability in water-level trends, increased withdrawals could alter the balance between high and low TDS groundwater. Such imbalances may induce the capture of streamflow from Castle Creek, reducing its flow and potentially stressing phreatophytic vegetation that relies on groundwater discharge. Furthermore, additional withdrawals could exacerbate the influence of evaporite-derived high-sulfate groundwater from the Paradox Formation, further degrading water quality. Preserving this sole-source aquifer's pristine drinking water status requires proactive water management, including sustainable groundwater extraction limits, enhanced monitoring of stream-aquifer interactions, and careful regulation of surface water diversions to maintain ecological and hydrological balance in Castle Valley.

INTRODUCTION

Purpose and Scope

Castle Valley is a rural community in southeast Utah that relies on groundwater as their sole source of drinking water supply. Local officials in Castle Valley have expressed concern about the potential impact that development may have on groundwater, especially considering drought conditions in the western United States. In addition, the preservation of groundwater quality and the potential for groundwater quality degradation are critical issues that need consideration when determining the extent and nature of future groundwater development in the valley. The primary goals of the study are to (1) characterize the hydrology and hydrogeology of the Castle Valley surface-drainage basin and the occurrence and flow of groundwater and surface water, (2) characterize groundwater levels, chemistry, and connection to surface water, and (3) develop a water budget constrains recharge and discharge components, including recharge and runoff,

streamflow, evapotranspiration (ET), well withdrawals, spring discharge, and change in groundwater storage. To achieve these goals, we collected water quality and environmental isotopic samples, measured water levels in wells, measured discharge from streams and springs to assess seepage conditions, and used the U.S. Geological Survey (USGS) Soil-Water-Balance (SWB) model to develop a water budget.

Study Area

Castle Valley is a northwest-trending valley in Grand County, nine miles (15 km) northeast of Moab in the Colorado Plateau physiographic province (Stokes, 1977). The valley extends 21 miles (34 km) from the Colorado River to the head of the watershed on Mount Waas. The valley is 8.5 miles (14 km) wide at the widest part, and has an area of about 53 square miles (137 km^2) (Figure 1). Elevation ranges from 4025 feet (1227 meters) above sea level along the Colorado River to the summit of Mount Waas at 12,331 feet (3758 meters). Castle Valley is a rural area in southeastern Utah (Figure 1) that is experiencing an increase in residential and groundwater development.

Castle Valley is bordered by Parriott and Adobe Mesas to the northeast, the La Sal Mountains to the southeast, Porcupine Rim to the west, and the Colorado River to the northwest (Figure 1). The headwaters of the perennial Castle Creek and ephemeral Placer Creek—the principal drainages of Castle Valley—originate in the La Sal Mountains (Figure 1). These streams flow into the valley on either side of Round Mountain, join near the town of Castle Valley, and then flow through a short, narrow canyon and enter the Colorado River. Castle Creek is the primary source of agricultural irrigation water in the valley. Culinary water is predominately from

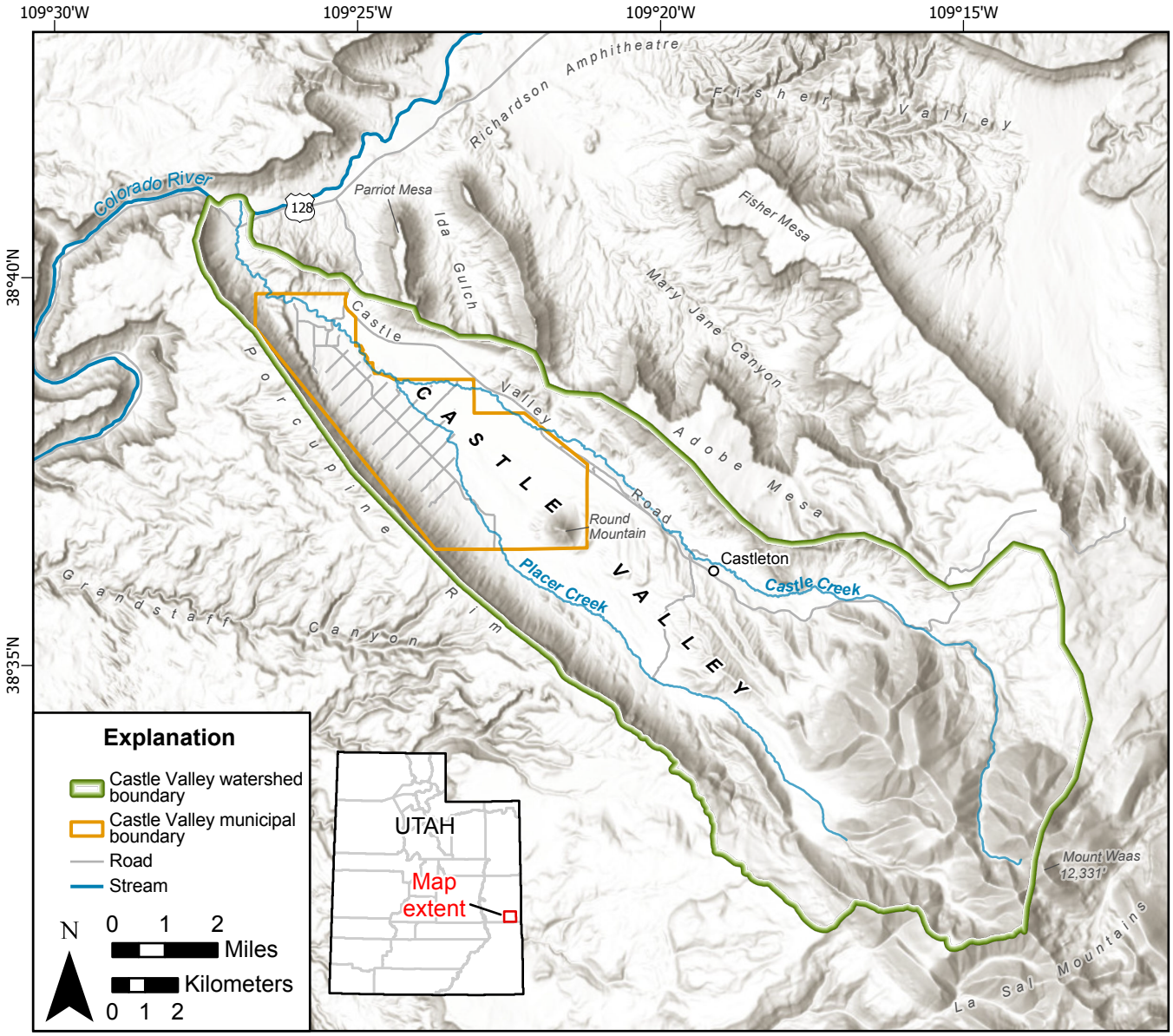

Figure 1. *Hydrologic and geographic features of Castle Valley.*

water wells that supply most of Castle Valley's drinking water and irrigation for individual properties. A number of wells, however, yield poor water quality and are only suitable for non-potable domestic use.

Population and Land Use

The majority of Castle Valley residents reside within the incorporated Town of Castle Valley. The 2020 census recorded 347 full-time residents within the town and the total population within the study area is 415 (U.S. Census Bureau, 2020). Land use within the valley is primarily residential, with parts allocated to irrigated cropland, limited commercial use, and seasonal winter cattle grazing. Currently, all residents utilize septic-tank systems for wastewater disposal.

Geologic Setting

Castle Valley lies within the central part of the Colorado Plateau physiographic province, which is characterized by relatively undeformed sedimentary strata that have been uplifted as a coherent block since the Late Cretaceous (Huntoon et al., 1982). The northwest part of the valley abuts the Colorado River corridor, where regional-scale uplift and subsequent erosion have exposed Pennsylvanian- through Jurassic-age strata that record the complex depositional and deformational history of the area.

The structure of Castle Valley is dominated by salt tectonics associated with the Paradox Basin, a large depositional basin that formed during Pennsylvanian time (Figure 2). The Paradox Formation, namesake of the basin, is primarily composed of halite with thinner sequences of clastic sediments, organic shales, and anhydrite. The formation is roughly 4500 feet (1370 meters) thick (Doelling, 2002) and underlies much of southeastern Utah.

Castle Valley belongs to a northwest-trending network of salt walls and collapsed anticlines that includes the Salt, Moab-Spanish, and Fisher Valley structures, collectively defining the region's structural grain (Figure 3) (Doelling, 2002; Trudgill, 2011). Structural evolution began during the Pennsylvanian Period, when passive salt diapirism occurred synchronously with sediment deposition, and continued through the Cretaceous. As overlying sedimentary rocks accumulated, they displaced Paradox Formation evaporites laterally, causing thinning within synclinal areas and upward migration into anticlinal features. This salt movement transformed originally horizontal sedimentary beds into steeply dipping or overturned units along the anticline flanks (Figure 3). Thickness of the Paradox Formation within Castle Valley's salt wall is estimated to be up to 3000 feet (900 meters) (Trudgill, 2011).

Due to its position relative to the other major structural features, Castle Valley falls within the "salt anticline region" of the Colorado Plateau, between the Uncompahgre Uplift to the northeast and the Monument Upwarp to the southwest (Trudgill, 2011). The valley's formation was influenced by both regional Laramide orogenic compression and local salt tectonics, resulting in a complex interplay of deformational processes. Structural extension accommodated by the Moab fault system to the south has also likely influenced salt movement in the region.

Geologic units surrounding Castle Valley include Pennsylvanian through Jurassic sedimentary rocks and Tertiary igneous rocks (Figure 4; Figure 5) (Doelling, 2001). Gypsum, mudstone, and shale of the Pennsylvanian Paradox Formation are exposed along the southwest margin of Castle Valley and around Round Mountain. These rocks also directly underlie Quaternary valley-fill deposits (Doelling, 2001). Sandstone, conglomerate, and mudstone of the Cutler Formation overlie the Paradox at the northwest end and central-northeast margin of the valley (Doelling and Ross, 1998; Doelling, 2001). Sandstone, siltstone, and mudstone of the Triassic Moenkopi and Chinle Formations, and Jurassic Wingate and Kayenta Formations and Navajo Sandstone of the Glen Canyon Group overlie the Cutler and form the cliffs along much of the northeast and southwest sides of the valley (Doelling, 2001). Round Mountain and the La Sal Mountains consist of intermediate composition Oligocene intrusive rocks (Doelling, 2001).

The valley fill consists mainly of alluvial-fan, mass-movement, and stream deposits (Doelling, 2001). Holocene stream deposits along Castle and Placer Creeks are generally poorly sorted sand, silt, and clay, with some gravel lenses. The amount of gravel in these deposits generally increases updrainage (Doelling and Ross, 1998). Coarse-grained older alluvium (including the Tertiary Geyser Creek Fanglomerate), composed of poorly sorted, sandy, cobble gravel with some small, localized accumulations of boulders, is exposed in the higher parts of Castle Valley and underlies the younger stream alluvium in lower Castle Valley (Snyder, 1996a, 1996b; Doelling and Ross, 1998; Lowe et al., 2004). Alluvial-fan deposits form apron-like gentle slopes at the base of Porcupine Rim and Adobe Mesa (Doelling and Ross, 1998; Doelling, 2001). The fans consist mainly of poorly sorted boulders, cobbles, and gravels in a crudely bedded fine-grained matrix (Doelling and Ross, 1998). Talus and colluvium, consisting of rockfall blocks, boulders, angular gravel, sand, and silt, are found along the southern part of Porcupine Rim, and mass-movement deposits are mapped along the upper reach of Placer Creek (Doelling, 2001).

Previous Work

Ford and Grandy (1997) and Ford (2006) measured water levels over several years and created potentiometric surface maps. They also attempted to assess the amount of groundwater flow in and out of Castle Valley. Ford (2006) estimated a discharge of 6800 acre-feet per year from Castle Valley. This report also presents static water-level data collected over a

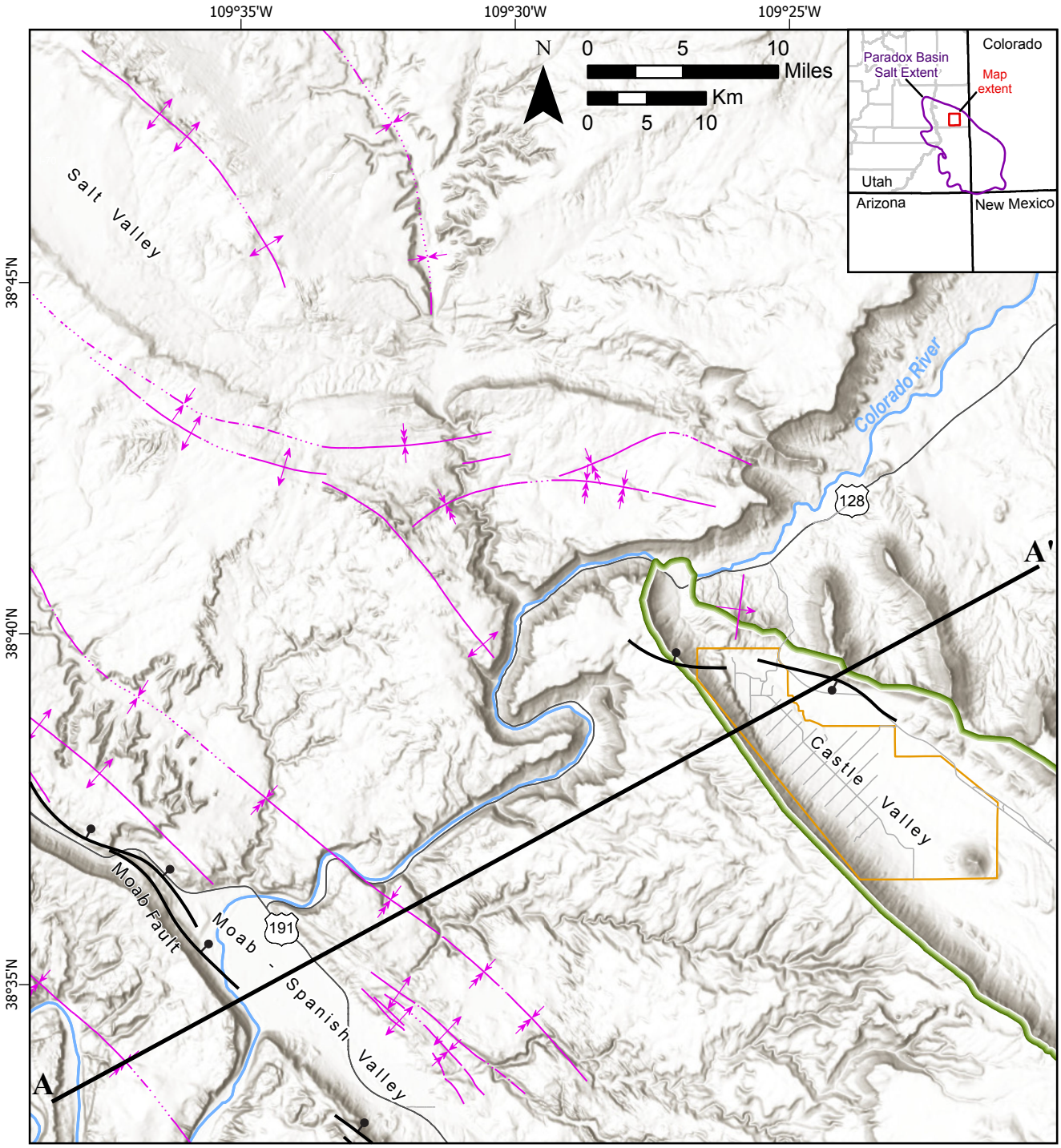

Explanation

- Axial trace of anticline – Dashed where approximately located, dotted where concealed
- Axial trace of monocline
- Axial trace of syncline – Dashed where approximately located, dotted where concealed
- Axial trace of asymmetrical syncline – Dashed where approximately located, dotted where concealed
- Normal fault – Bar and ball on down-thrown side
- Town of Castle Valley boundary
- Study area boundary
- Road
- Stream

Figure 2. *Moab and Castle Valley area fault- and diapir-related folds within the Paradox Basin with geologic cross section A-A' shown.*

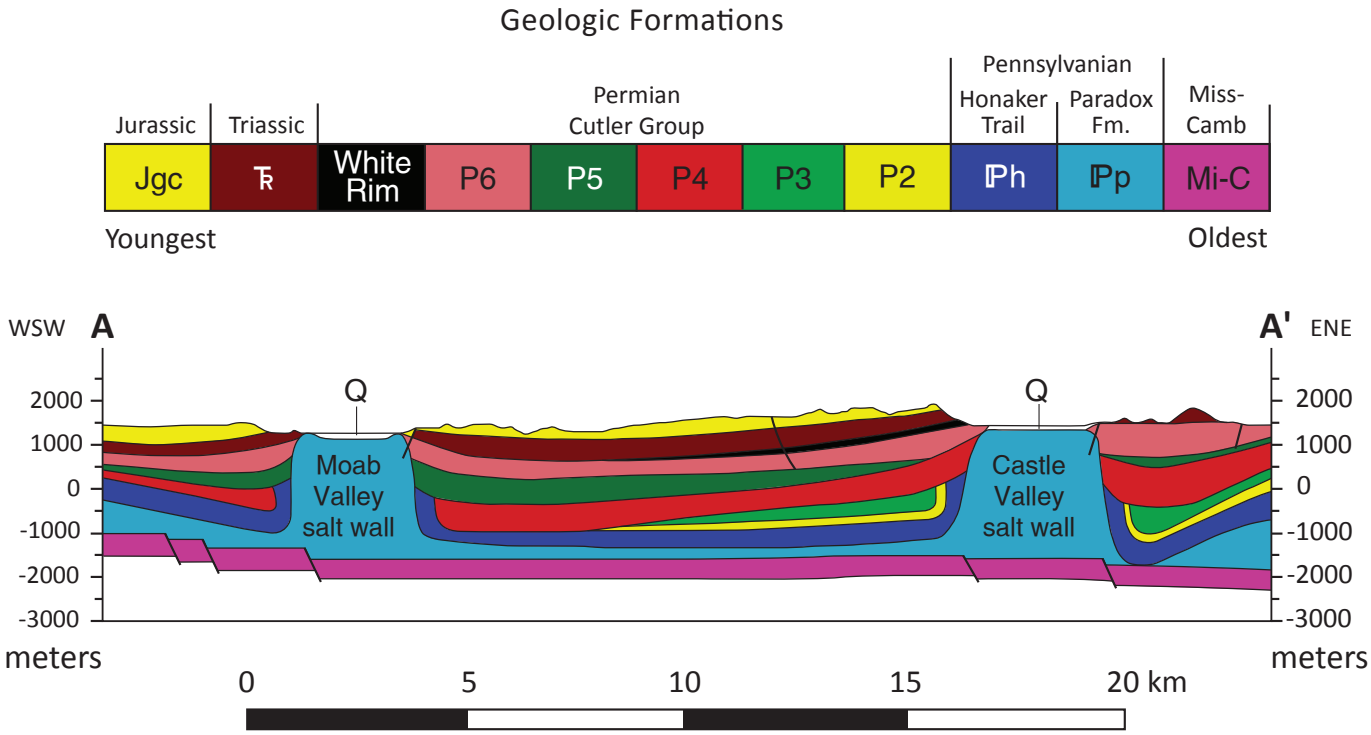

Figure 3. *Geologic cross section showing Paradox Formation salt walls and their relationship to adjacent Mississippian through Jurassic strata, modified from Trudgill (2011). See Figure 2 for cross section location.*

five-year period, which showed an initial decline followed by a rise correlated to precipitation patterns. Ford's (2006) recharge (inflow) sources were precipitation, groundwater flow, and groundwater gained from Castle Creek near Castleton, and the discharge (outflow) was attributed to ET (consumptive use by crops and riparian areas), domestic wells, and discharge of Castle Creek to the Colorado River near Utah State Route 128.

Lowe et al. (2004) assessed the impact of increasing residential development on the valley-fill aquifer in Castle Valley. The study classified groundwater quality using Utah's total dissolved solids (TDS)-based system and applied a mass-balance groundwater flow model to evaluate the effects of projected septic tank use. In the northwestern part of the valley, Lowe et al. classified groundwater as Class IA (Pristine) or II (Drinking Water quality), with TDS ranging from 204 to 2442 mg/L (average 785 mg/L) and average nitrate concentrations of 0.52 mg/L. To protect water quality, the study recommended septic-system densities of 5 to 15 acres per system based on flow simulations. Wallace and Lowe (2012) documented an updated groundwater quality classification (Wallace and Lowe, 2007), which leveraged new monitoring well data to extend the Class IA area to the southeast.

Kolm and van der Heijde (2016, 2020) compiled data to provide an estimate for a water budget. Their inflow and outflow estimates of groundwater recharge and discharge were balanced at ~5530 acre-feet per year. Their preliminary water budget estimated 72% of recharge to the valley-fill aquifer is from the La Sal Mountain subsystem. This study estimated 10% of the total water storage as recoverable ("variable" or "dynamic" storage). The calculations provide a range of total average water volume (aquifer storage) for the valley-fill aquifer of 42,160 to 126,490 acre-feet and variable storage of 4220 acre-feet to 12,650 acre-feet. They include caveats to indicate that only a portion of this water is recoverable based on their storage capacity calculations.

Bailey (written communication, February 21, 2024) conducted an in-depth review of Kolm and van der Heijde's (2016, 2020) Hydrologic and Environmental System Analysis (HESA) and identified several areas to enhance future water budget studies that include (1) improving documentation to support assumptions, especially regarding specific yield and fracture zones; (2) implementing more recently available data; and (3) conducting more detailed mapping to provide better context and orientation.

Hydrogeology

Groundwater in Castle Valley occurs in two types of aquifers: (1) valley-fill deposits, and (2) fractured bedrock. The valley-fill aquifer is the most important source of drinking water in Castle Valley (Lowe et al., 2004; Wallace and Lowe, 2012). The valley fill consists predominantly of gravelly stream alluvium and alluvial-fan deposits that are generally coarser grained near source areas at the base of Porcupine Rim and the La Sal Mountains, and finer grained along the lower reaches of Castle Creek (Snyder, 1996a, 1996b; Doelling and Ross, 1998).

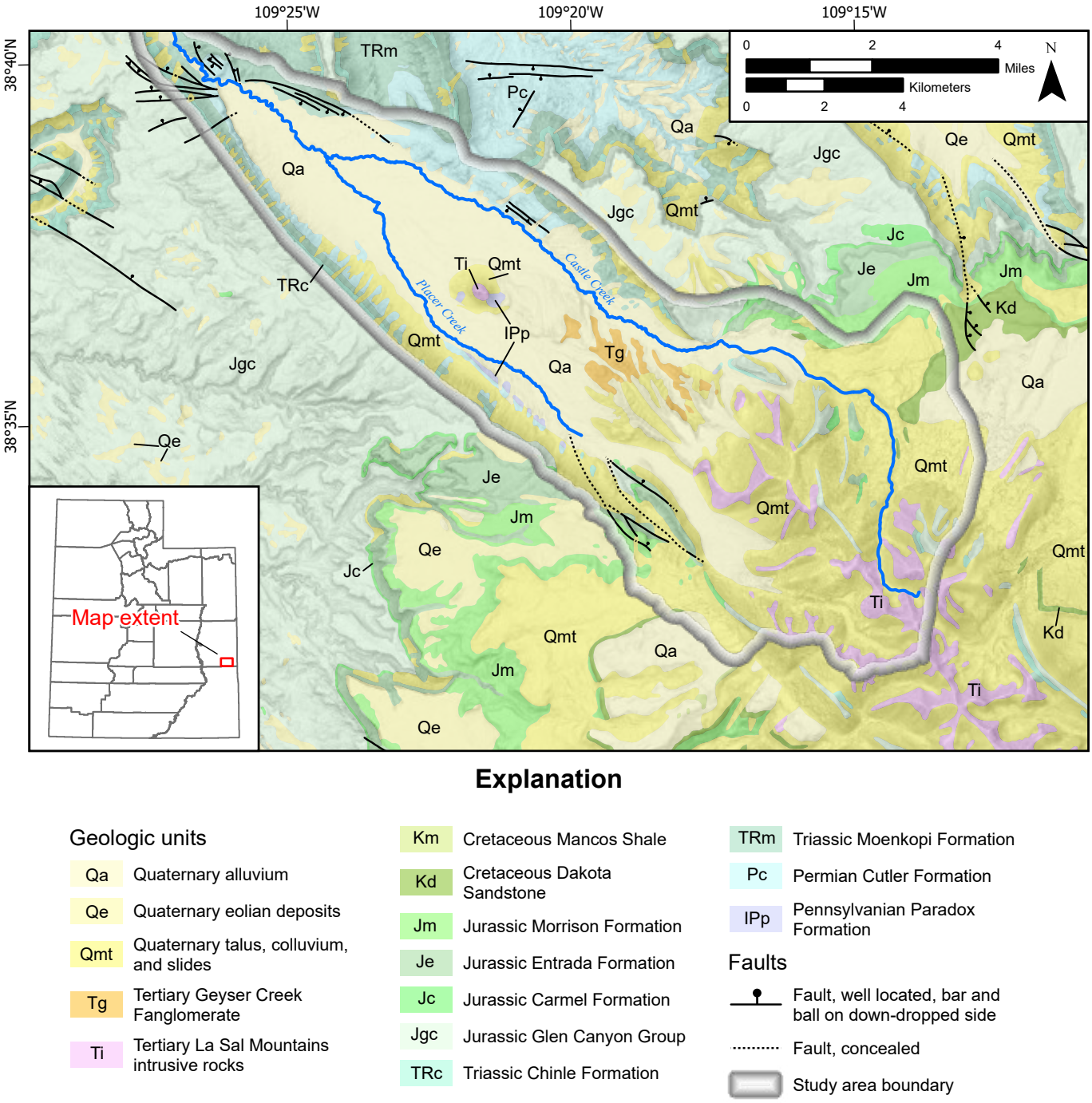

Figure 4. *Simplified geologic map of the Castle Valley area, modified from Doelling, (2001).*

Groundwater in fractured-rock aquifers is recharged mostly from infiltration of precipitation and streamflow and flows primarily through fractures. Blanchard (1990) reported that approximately 30 wells are completed in the Cutler Formation aquifer along the base of Porcupine Rim on the west side of the valley. A smaller number of wells (<10) are completed in the Moenkopi Formation along the east side of the valley. Although the number of wells completed in bedrock has increased slightly since these estimates, the Cutler Formation is the main fractured-rock aquifer currently used in Castle Valley. Recharge to the Cutler Formation aquifer includes infiltration from precipitation from upland areas, including partially from the La Sal Mountains (Doelling and Ross, 1998; Masbruch and Shope, 2014). Bedrock well depth completions are typically 150 to 300 feet (45–90 m) below the land surface (Snyder, 1996a, 1996b).

Groundwater Quality

Groundwater quality in Castle Valley is generally good and is suitable for most uses (Lowe et al., 2004; Wallace and

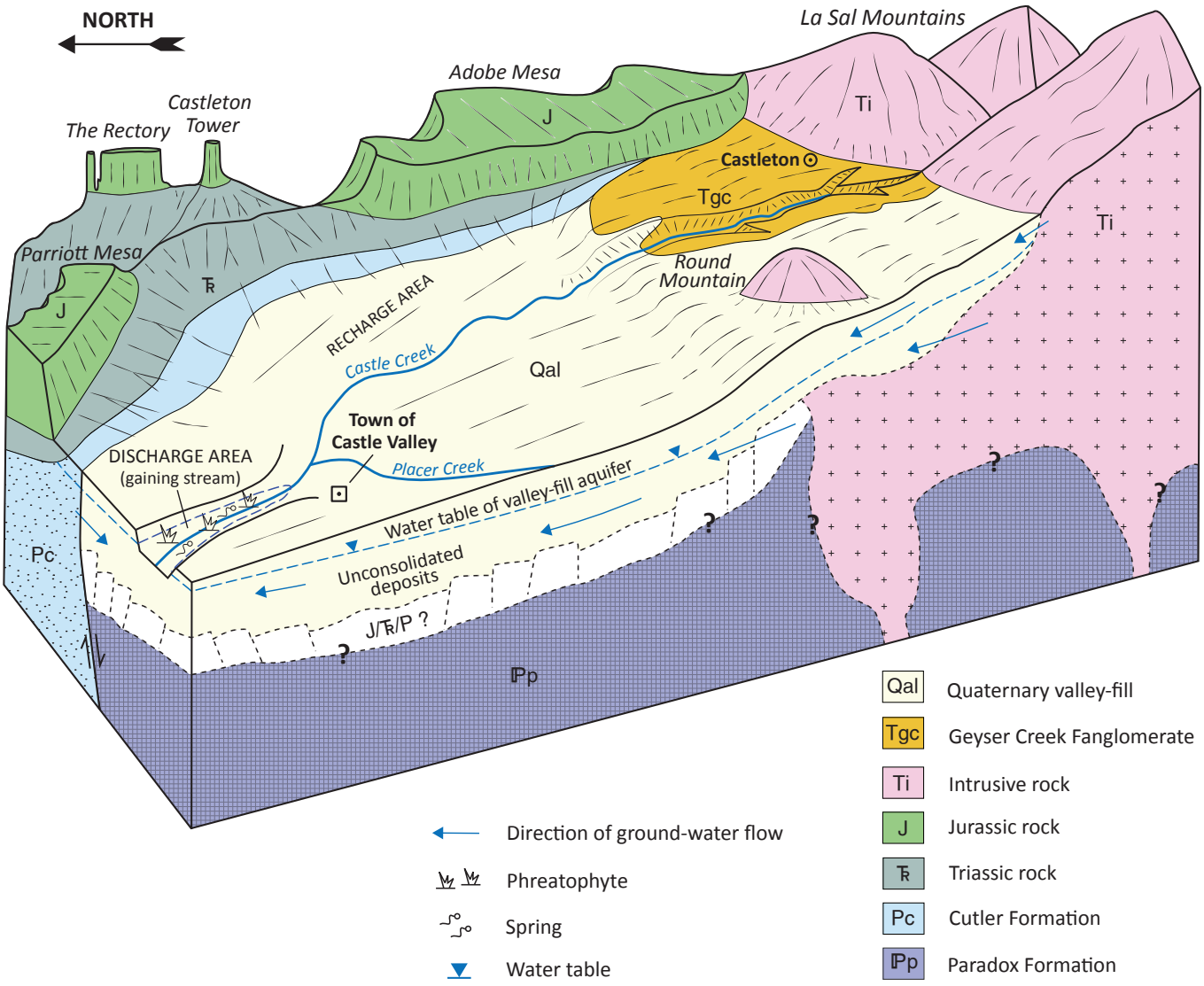

Figure 5. *Conceptual block diagram of Castle Valley illustrating likely groundwater flow paths and bedrock units (modified from Snyder, 1996a).*

Lowe, 2012). Class IA (Pristine groundwater) areas cover about 74% of total valley-fill material, and primarily exist in the central part of the valley along Castle and Placer Creeks and the southern margin of the valley. Class II (Drinking Water Quality groundwater) covers about 26% of total valley fill and exists along the western margin and northwestern end of the valley (Wallace and Lowe, 2012). Ford (2006) reported higher TDS concentrations along the northwest margins of Castle Valley where the Cutler Formation is encountered at relatively shallow depths. Relatively high TDS concentrations are also found around Castleton and at the northwest end of the valley where the Paradox Formation is exposed (Wallace and Lowe, 2012).

The Cutler Formation in Castle Valley typically contains calcium-magnesium-sulfate- or calcium-magnesium-sodium-sulfate-type water (Blanchard, 1990). Groundwater from wells completed in the Cutler Formation is generally higher in TDS concentration than groundwater from wells completed in adjacent valley fill (Snyder, 1996a; 1996b). The shallower wells in northeastern and southeastern Castle Valley have relatively low TDS values possibly due to receiving some recharge from the valley-fill aquifer. Wells at the base of Porcupine Rim have higher TDS values and gypsum along drainages may indicate proximity to Paradox Formation evaporites (Snyder, 1996a, 1996b). Blanchard (1990) reported that groundwater samples from three wells in the Cutler Formation near the Town of Castle Valley had TDS concentrations ranging from 1420 mg/L to 3450 mg/L.

The high TDS values in the valley-fill aquifer and Cutler Formation may result from a combination of three possible factors: (1) long residence time and flow path, (2) dissolution of fine-grained constituents within the Cutler Formation, and (3) hydraulic connection to the Paradox Formation evaporites beneath and adjacent to the Cutler Formation.

GROUNDWATER LEVELS

To create a potentiometric surface map and identify areas of water-level change, we measured groundwater elevations in 31 wells in November 2023, 34 wells in May 2024, and 31 wells in November 2024 (Figure 6; Appendix A Tables A-1 and A-2). Wells were selected based on their distribution across the valley and accessibility.Water-level measurements were recorded using an electronic water-level meter and a graduated steel tape with an accuracy of ±0.01 feet (Cunningham and Schalk, 2011; Jelinski et al., 2015). We also used a Trimble GNSS RTK GPS instrument to collect ground surface coordinates and elevation data at each well location, with a horizontal precision of 0.007 meters and a vertical precision of 0.01 meters. Groundwater elevation is calculated as the difference between the stickup elevation and depth to groundwater measurements. The potentiometric surface map is based on data collected during spring 2024 (Figure 7). We also applied Mann-Kendall analysis using the "pymannkendall" package in Python (Hussain and Mahmud, 2019) to an eight-year period of monitoring well data collected in Castle Valley from 2016 to 2024 to determine whether significant water-level trends exist (Figure 8).

Groundwater depths range from approximately 8 feet (2.4 meters) below ground surface (bgs) at well CV7 to nearly 220 feet (67 meters) bgs at well CV1 (Figure 9). The potentiometric surface generally mirrors the regional topography. Groundwater movement is predominantly from higher elevations in the southeast toward lower elevations in the northwest and the Colorado River (Figure 7).

Repeat observations in Castle Valley monitoring wells indicate long-term stability of groundwater elevations. On average, groundwater levels declined by 0.2 (0.061 m) feet between fall 2023 and spring 2024, with a decrease of 0.5 feet (0.15 m) observed from fall 2023 to fall 2024 (Appendix A Table A-2). A comparison of groundwater levels recorded in 1994 (Ford and Grandy, 1997) with those measured in 2024 indicates an average increase of 1.45 feet (0.048 ft/yr) (Table 1).

The Mann-Kendall analysis, using the 2016–2024 depth-to-water record summary (Table 2), confirms that monitoring wells showed no significant change in groundwater level from 2016 to 2024 (Figure 8; Table 3). Although some wells show apparent trends in the raw data, these are not statistically significant over the monitoring period. This statistical analysis helps distinguish real trends from normal hydrologic variation.

A consistent seasonal pattern is evident across all monitoring locations, with groundwater levels typically 0.16 feet (0.05 m)

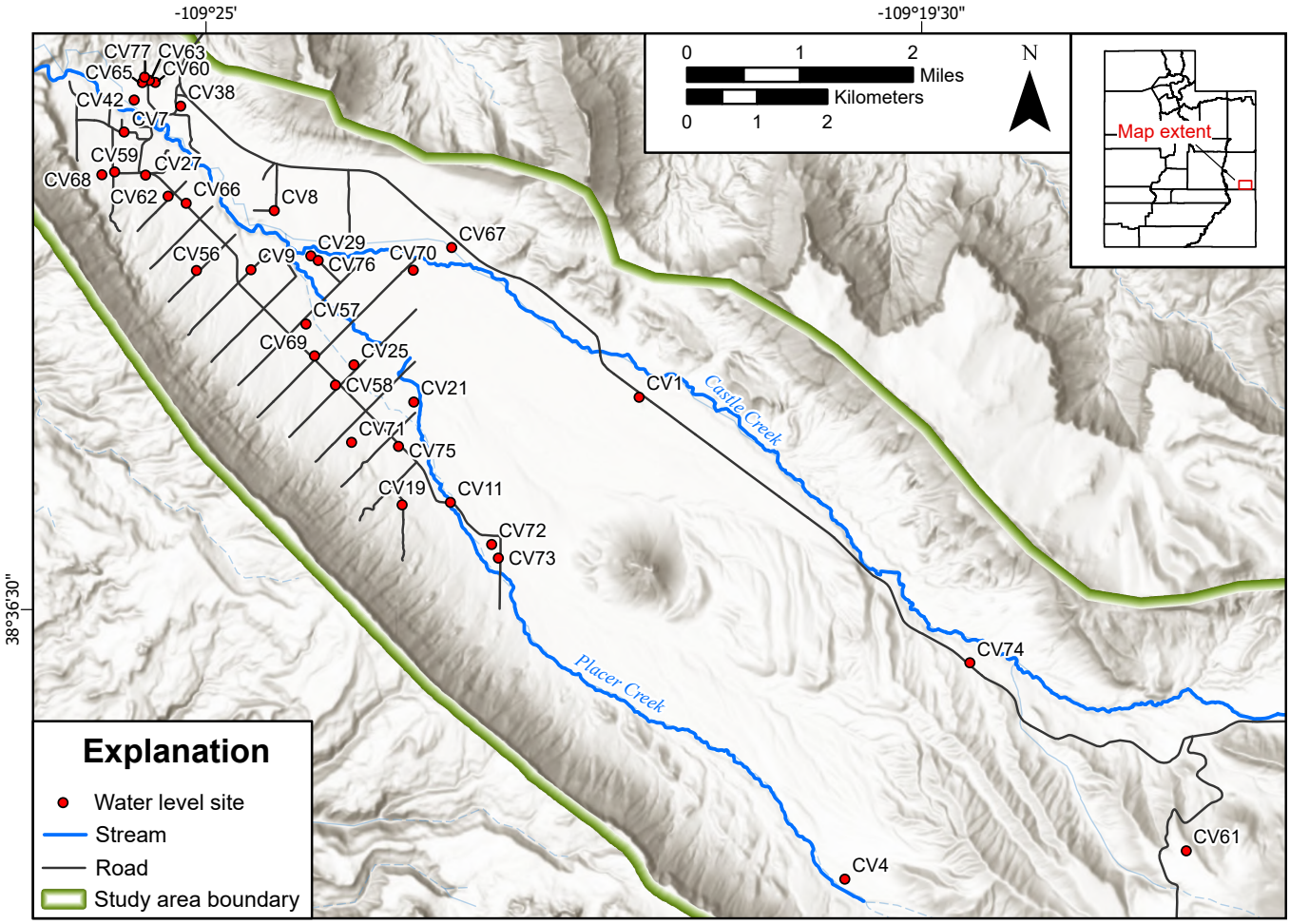

Figure 6. *Site locations of water levels taken from fall 2023 to fall 2024. Well labels correspond to the "Site ID" column of Appendix A Table A-2.*

lower during fall compared to spring. This pattern reflects the annual hydrologic cycle, with spring recharge from snowmelt and precipitation and fall drawdown from irrigation and natural discharge.

HYDROSTRATIGRAPHY

Valley-fill Aquifer Lithology

To define the character and extent of the basin fill and bedrock aquifers, we entered lithology data from well logs (Utah Division of Water Rights, 2024) into a well management program, constructed cross sections through the valley fill and into underlying bedrock where possible, and identified laterally continuous lithologic units. We chose cross section lines based on the distribution of well logs within the study area (Figure 10) and selected 44 well logs for subsurface geology interpretation based on their proximity to the cross sections. Wells used in cross sections are labeled by Utah Division of Water Rights Well Identification Number (WIN) on Figures 8 and 9. The cross sections assist in interpreting valley-fill stratigraphy and thickness, water levels, flow paths, groundwater–surface-water interactions, and constructing the conceptual flow model. Based on well log analysis, we divided the valley fill in Castle Valley into four units: clay, predominantly fine grained (clay and silt), predominantly coarse grained (sand and gravel), and mixed grain size.

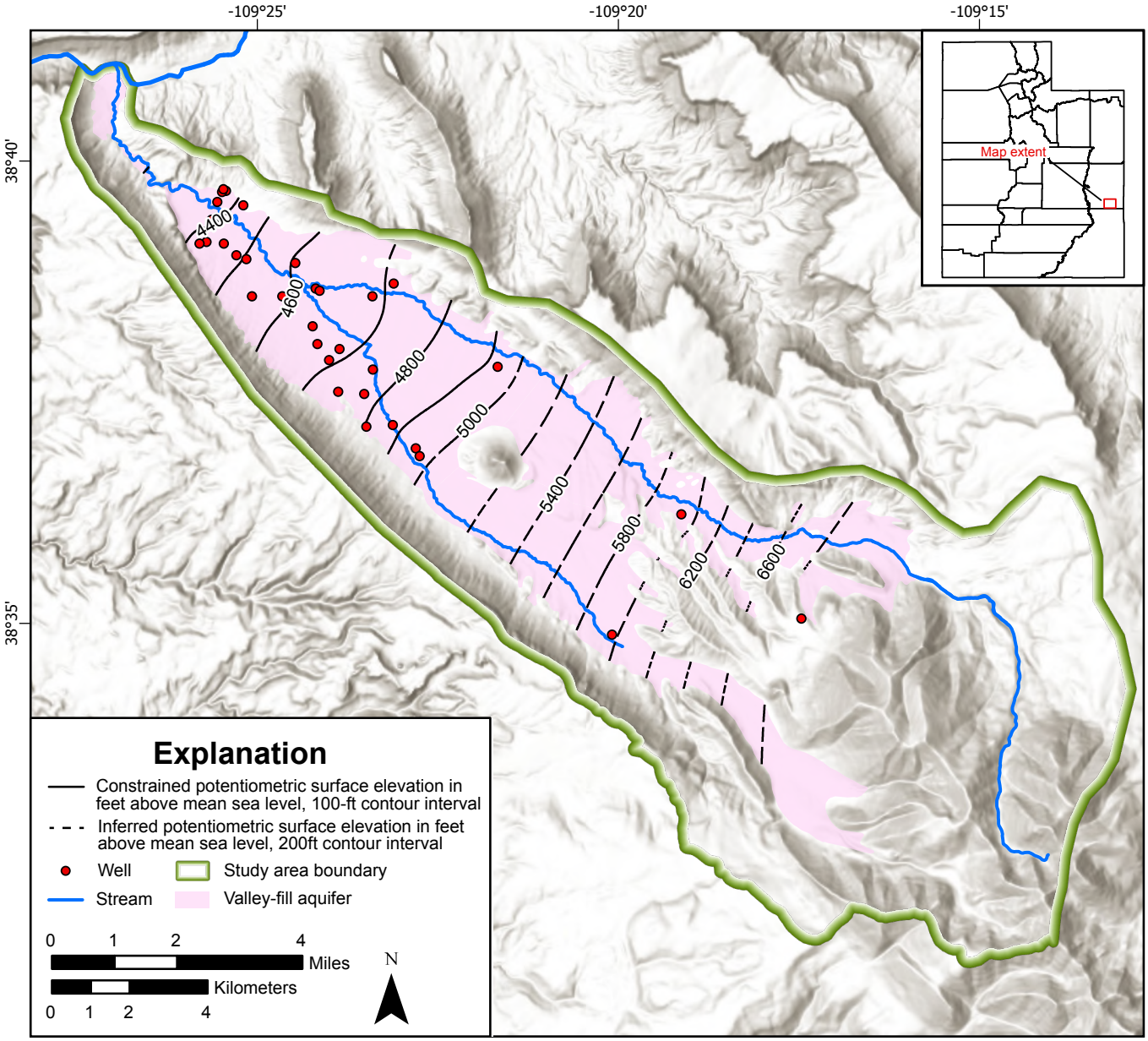

Figure 7. *Potentiometric surface map of water levels from wells measured during spring 2024. Note that contour interval size increases above the 5000-foot contour, meaning that the contour spacing does not reflect the substantially greater hydraulic gradient in the southeastern part of the valley.*

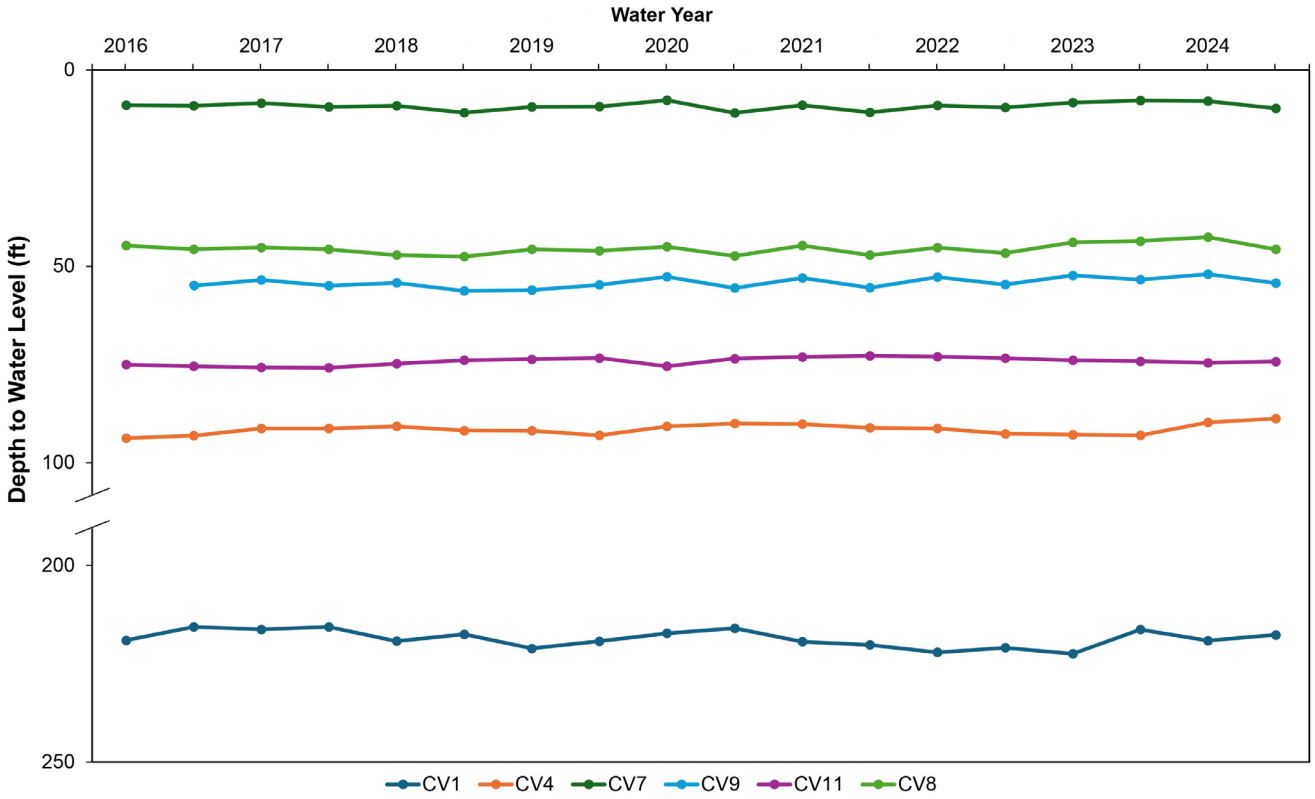

Figure 8. *Groundwater levels for Castle Valley monitoring wells measured between 2016 and 2024.*

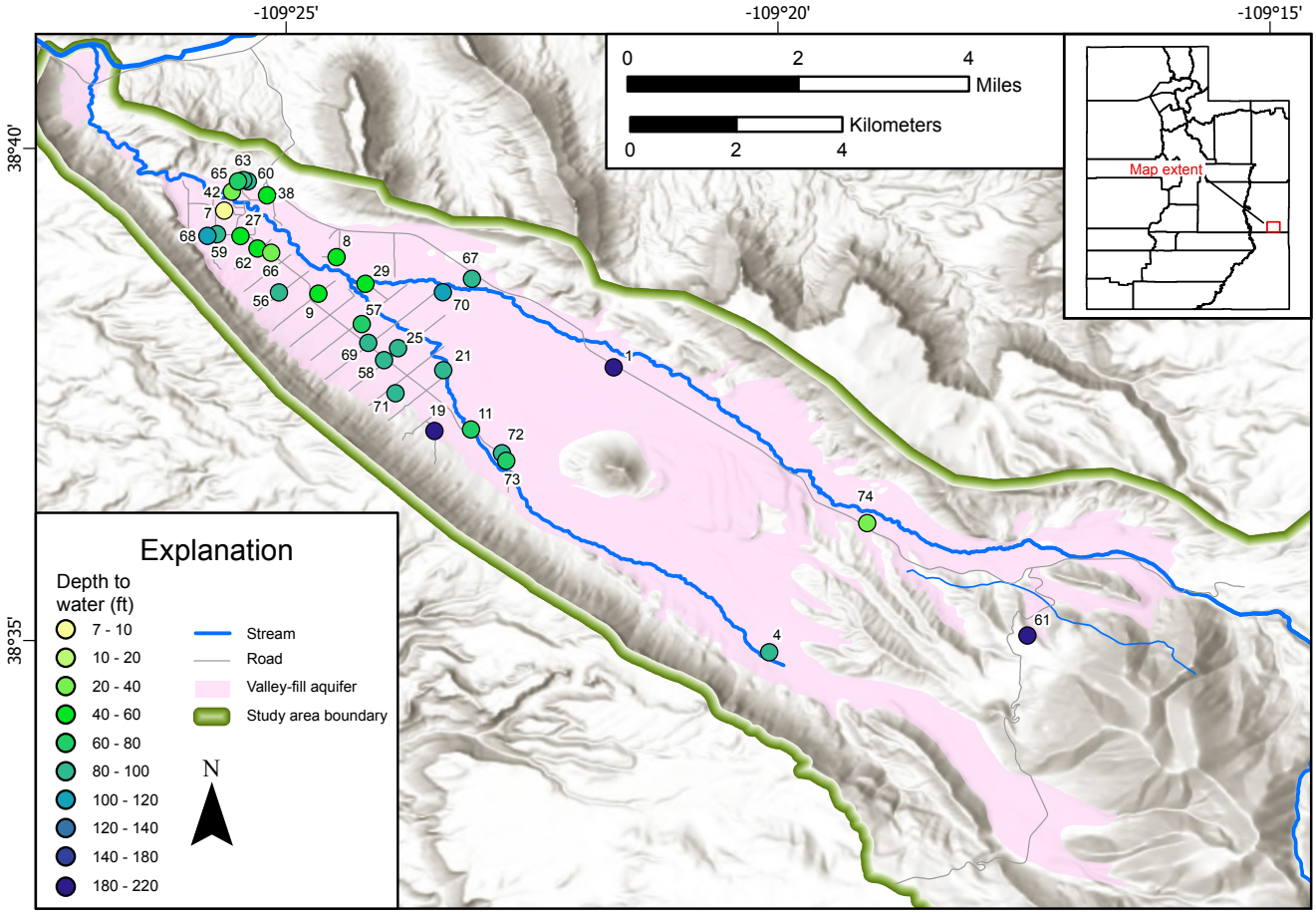

Figure 9. *Depth to water in wells measured during the fall 2023 water level run. Circle colors show depth-to-water classes (7 to 220 ft below land surface); numbers label wells.*

Table 1. *Changes in depth to groundwater from 1994 to 2024 for selected Castle Valley wells. A positive change indicates an increase in depth to water or lower groundwater elevation; a negative change indicates a decrease in depth to water or higher groundwater elevation. Count is a measure of how many times the water level was measured in each well.*

Site ID	Lot #	Depth to water 1994 (ft)	Depth to water 2024 (ft)	Avg (ft)	Change (ft)	Count
CV70	194	-110.68	-108.96	-109.82	1.72	2
CV71	287	-94.09	-97.95	-96.02	-3.86	2
CV73	356	-77.66	-80.32	-78.83	-2.54	2
CV68	401	-98.23	-101.14	-99.69	-2.91	2
CV65	432	-71.87	-71.97	-71.92	-0.10	2
CV38	439	-43.37	-44.39	-43.88	-1.02	2

Table 2. *Depth to water (DTW) statistics for Castle Valley monitoring wells, 2016 through 2024. Count is a measure of how many times the water level was measured in each well.*

Well	Average DTW (ft)	Min DTW (ft)	Max DTW (ft)	Range DTW (ft)	Count
CV1	218.59	215.60	222.45	6.85	18
CV4	91.47	88.74	93.69	4.95	18
CV7	9.20	7.71	10.94	3.23	18
CV9	54.11	51.96	56.22	4.28	17
CV11	74.18	72.74	75.80	3.06	18
CV8	45.51	42.56	47.51	4.96	18

Table 3. *Mann-Kendall trends for Castle Valley monitoring wells.*

Well	Trend	Significance	p-value	Kendall Tau	Slope
CV1	No trend	Not significant	0.0748	0.3137	0.170
CV4	No trend	Not significant	0.16	-0.2484	-0.0967
CV7	No trend	Not significant	0.7049	-0.0719	-0.0109
CV9	No trend	Not significant	0.0578	-0.3456	-0.1342
CV11	No trend	Not significant	0.1116	-0.2810	-0.0967
CV8	No trend	Not significant	0.2241	-0.2157	-0.0783

Note: Significance based on $\alpha = 0.05$. p-value < 0.05 indicates a statistically significant trend.

Scattered clay lenses are present in Castle Valley, but none are extensive enough to act as confining layers (Snyder, 1996a). Valley-fill well depths range from 58 to 367 feet (18–112 m) and are typically less than 150 feet (45 m) below the land surface. The estimated maximum valley-fill aquifer thickness is 410 feet (125 m) in the valley center, an increase from the previous estimate of 350 feet (107 m) along Castle Creek (Lowe et al., 2004).

Cross section A-A′ trends northwest-southeast through Castle Valley, generally parallel to Castle Creek (Figure 11). At the northwest end of the cross section, the lithologic log for an exploratory well that was abandoned (WIN 19493) indicates Moenkopi Formation at ~70 feet (21 m) bgs. This shallow depth may indicate the presence of a radial fault in the subsurface, a feature commonly found at the nose end of salt walls in the Paradox Basin (Giles et al., 2017; Escosa et al., 2019). At least one well (WIN 6810) in the center of the cross section is completed in bedrock at a depth of 130 feet (40 m) bgs, but the well log provides no clear geologic unit description. Maximum unconsolidated thickness is poorly constrained along most of the cross section, but is locally at least 250 feet (76 m) thick (WIN 23205). Unconsolidated deposits are primarily coarse and medium- grained, with rare fine-grained and clay interbeds. Basin-fill thickens along the valley axis as bedrock elevations decrease due to salt dissolution collapse.

Cross section B-B′ trends southwest-northeast across the northwest part of Castle Valley (Figures 8 and 9). Two wells at the southwest end of the cross section are completed in Cutler Formation and three wells at the northeast end are completed in the Moenkopi and Cutler Formations. Unconsolidated deposits on the valley margins range in thickness from 20 to 60 feet (6–18 m) and are predominantly fine grained and mixed grained, with minor clay lenses. Unconsolidated deposits in the valley center are almost exclusively coarse grained. The total thickness of unconsolidated deposits in the valley center is poorly constrained in this cross section, but is presumed to be locally greater than 125 feet (38 m), and possibly up to 200 feet (61 m), based on data from a nearby well not used in this cross section (WIN 8511). At least one well (WIN 239) in the valley center,

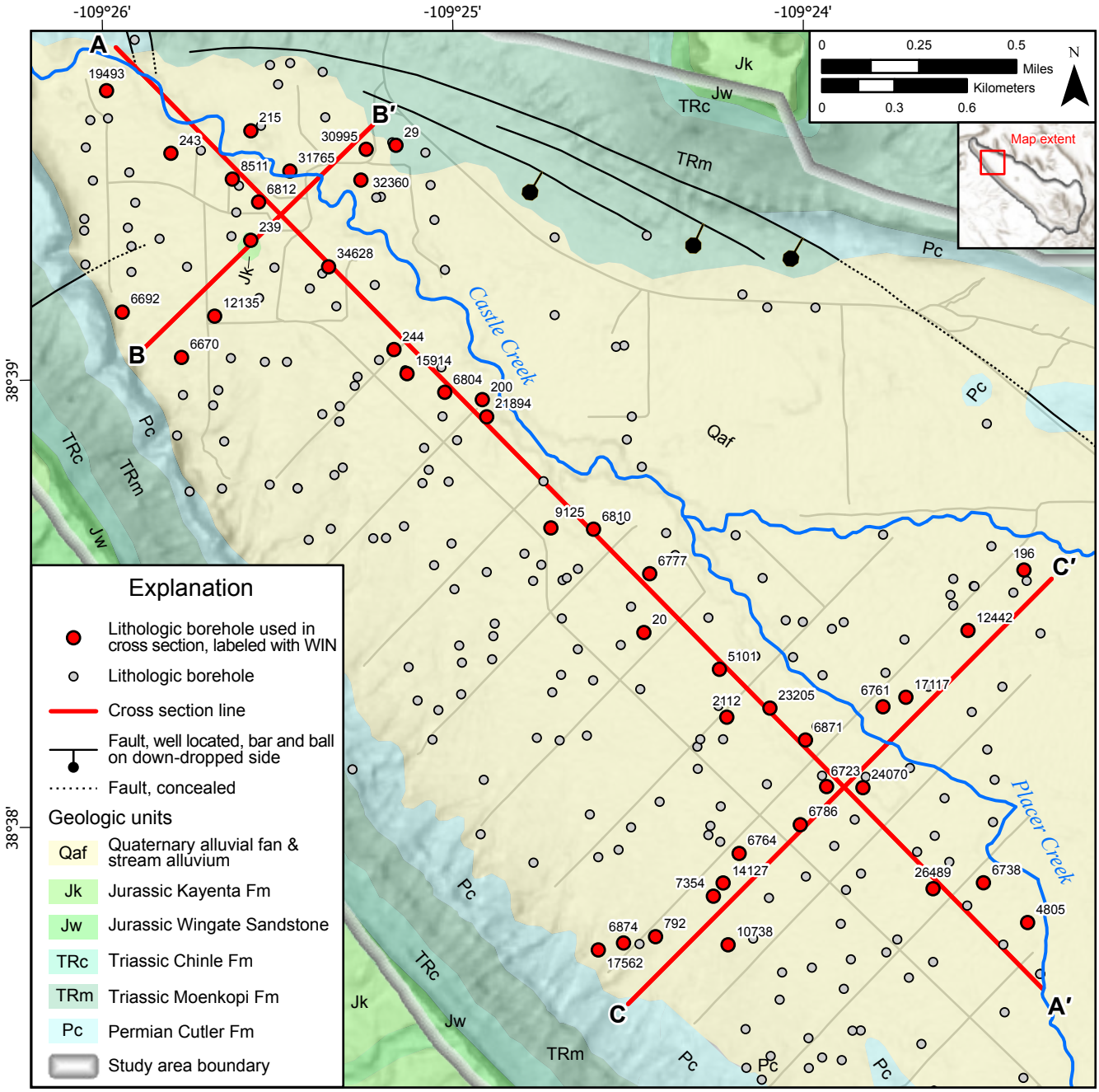

Figure 10. *Geologic map and location of cross sections and lithologic boreholes shown on Figure 11. Lithologic boreholes used to construct the cross sections are labeled with a Utah Division of Water Rights assigned and searchable well identification number (WIN). Geologic map and units modified from Doelling (2002).*

drilled to 40 feet (12 m) bgs, is completed in Jurassic Kayenta Formation that locally overlies the Paradox Formation.

Cross section C-C′ trends southwest-northeast across the southernmost concentration of wells within the Town of Castle Valley (Figure 10). Most wells at the southwest end of the cross section are completed in Cutler Formation. Overlying unconsolidated deposits, predominantly mixed-grain size, range in thickness from 0 to 60 feet (18 m). Unconsolidated deposits near the northeast valley margin along this cross section are mixed- and coarse-grained and are ~90 feet (27 m) thick. These deposits overlie the Moenkopi Formation. Unconsolidated deposits in the valley center are a mix of fine- to coarse-grain size, with sporadic clay lenses and generally grade from coarse to fine from southwest to northeast. This gradation may reflect the difference in source rock composition on opposite sides of the valley. Unconsolidated fill in this part of the valley center is poorly constrained, but is at least 200 feet (61 m). Based on the lithology at the northeast end of the cross section (WIN 196), there are likely one or more concealed normal faults associated with the collapse of the salt-core anticline that have dropped Moenkopi Formation down relative to the underlying Cutler Formation. Similar faults are mapped to the north (Doelling, 2002).

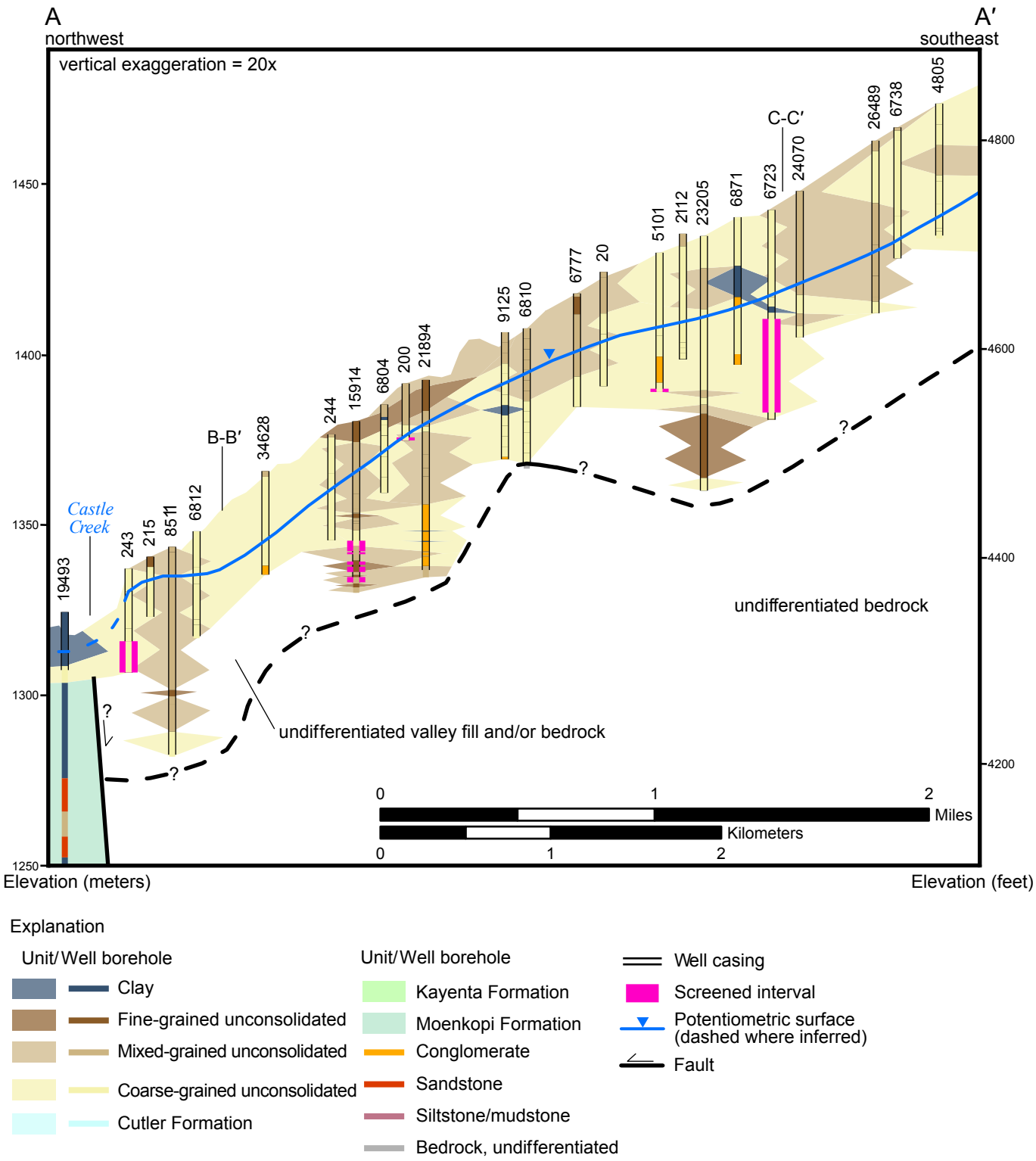

Figure 11. *Hydrostratigraphic cross sections. See Figure 10 for cross section location. Potentiometric surface from spring 2024. Well boreholes labeled with WIN. Note that vertical exaggeration in cross section A-A′ is greater than that in cross sections B-B′ and C-C′.* ***A)*** *Cross section A-A′ along the primary axis of Castle Valley.* ***B)*** *Cross section B-B′ perpendicular to the primary axis of Castle Valley in the northwest of the study area.* ***C)*** *Cross section C-C′ perpendicular to the primary axis of Castle Valley.*

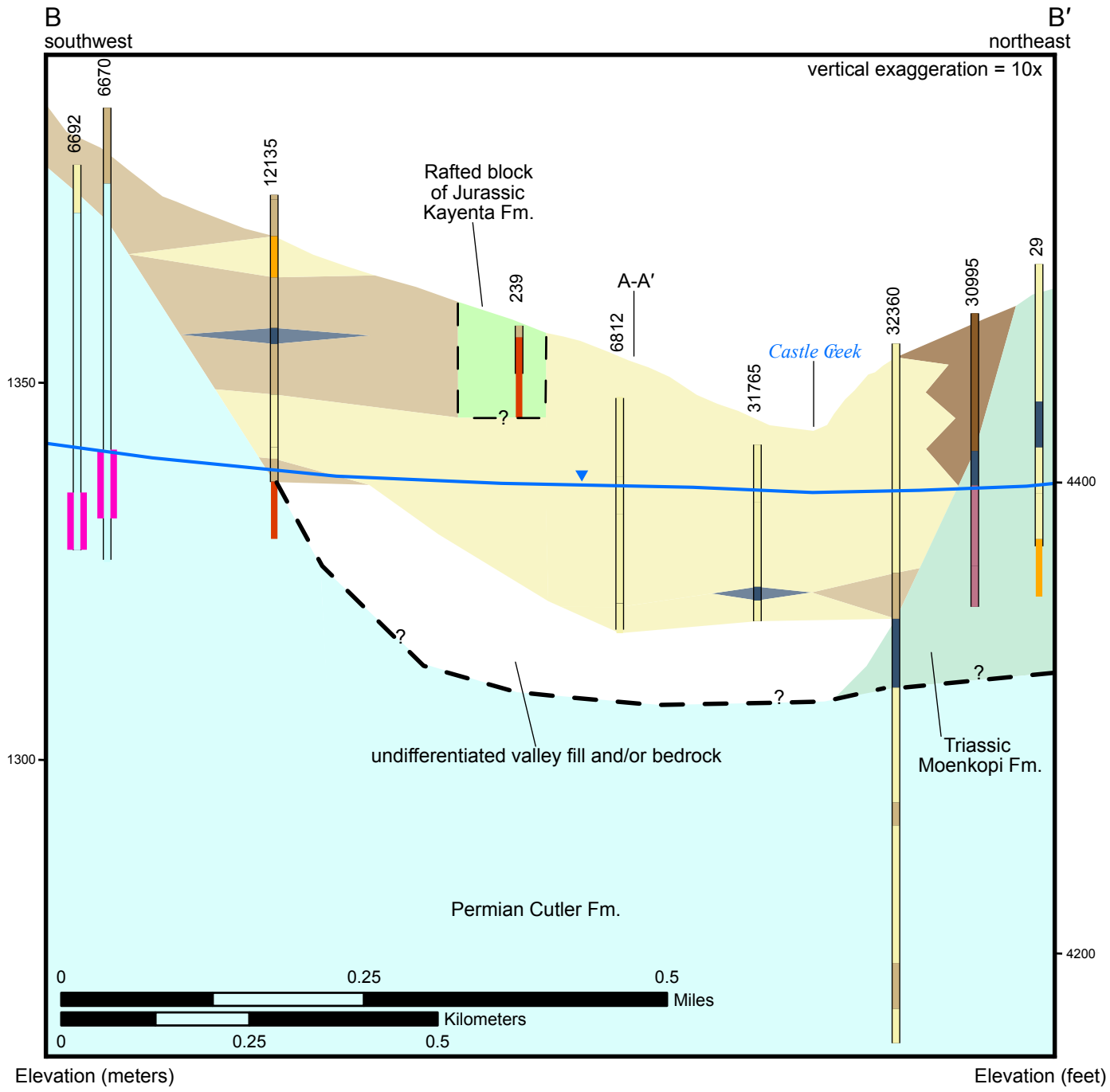

Figure 11 Continued. *Hydrostratigraphic cross sections. See Figure 10 for cross section location. Potentiometric surface from spring 2024. Well boreholes labeled with WIN. Note that vertical exaggeration in cross section A-A′ is greater than that in cross sections B-B′ and C-C′.* ***A)*** *Cross section A-A′ along the primary axis of Castle Valley.* ***B)*** *Cross section B-B′ perpendicular to the primary axis of Castle Valley in the northwest of the study area.* ***C)*** *Cross section C-C′ perpendicular to the primary axis of Castle Valley.*

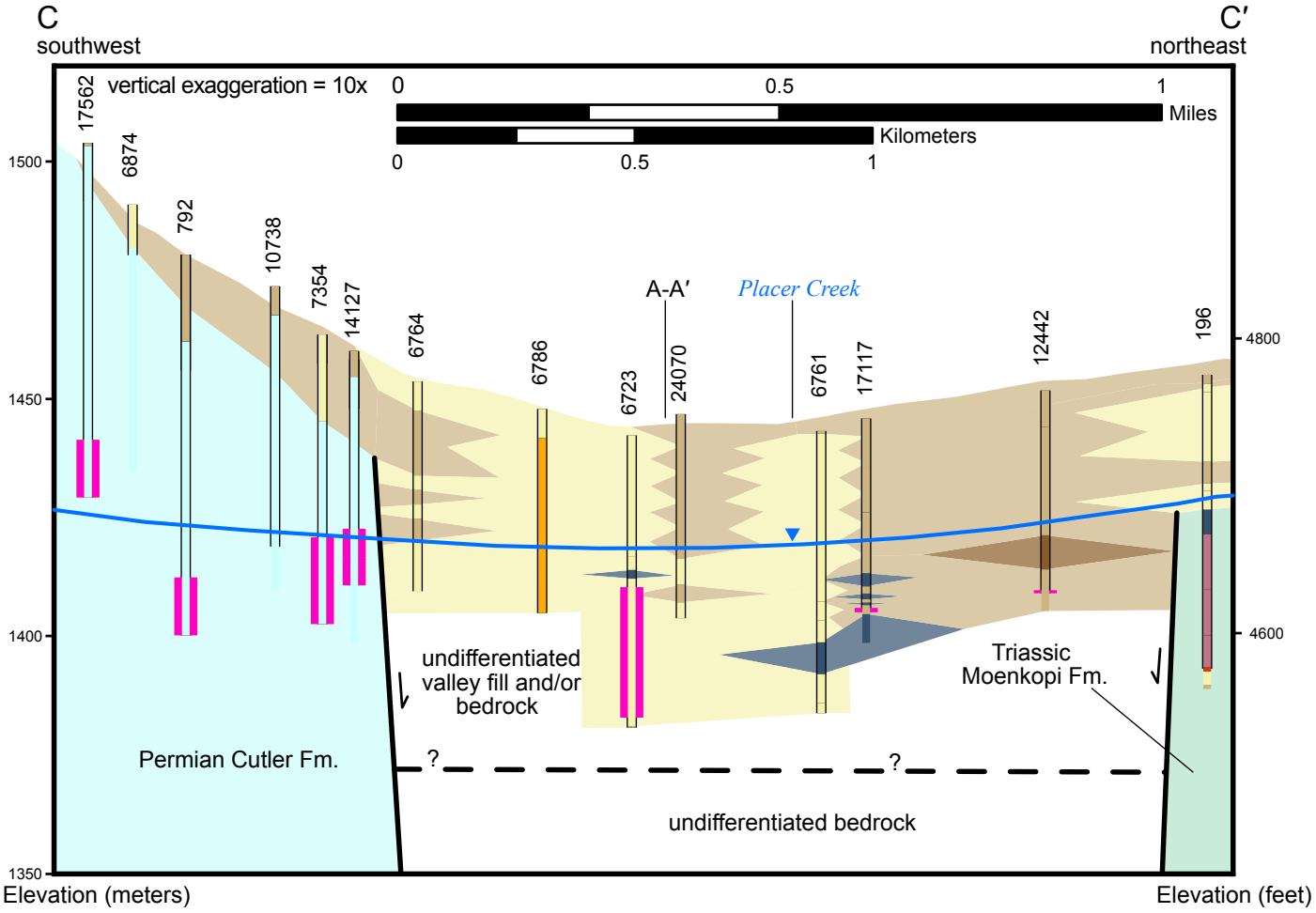

Figure 11 Continued. *Hydrostratigraphic cross sections. See Figure 10 for cross section location. Potentiometric surface from spring 2024. Well boreholes labeled with WIN. Note that vertical exaggeration in cross section A-A′ is greater than that in cross sections B-B′ and C-C′.* ***A)*** *Cross section A-A′ along the primary axis of Castle Valley.* ***B)*** *Cross section B-B′ perpendicular to the primary axis of Castle Valley in the northwest of the study area.* ***C)*** *Cross section C-C′ perpendicular to the primary axis of Castle Valley.*

Transmissivity

To characterize the aquifers in Castle Valley, we estimated transmissivity by compiling data from aquifer tests and drillers' well logs in the valley-fill and bedrock aquifers, including wells completed in the Cutler and Moenkopi Formations. Aquifer test data is generally more reliable, but specific capacity data in well logs is more common. Data from one aquifer test in the valley-fill aquifer yielded a transmissivity of 357 ft^2/day, whereas data from an aquifer test in the Moenkopi Formation yielded a transmissivity of 2693 ft^2/day (Figure 12). We calculated transmissivity from well logs using the TGUESS algorithm of Bradbury and Rothschild (1985), which utilizes the Cooper and Jacob (1946) solution of the Theis (1935) equation. To derive transmissivity from specific capacity data, we estimated storativity using the equation

$$S = Sy + (Ss * b) \quad (1)$$

Where:

S = storativity

Sy = specific yield

Ss = specific storage

b = aquifer thickness

We based Sy and Ss on published values for aquifer materials from Johnson (1967) and Domenico (1972) and based b on well logs, using length of screened or perforated interval.

We estimated transmissivity from specific capacity data for the valley-fill aquifer (n = 12) using a storativity of 0.25 and for the bedrock aquifer (n = 13) using a storativity of 0.1. Valley-fill aquifer transmissivities ranged from 42 to 12,900 ft^2/day, with a geometric mean of 379 ft^2/day (Figure 13). Bedrock aquifer transmissivities ranged from 3.5 to 1838 ft^2/day, with a geometric mean of 119 ft^2/day.

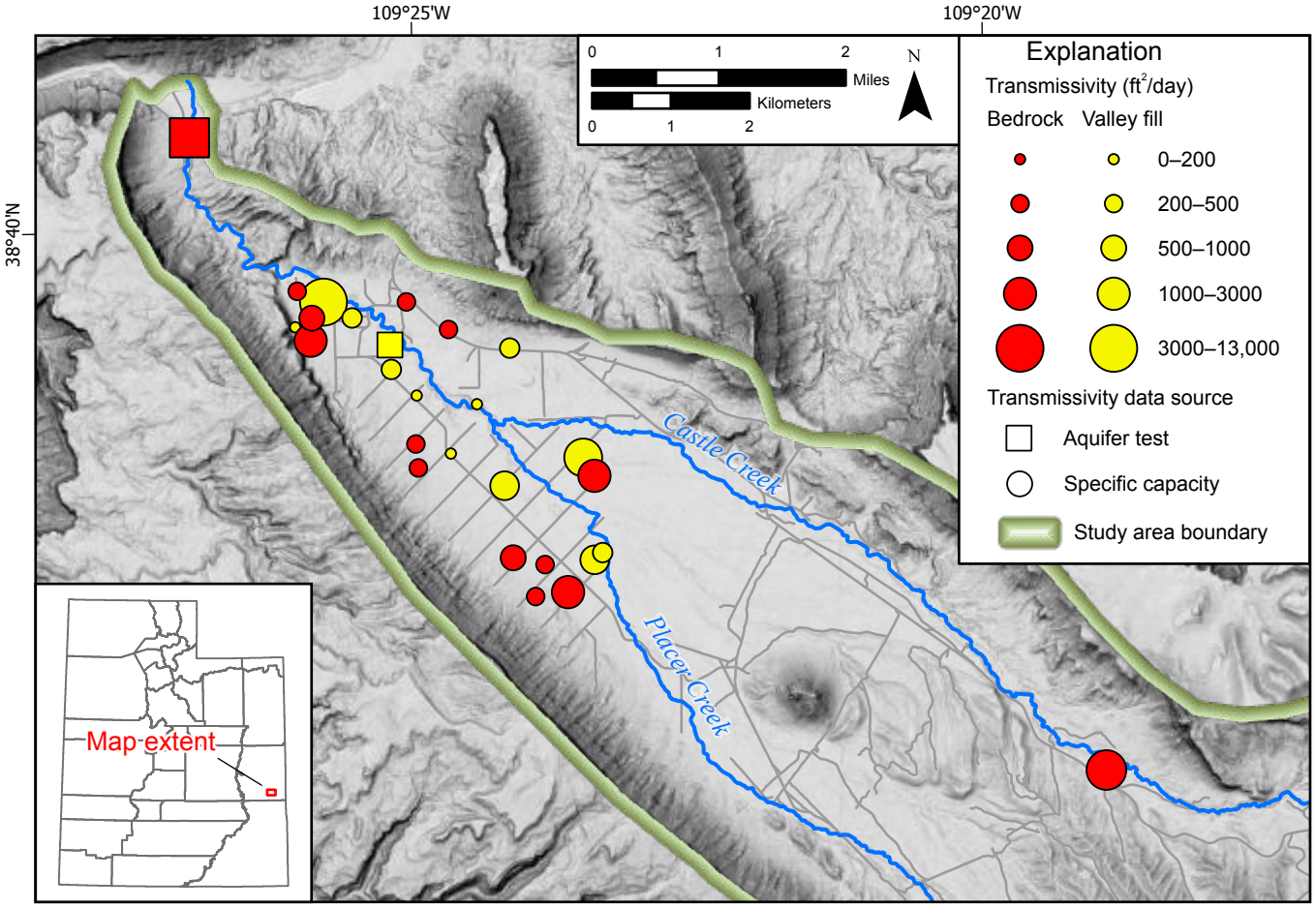

Figure 12. *Transmissivity map compiled from aquifer test and specific capacity data.*

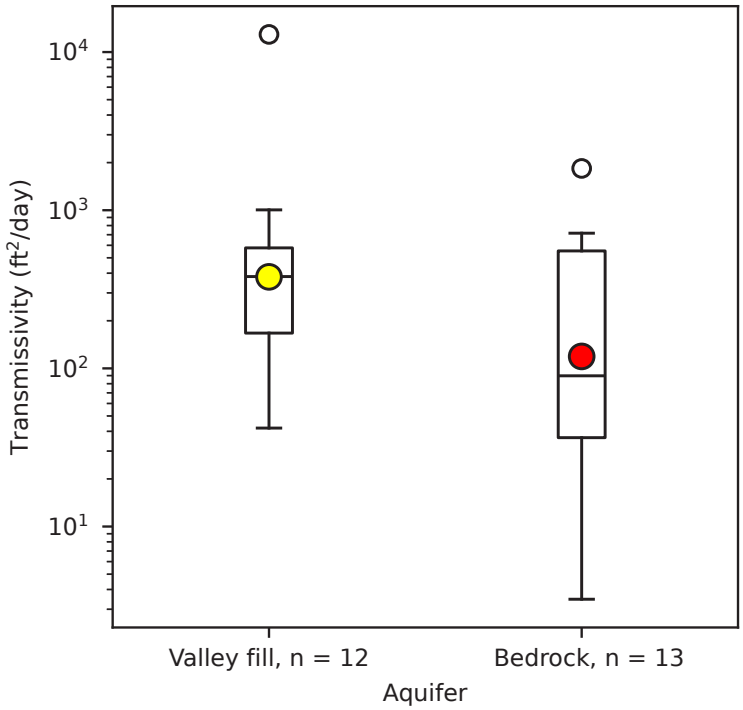

Figure 13. *Box and whisker plots of specific capacity data for study area aquifers. Geometric means shown as colored circles.*

STREAMFLOW AND DISCHARGE

Methods

Discharge measurements provide the foundation for understanding groundwater-surface water interactions. These measurements constrain streamflow gains or losses due to groundwater exchange and estimate groundwater discharge from springs. To determine stream discharge, we used an electromagnetic current velocity meter to measure velocity across a transect and the 0.6-depth method to compute the cross sectional area (Buchanan and Somers, 1969). Site locations where discharge measurements were taken are shown in Figure 14.

We conducted flow measurements at 20 sites along Castle Creek in fall 2023 and at 15 sites in spring 2024 (Appendix A Tables A-1 and A-3). Seepage runs were taken along Castle Creek in November 2023 (base flow conditions) and May 2024 (high flow conditions) to assess stream loss and or gain across Castle Valley. Base flow measurements, taken in late fall after the irrigation season ended, clearly represent

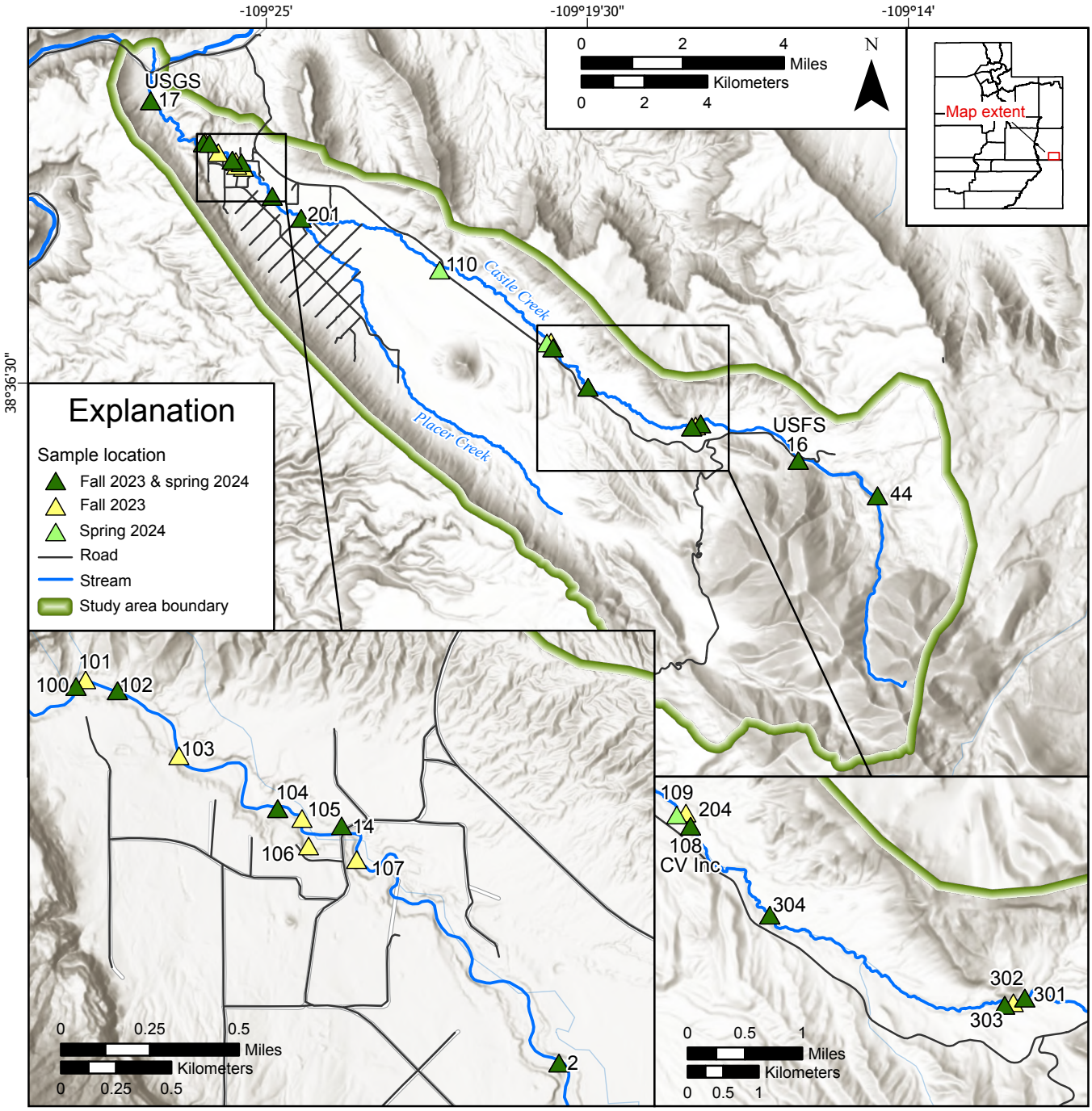

Figure 14. *Discharge measurement locations along Castle Creek showing seasonal sampling periods (fall 2023 and spring 2024).*

groundwater contributions to streamflow, as other surface inputs are minimal. High flow measurements, conducted in late spring, captured snowmelt from the La Sal Mountains and irrigation use.

Each seepage study was completed during a single day. Data collection spanned from the headwaters of Castle Creek in the Willow Basin area to USGS gage 09182400 near the Red Cliffs Lodge diversion, the farthest downstream point before Castle Creek discharges into the Colorado River. Three teams collected measurements simultaneously to minimize variability in streamflow conditions. We also collected monthly discharge measurements at three fixed locations along Castle Creek from November 2023 to December 2024 to track seasonal flow variations. Placer Creek was not included in seepage studies because it is an ephemeral stream and typically flows only during late spring runoff from the La Sal Mountains. During the spring 2024 runoff, Placer Creek did not flow and only experienced short-duration, high-flow events later in the summer and fall.

Ford (2007) and Ford and Grandy (1997) described variable hydrologic conditions along Castle Creek, identifying gaining and losing stream reaches (Figure 15). From its headwaters to the DSA irrigation diversion (now Castle Valley Inc. diversion (CVInc on Figure 14)) the creek gains flow. Below the diversion, the channel remains dry until seeps, springs, and irrigation return flows restore streamflow just downstream of the Placer and Castle Creek confluence. From there, Castle Creek continues to gain water as it flows toward its confluence with the Colorado River. We were unable to take flow measurements in most of the losing section of Castle Creek during the spring seepage run due to insufficient water and unsuitable channel geometry. During the spring measurement the Castle Valley Inc. diversion was already operational. At the confluence of Placer Creek and Castle Creeks (sample site CV201) flow was measured at 1.3 cfs, whereas upstream site CV204 measured 2.6 cfs, indicating a loss in flow. Notably, seeps above site CV201 contribute to the creek, initiating a gaining reach again.

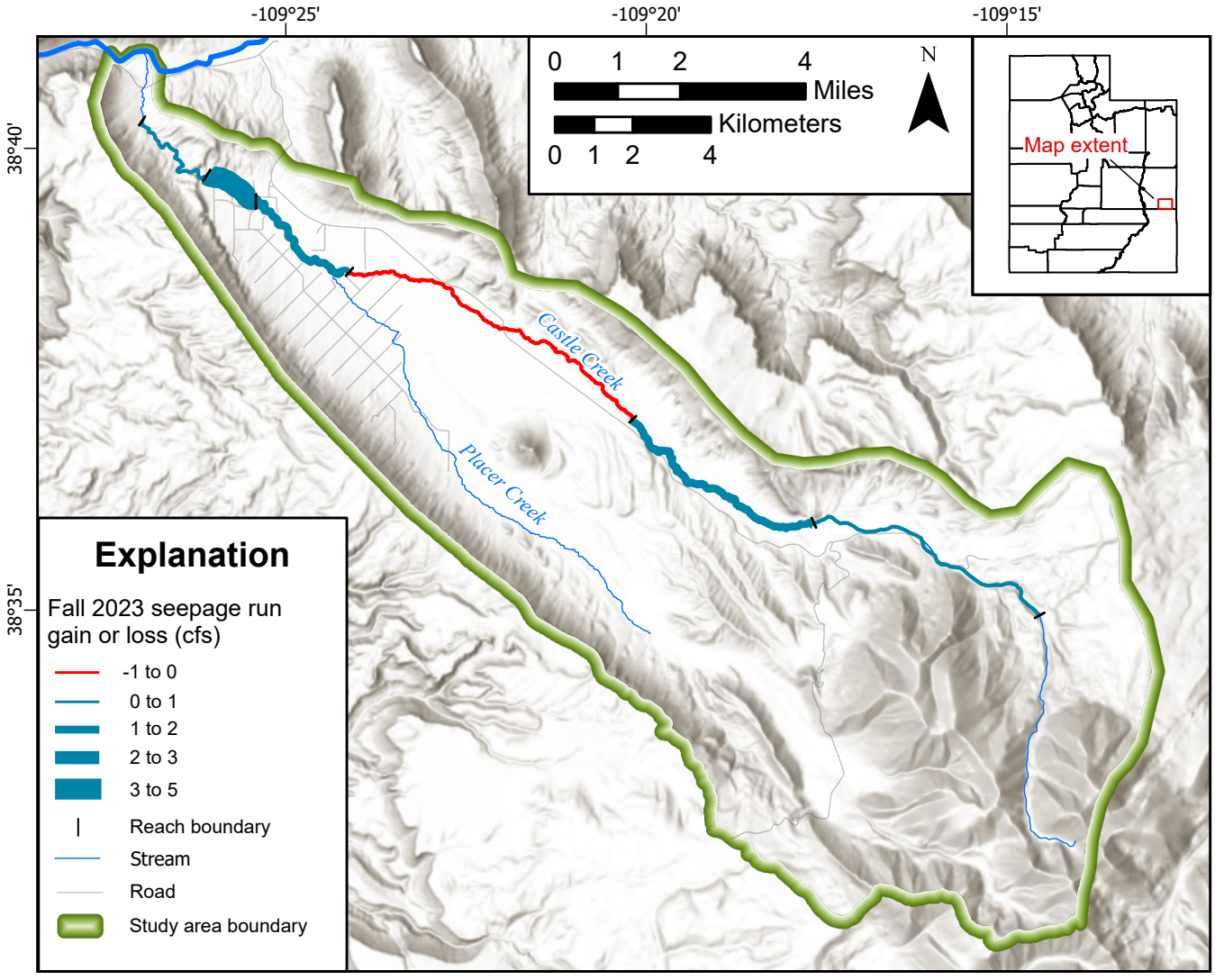

Figure 15. *Gaining and losing reaches of Castle Creek during the fall 2023 seepage run.*

We calculated water gains and losses for specific reaches of Castle Creek by comparing the flow measured at each location to the flow at the nearest upstream site, accounting for tributary inflows and diversions using the following equation:

$$\textit{Gain or loss} = \textit{downstream flow} - (\textit{upstream flow} + \textit{tributary} - \textit{diversion}) \quad (2)$$

Negative values indicate a flow loss between upstream and downstream locations, whereas positive values signify a gain from groundwater or other inputs. The error in these calculations is the sum of the individual measurement errors and likely represents an overestimate of the actual uncertainty in each calculation.

During the seepage runs conducted in November 2023 and May 2024, we also collected discharge measurements at spring locations throughout the study area (Figure 16). For larger flows, we used an electromagnetic current velocity meter in conjunction with the 0.6-depth method to measure stream velocity across transects and calculate cross-sectional area. For smaller springs with lower discharge, we utilized a portable v-notch weir or manual volumetric methods, such as timing the fill of graduated containers (e.g., 5-gallon, 1-gallon, or pint-size buckets) with a stopwatch.

Results

Streamflow

Near the headwaters of Castle Creek, the average discharge was measured at just 0.12 cubic feet per second (cfs), with flows steadily increasing downstream towards the CV Inc. diversion, where discharge reached 2.60 cfs in the fall and 3.28 cfs in the spring. During the spring seepage run, we recorded a discharge of 2.14 cfs at a diversion channel downstream of the CV Inc. diversion (site CV110). After the confluence of Placer and Castle Creeks, flows were 1.30 cfs in the fall and 1.02 cfs in the spring.

Downstream of the confluence, flow in Castle Creek increases, indicative of gaining-stream conditions sustained by seeps and springs in the northern reach. The majority of this increase occurred in the northwestern section of the creek, between sites CV106 and CV100, as the channel flows toward site CV17 (USGS gage 9182400).

Decreased discharge observed during the spring seepage run may be attributed to irrigation diverting water from Castle Creek and the fluctuating temperatures in the La Sal

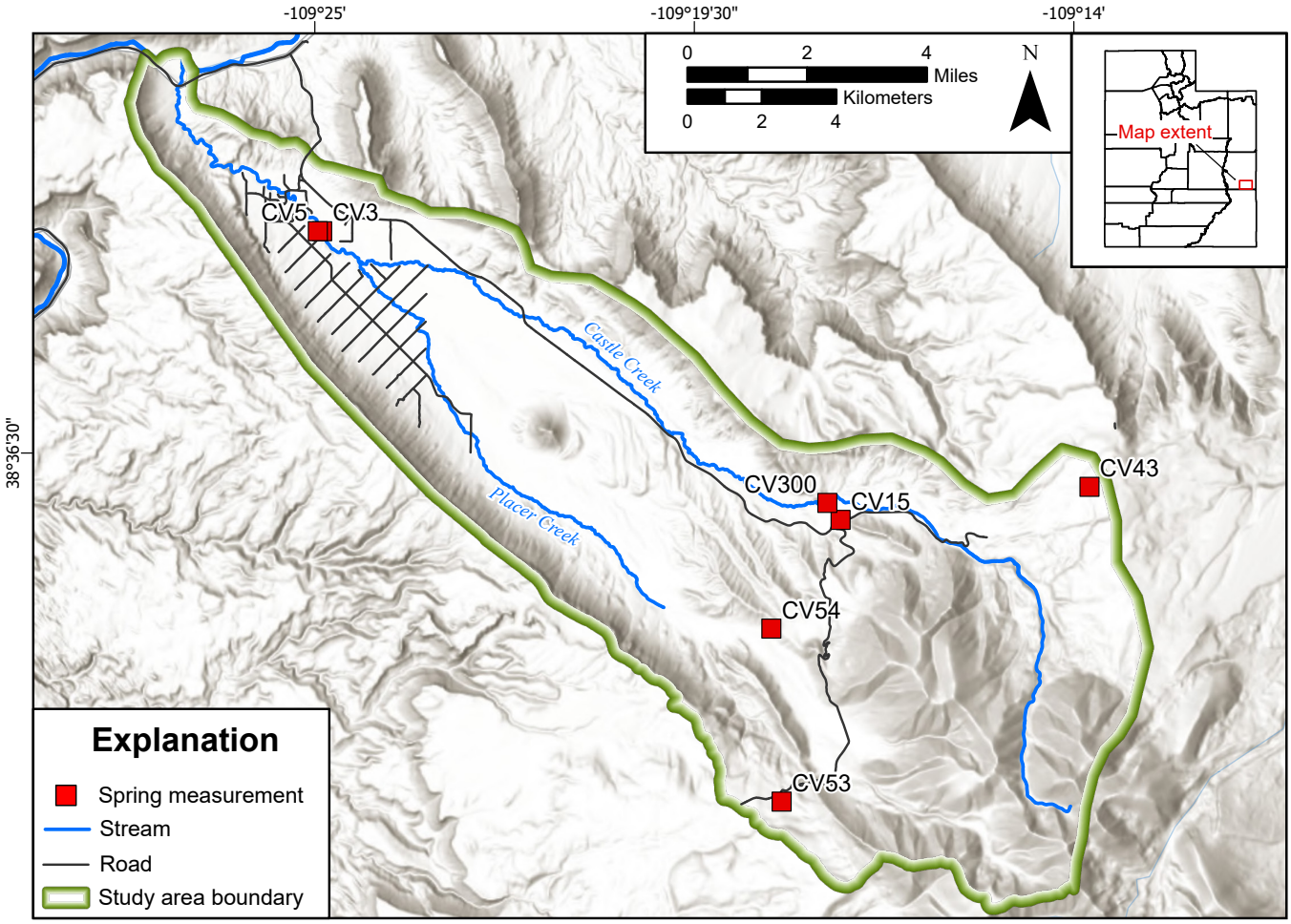

Figure 16. *Measurement locations of springs within the study area.*

Mountains, which might have slowed the rate of snowmelt into the creek.

Additional measurements were taken at three locations repeatedly between November 2023 and November 2024. These measurements provided insight into changing conditions in Castle Creek throughout the year (Table 4).

In 2024, Castle Creek gained approximately 3788 acre-feet from where it flows into the eastern extent of the valley-fill aquifer to USGS gage 9182400 (Table 5). Results indicate that Castle Creek is a gaining stream system overall, especially in the northernmost reaches. Castle creek loses streamflow between the Castle Valley Inc. diversion and the confluence of Placer and Castle Creeks. This groundwater seepage is critical to maintaining baseflow in Castle Creek throughout the year and supports both riparian habitat and downstream water users.

Spring Flow

Four springs (sites CV3, CV5, CV15, and CV300) contribute flow to Castle Creek, resulting in measurable gains along the creek (Figure 17). Average annual discharges ranged from 0.005 cfs to 1.17 cfs. Site CV15 exhibits the highest discharge at 1.17 cfs and flows into Castle Creek. Sites CV3 and CV5 are at the northwest end of Castle Valley that flow directly into Castle Creek, with annual discharge measurements of 0.20 cfs and 0.21 cfs, respectively.

Table 4. *Measured monthly streamflow for Castle Creek.*

Site Name	Latitude	Longitude	Date	Discharge (cfs)	Rating (%)	Discharge Error (cfs)
USFS	38.59138	-109.26500	November 2023	0.0956	8	0
			January 2024	0.6	8	0
			February 2024	0.516	10	0.1
			March 2024	0.442	10	0
			April 2024			
			May 2024	1.677	8	0.1
			June 2024	1.782	8	0.1
			July 2024	1.445	10	0.1
			August 2024	0.839	8	0.1
			September 2024	0.71	8	0.1
			October 2024	0.878	8	0.1
			November 2024	0.426	10	0
CV INC	38.61733	-109.33632	November 2023	2.146	8	0.2
			January 2024	2.165	8	0.2
			February 2024	2.25	8	0.2
			March 2024	2.161	8	0.2
			April 2024	2.4164	10	0.2
			May 2024	2.904	8	0.2
			June 2024	4.148	8	0.3
			July 2024	3.325	10	0.3
			August 2024	2.12	8	0.2
			September 2024	2.38	8	0.2
			October 2024	1.992	8	0.2
			November 2024	2.549	8	0.2
USGS	38.67158	-109.44978	November 2023	7.463	8	0.6
			January 2024	6.915	8	0.6
			February 2024	6.869	8	0.5
			March 2024	6.987	8	0.6
			April 2024	5.9436	10	0.6
			May 2024	5.502	8	0.4
			June 2024	7.131	8	0.6
			July 2024	4.02	10	0.4
			August 2024	6.464	8	0.5
			September 2024	4.383	8	0.4
			October 2024	3.879	8	0.3
			November 2024	7.5	8	0.6

Table 5. *Castle Creek streamflow analysis showing mean flow rates and annual volumes at key monitoring locations, with calculated reach gains and losses indicating groundwater contributions from the valley-fill aquifer.*

	Mean flow (cfs)	Mean annual volume (ac-ft)	Reach gain/loss (ac-ft)
USFS	0.86	619	1224
CV Inc	2.55	1844	
USGS	6.1	4408	2564
Total gain			3788

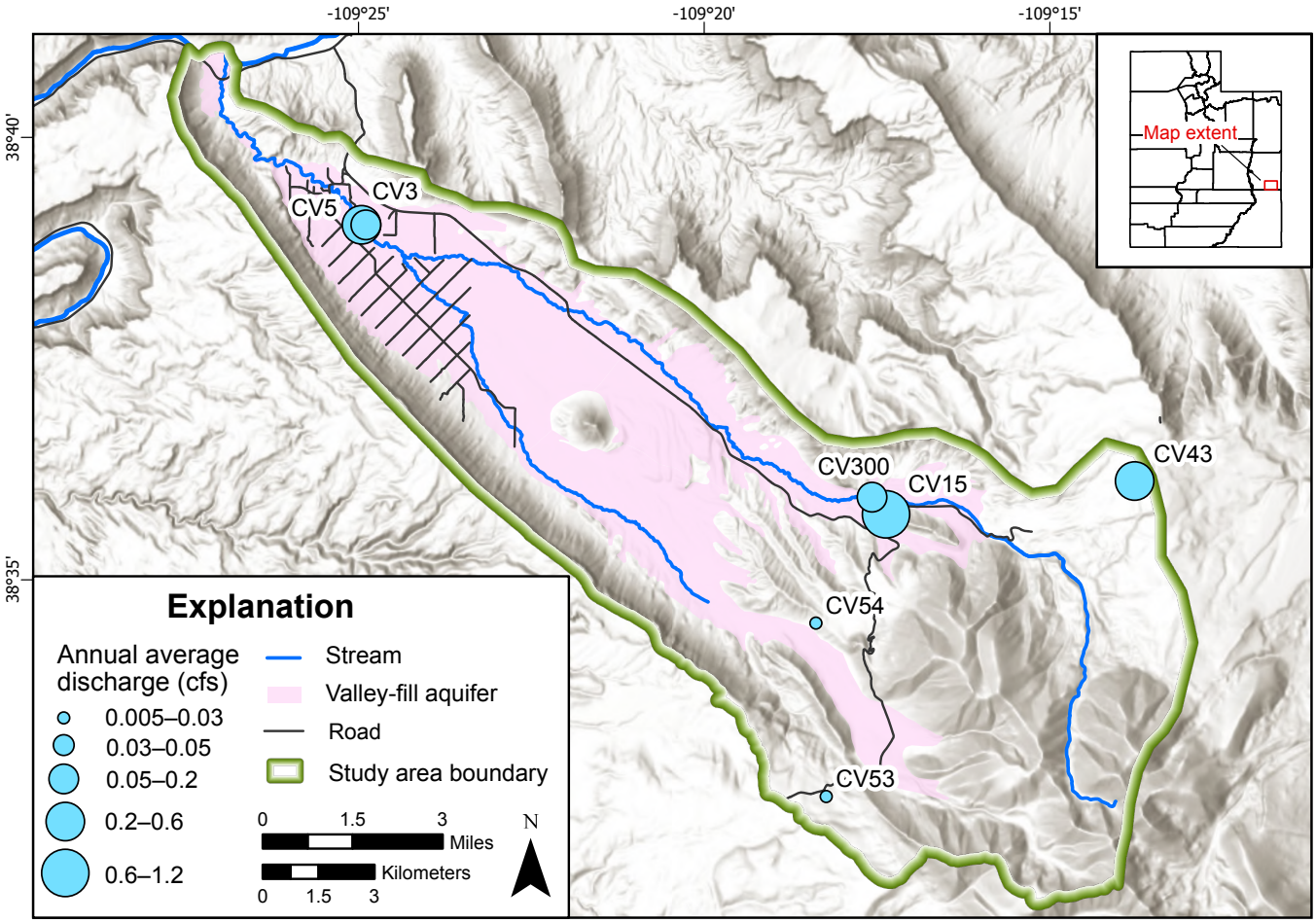

Figure 17. *Annual average discharge (cfs) from spring locations taken during seepage runs in fall 2023 and spring 2024.*

GROUNDWATER CHEMISTRY

The composition of geologic materials within a drainage basin and the duration of water exposure to these materials play a crucial role in shaping water chemistry (Winter et al., 1998). Analyzing groundwater and surface-water chemistry helps assess water quality and provides valuable insights into the overall groundwater system. By examining water chemistry from wells, springs, and streams at different locations and depths, along with other physical data, we can better interpret groundwater flow patterns and their interactions with surface water.

Methods

In October 2023, we collected chemistry samples from 21 sites, including 17 wells, 2 springs, and 2 stream locations (Figure 18; Appendix A Tables A-1 and A-4). Most wells are domestic and used regularly and were run for at least 15 minutes before sampling. For the six monitoring wells, three well volumes were purged before sampling. Field parameters including temperature, pH, and specific conductivity were measured at 18 additional wells, 14 springs, and 4 stream sites (Figure 18; Appendix A Table A-4). We analyzed selected

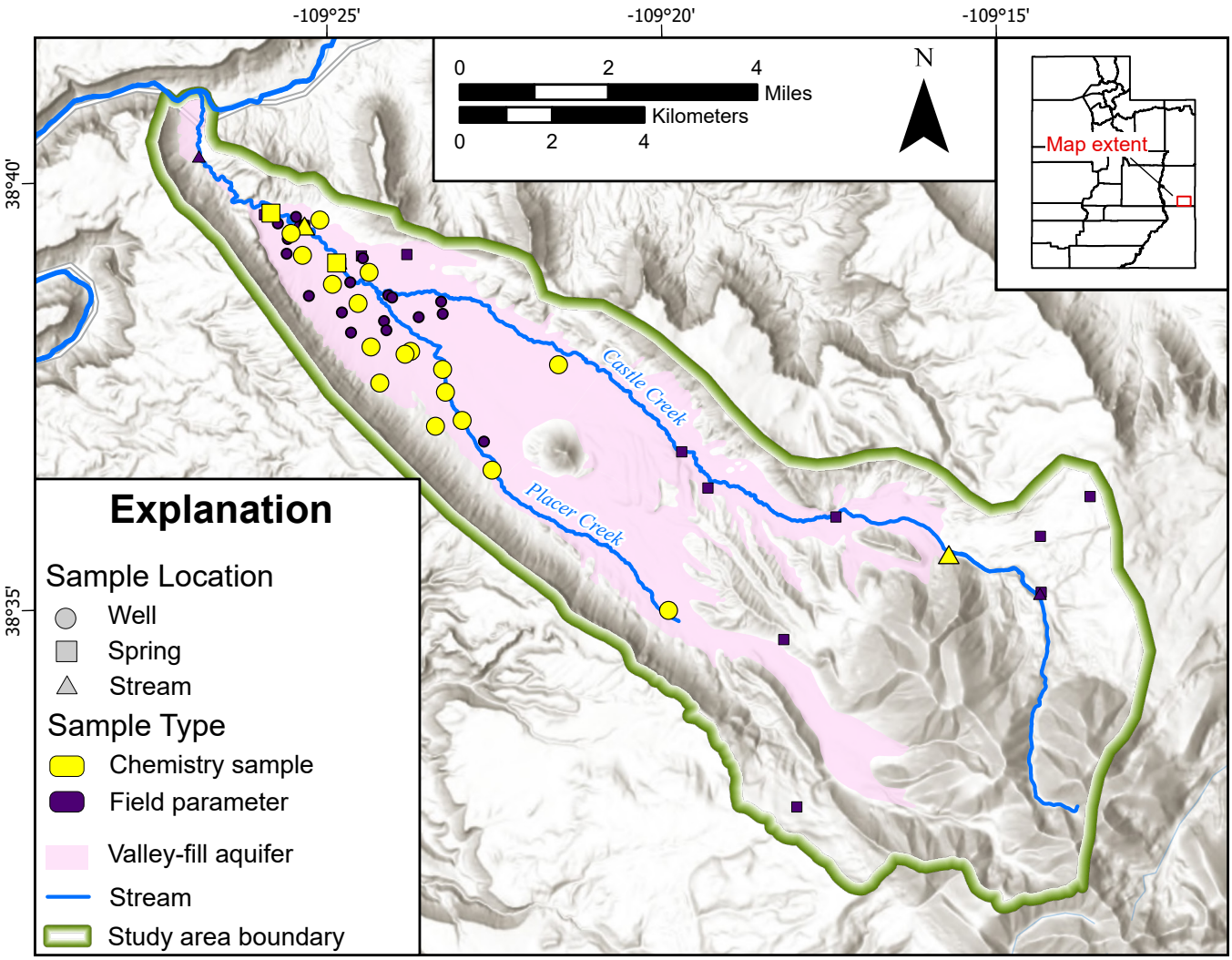

Figure 18. *Water chemistry sampling and field parameter locations.*

wells for TDS, major ions, and nitrate. Samples were collected in lab-provided bottles and stored on ice until delivery to the Utah Department of Health's Chemical and Environmental Services Division of the Utah Public Health Laboratory for analysis. To calculate TDS, a conversion factor of 0.69 was used in Castle Valley wells that only have specific conductance measurements. This number is based on Hem's (1985) equation for estimating TDS from specific conductance. The newly collected data are supplemented with information from previous studies (Lowe et al., 2004; Wallace and Lowe, 2012).

Results

Total Dissolved Solids and Major Ion Chemistry

Groundwater total-dissolved-solids concentrations within Castle Valley vary throughout the study area, ranging from 189 to 2565 mg/L. The mean TDS concentration in the study area is 856.5 mg/L (Figure 19). Increased concentrations are measured along the eastern and western margins of the valley-fill aquifer, with higher concentrations documented along the western side beneath Porcupine Rim (Figures 20 and 21). The higher TDS concentrations in the valley-fill aquifer occur in areas where the Cutler Formation and adjacent Paradox Formation evaporites lie in the shallow subsurface.

TDS in Castle Creek generally increases down valley towards the Colorado River. Concentrations rise from 103 mg/L at the headwaters (site CV45) to 2440 mg/L at the downstream USGS gage 09182400 (site CV17) (Appendix A Table A-4). The highest TDS levels are in the northwestern reach of the creek, near the town boundary. This increase may be related to a local hydraulic connection with water in the Paradox Formation (Snyder, 1996a), and also corresponds to elevated TDS levels in groundwater within the same area.

A Piper diagram of chemistry type (Figure 22) shows that groundwater in Castle Valley is predominantly calcium-bicarbonate and calcium-sulfate type, with calcium-bicarbonate in the valley center and calcium-sulfate in the remainder of the study area. Castle Creek shows marked changes in

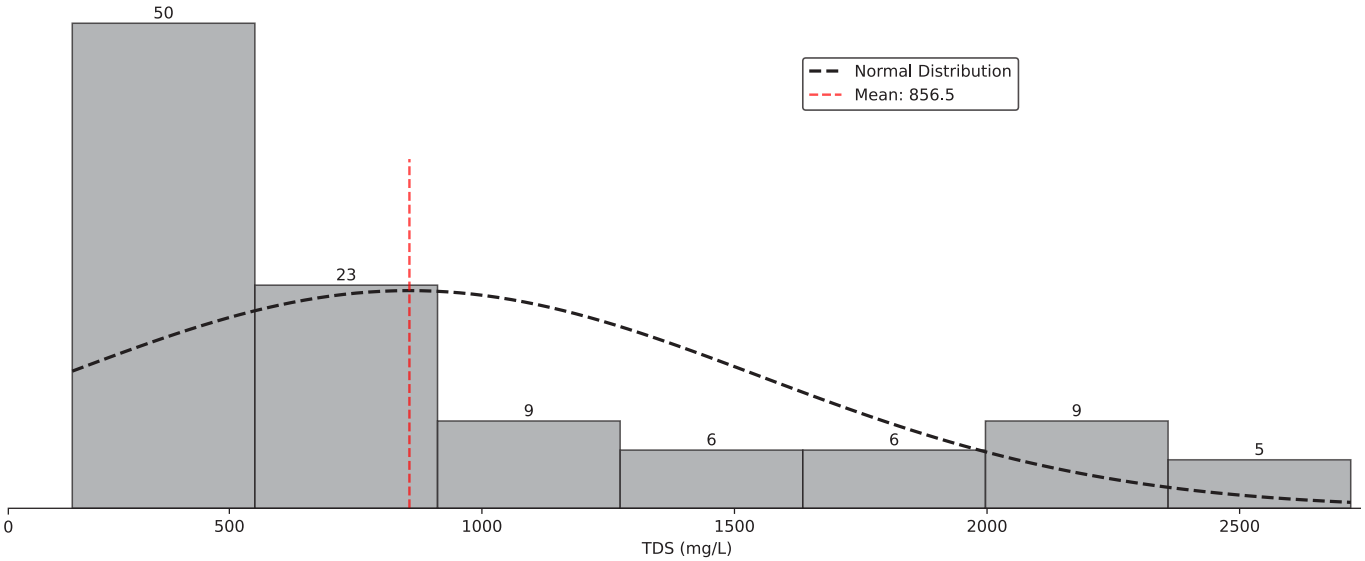

Figure 19. *Histogram showing TDS distribution (n = 108) for groundwater samples in Castle Valley. Numbers above each bar indicate the number of samples in that TDS range. Data show positive skew with mean TDS concentration of 856.5 mg/L.*

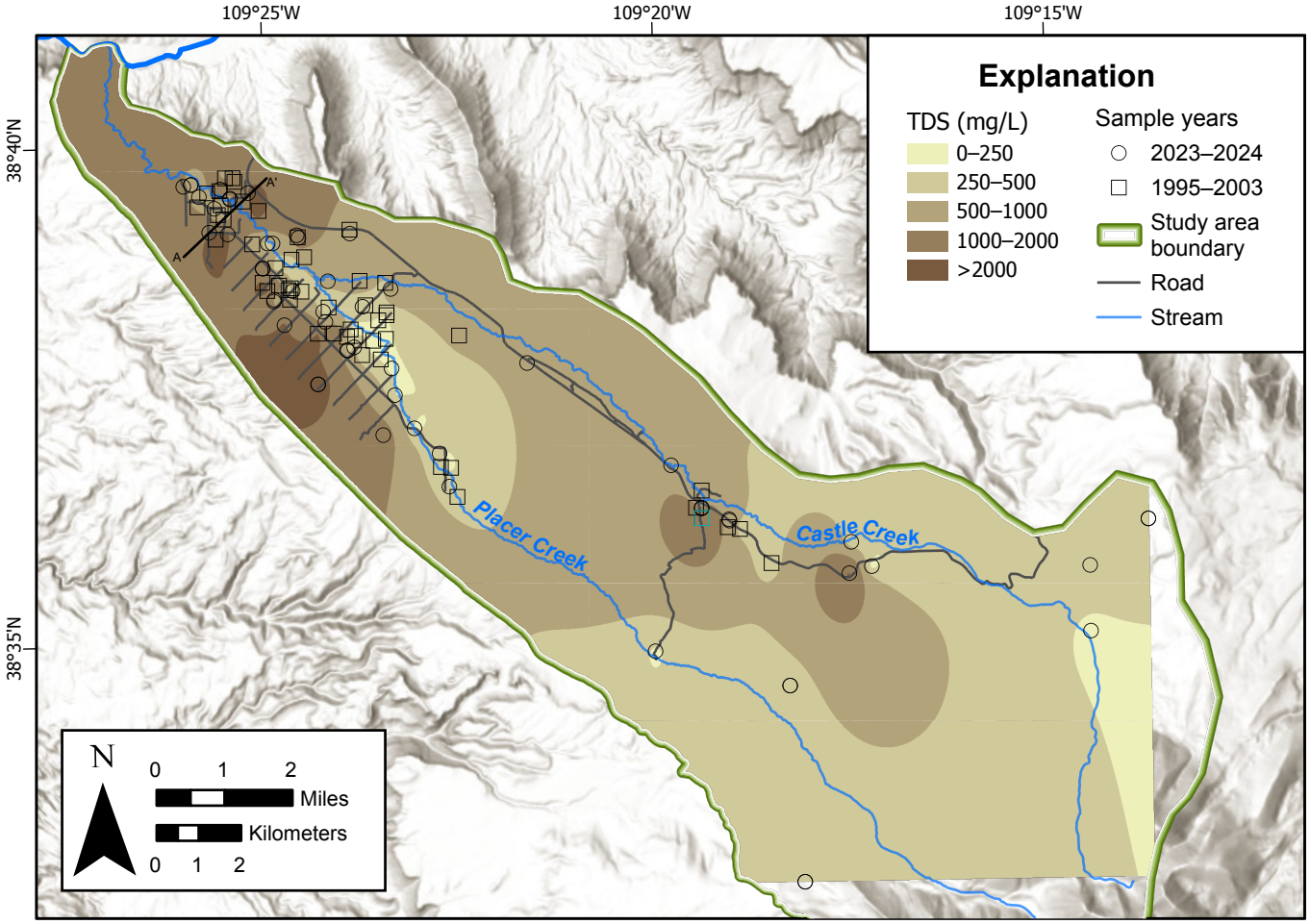

Figure 20. *Spatial distribution of TDS in groundwater across the study area, with concentrations ranging from 2565 mg/L (brown) to 185 mg/L (beige). Sample locations are marked by circles (2023–2024 sampling) and squares (1995–-2003 data) (Lowe et al., 2004). TDS raster created using Topo to Raster interpolation method. Large areas in central and southeast parts of the valley lack wells or springs, which introduces uncertainty in interpolated TDS concentrations in those regions.*

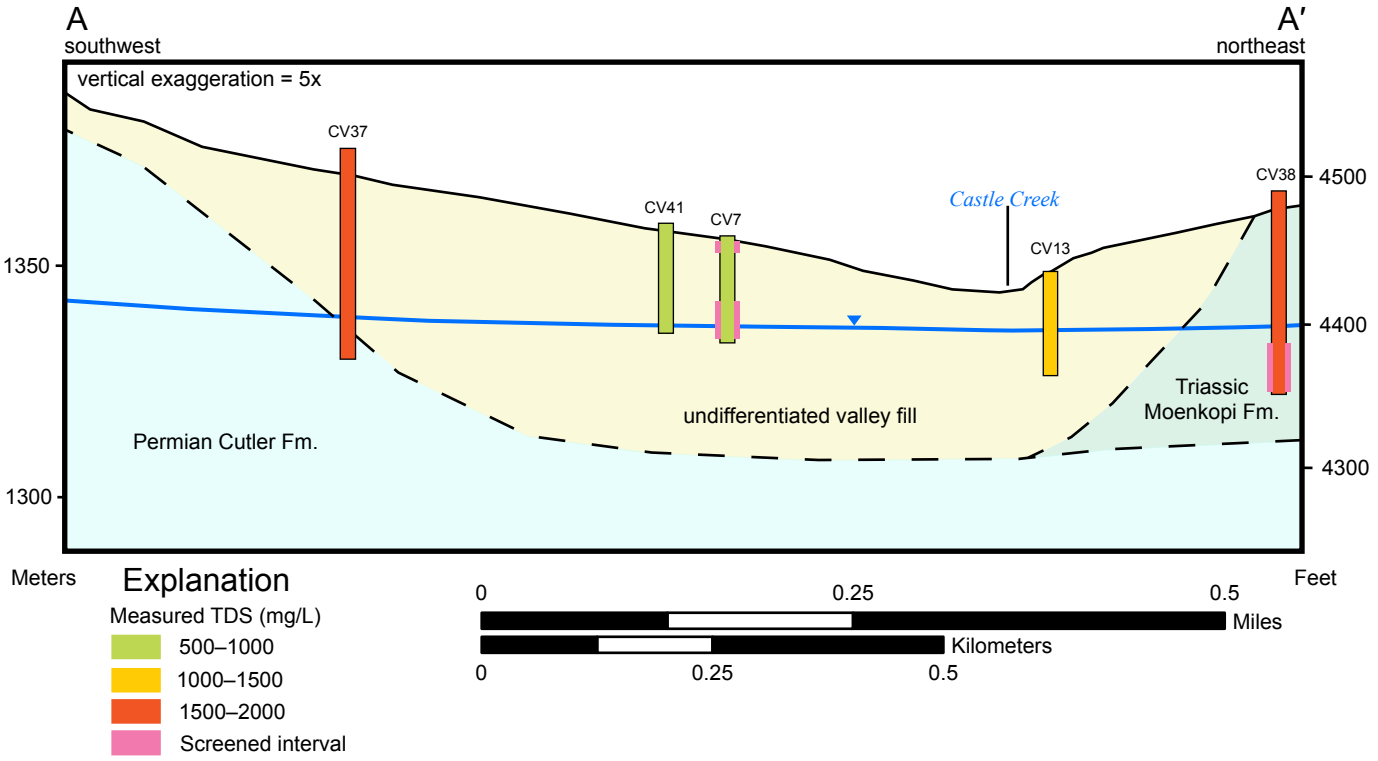

Figure 21. *Cross section showing TDS data for wells in the northern region of Castle Valley from fall 2023. Screened intervals are shown for wells CV7 and CV38, open boreholes for CV41 and CV13. Detailed well construction information is unavailable for CV37.*

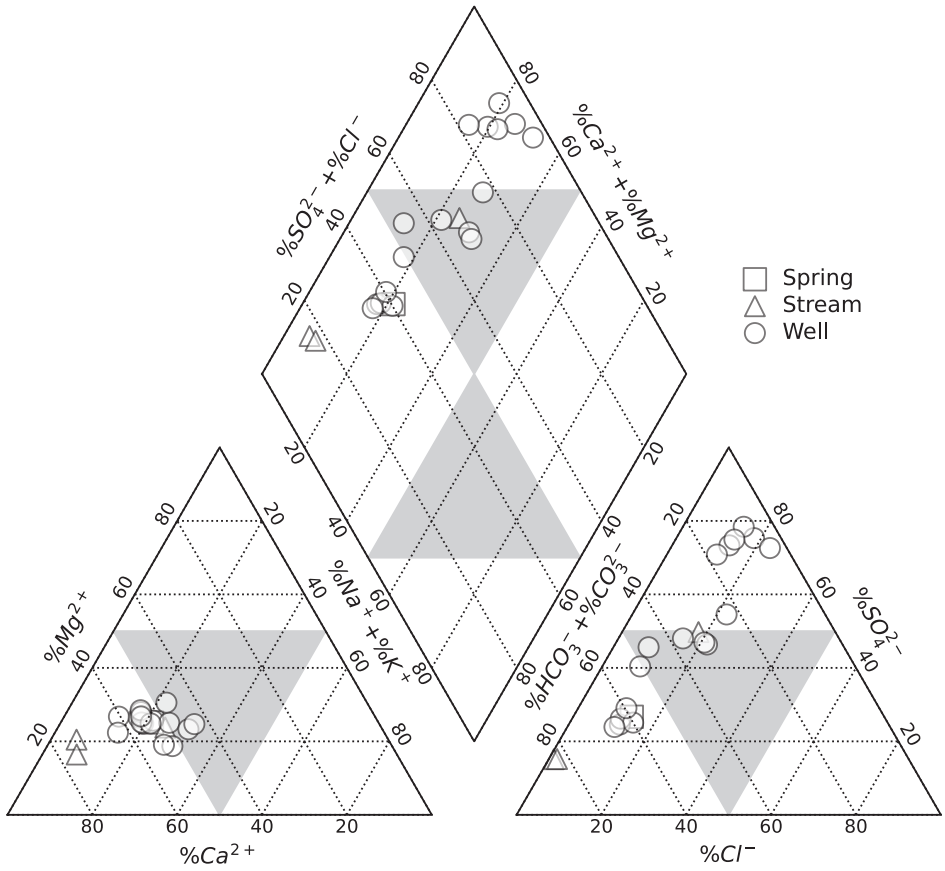

Figure 22. *Piper diagram of general chemistry samples from Castle Valley. The left triangle displays relative proportions of cations (calcium, magnesium, sodium, and potassium), and the right triangle shows anions (carbonate, bicarbonate, sulfate, and chloride).*

chemistry as it flows downstream, with increasing dissolved solids presumably sourced from seeps, springs, and small tributaries along with groundwater in various locations. The anion triangle on the bottom right of Figure 22 reveals a gradient between groundwater dominated by bicarbonate, reflecting shallow groundwater interaction with carbonate rocks, and sulfate, likely from gypsum dissolution in Cutler and Paradox Formation-derived sediments and rocks.

Nitrate

Nitrate concentrations in groundwater ranged from <0.1 to 2.16 mg/L (Figure 23; Appendix A Table A-4). At all sites, nitrate concentrations remained below 1 mg/L except for a monitoring well adjacent to an irrigated alfalfa field that had a concentration of 2.16 mg/L (well CV8; Appendix A Table A-4). This monitoring well has had concentrations of nitrate around 1.5 to 2 mg/L for over a decade, suggesting potential seasonal influences from irrigation return flows (Wallace and Lowe, 2012). Figure 23 depicts the new nitrate samples augmented with previous data from Wallace and Lowe (2012). Nitrate concentration data from this study and historical data from previous publications (Lowe et al., 2004; Wallace and Lowe, 2012) show a broader range of <0.1 to 4.27 mg/L across 46 wells.

Sulfate

Sulfate concentrations in the study area range from 14.2 to 1460 mg/L (Appendix A Table A-4). Almost one-half of all samples analyzed for sulfate have concentrations that

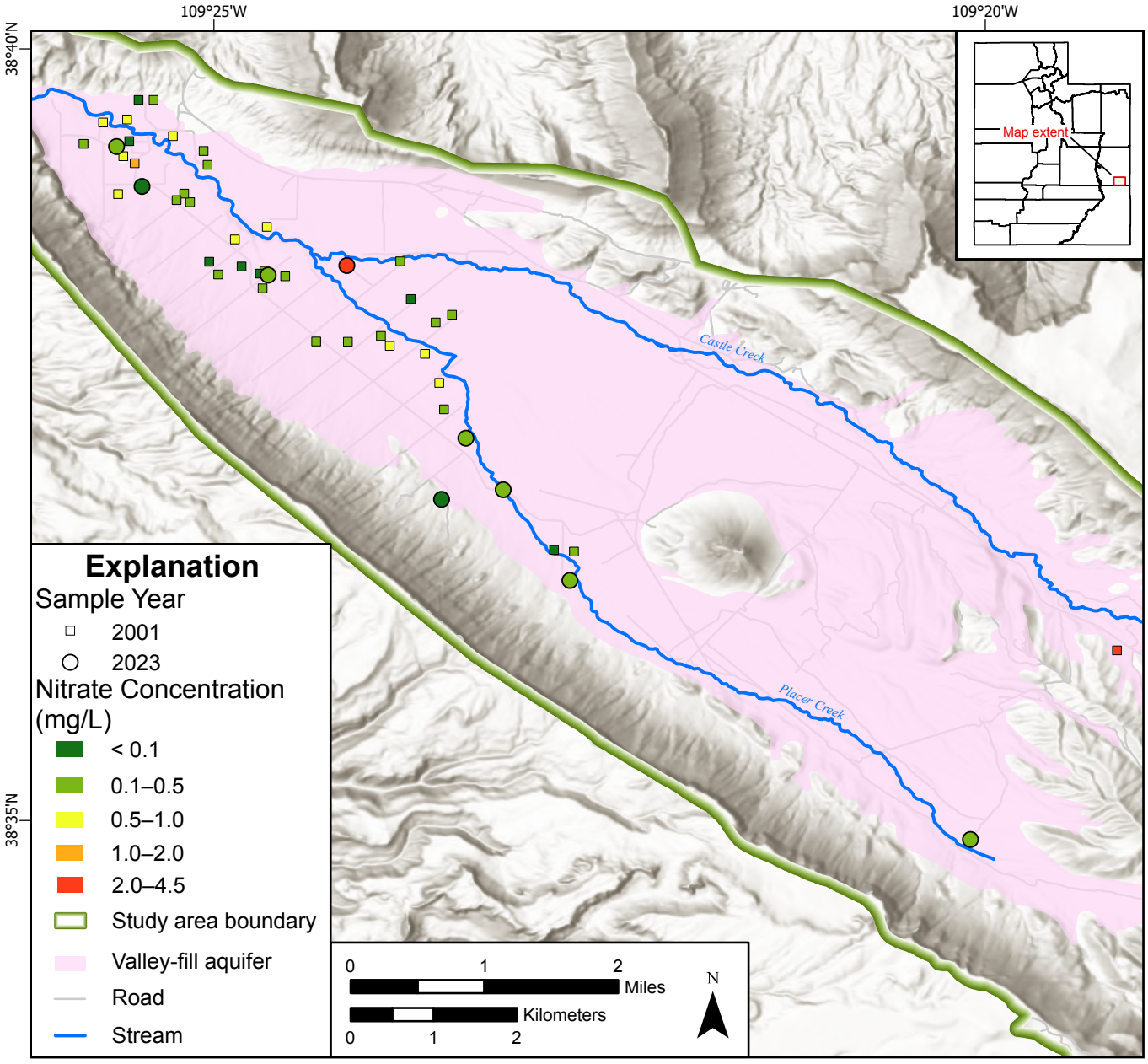

Figure 23. *Nitrate sample locations and concentration ranges.*

exceed the 250 mg/L EPA secondary drinking water standard for sulfate (Figure 24). Sulfate is a common constituent in many sedimentary rocks in Castle Valley in outcrop and in the subsurface, especially in the Cutler, Paradox, and Moenkopi Formations and to a lesser extent in the Chinle Formation. Higher sulfate concentrations correlate with proximity to these formations. In the following section, we use sulfate isotopes to aid with determining the source of sulfate in the subsurface.

ENVIRONMENTAL TRACERS

Environmental tracers are naturally occurring or anthropogenic chemicals or isotopes that can define water sources and flow processes such as recharge, flow rate, geologic subsurface interactions, residence times, and mixing. Ideal tracers have well-defined input sources and input histories, are inert (no reactions) or geochemically conservative (limited reactions), have transport mechanisms identical to water, and are detected precisely and economically. The use of multiple tracers provides a more comprehensive understanding of groundwater systems. In our study, we analyzed water samples for a suite of stable and radioactive isotopes that include oxygen-18, deuterium, and tritium in water molecules; carbon-14 and carbon-13 in dissolved inorganic carbon (DIC); and sulfur-34 and oxygen-18 in dissolved sulfate.

Methods

Stable Isotopes of Water

Oxygen-18 (^{18}O) and deuterium (^{2}H) are naturally occurring stable isotopes of oxygen and hydrogen. Water molecules containing the lighter isotopes (i.e., $^{1}H_2{}^{16}O$) and heavier isotopes (i.e., $^{2}H^{1}HO$ and $H_2{}^{18}O$) fractionate preferentially during phase changes such as evaporation and condensation.

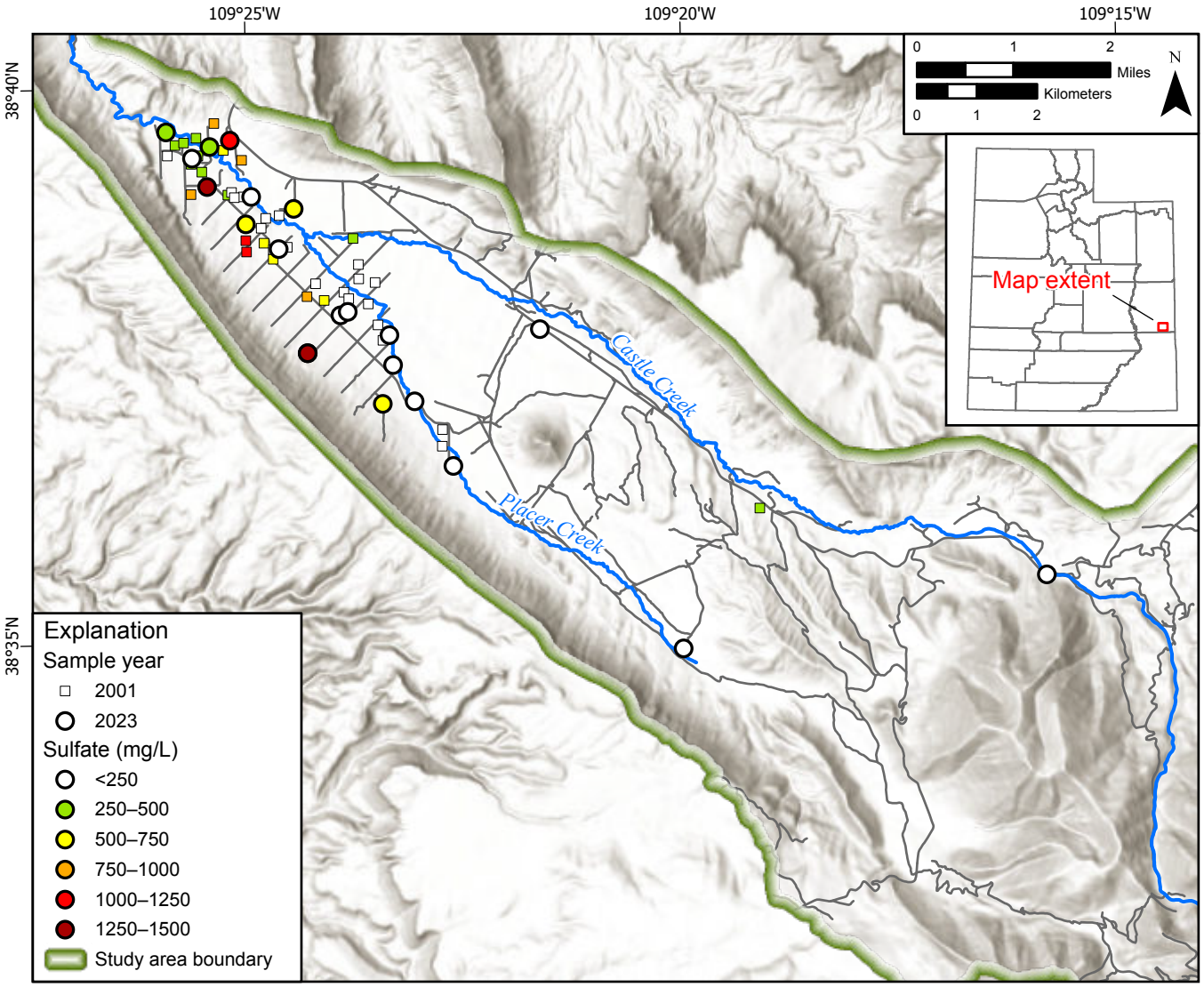

Figure 24. *Sulfate concentration in Castle Valley groundwater.*

Values for ^{18}O and ^{2}H are expressed as ratios in delta notation (δ) per mill (‰) relative to a reference standard:

$$\delta x = (Rx/Rstandard - 1) \times 1000 \quad (3)$$

where:

δx = delta notation of the sample x (in per mill, ‰)

Rx = isotopic ratio of $^{2}H/^{1}H$ or $^{18}O/^{16}O$ in the sample (no units)

Rstandard = isotopic ratio of $^{2}H/^{1}H$ or $^{18}O/^{16}O$ in the standard (no units)

The reference standard for ^{18}O and ^{2}H is Vienna Standard Mean Ocean Water (VSMOW) (Gonfiantini, 1978). The global meteoric water line (GMWL) represents approximate isotopic composition for $\delta^{18}O$ and $\delta^{2}H$ of precipitation (Craig, 1961; Rozanski et al., 1993; Clark and Fritz, 1997) (Figure 25):

$$\delta^{2}H = 8(\delta^{18}O) + 10 \quad (4)$$

Larger fractions of heavier isotopes are considered "enriched" (less negative) and smaller fractions of heavier isotopes are considered "depleted" (more negative). Precipitation can be enriched or depleted depending on origin, distance inland, elevation, form of precipitation, and event intensity. Precipitation at high elevation, inland areas, and snow is more depleted relative to precipitation at low elevation, coastal areas, and rain (Clark and Fritz, 1997). Regionally, precipitation generally plots along a local meteoric water line (LMWL), which differs slightly from the GMWL (Clark and Fritz, 1997). During evaporation of groundwater or surface water, $\delta^{18}O$ is enriched relative to $\delta^{2}H$, so samples that have been partially evaporated deviate from the LWML and tend to plot below the GWML.

Water samples from wells, springs, precipitation, and streams were analyzed for oxygen-18 and deuterium. All stable isotope samples were field-filtered with disposable 0.45-µm disc filters into 10 mL snap-cap or crimp-cap vials with no head space. Isotopic analysis of $\delta^{18}O$ and $\delta^{2}H$ was performed by cavity ring-down spectrometry at the University of Utah Stable Isotope Ratio Facility for Environmental Research (SIRFER).

Tritium

Tritium (^{3}H) provides a semi-quantitative age of groundwater recharge (Clark and Fritz, 1997). Tritium is an unstable isotope of hydrogen with a half-life of 12.32 years, therefore tritium concentration in groundwater isolated from other water will decrease by one-half after 12.32 years. Tritium is produced naturally in the upper atmosphere in small quantities, but above-ground thermonuclear testing from 1952 to the late 1970s added tritium to the atmosphere in amounts that far exceed the natural production rates, and, as a result, tritium concentrations in precipitation also increased. The amount of tritium in the atmosphere from weapons testing peaked in the early to mid-1960s and has been declining since atmospheric

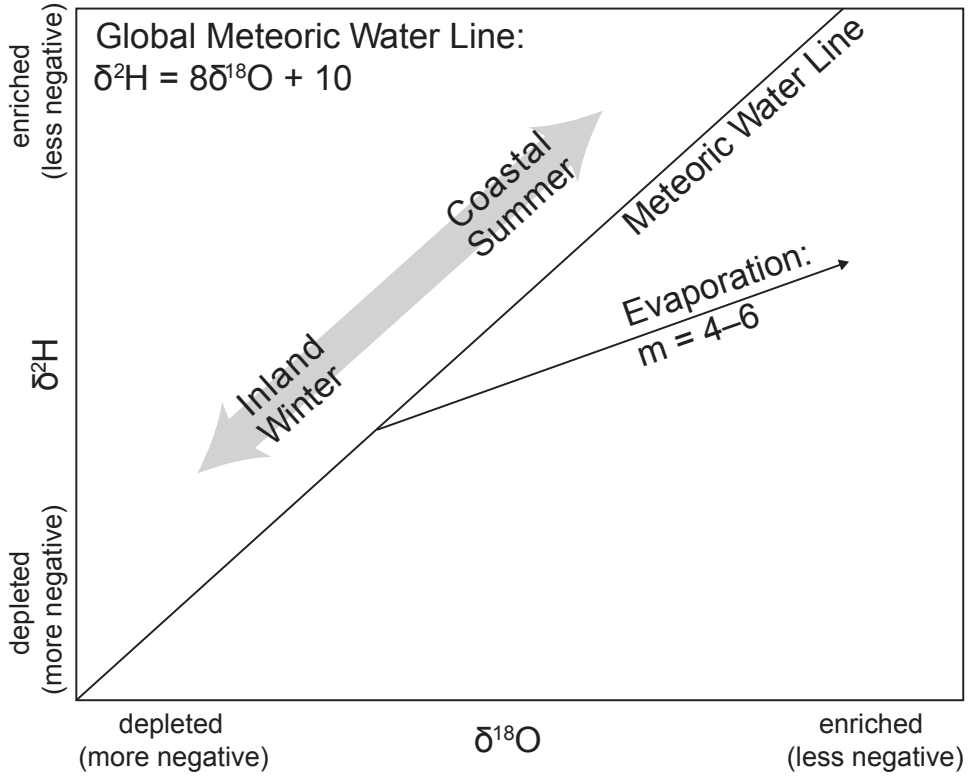

Figure 25. *Relation of oxygen-18 to deuterium in waters, including some factors that affect depletion and enrichment. Modified from Clark and Fritz (1997).*

nuclear testing ceased. Tritium concentrations in water are reported in tritium units (TU). One TU represents one tritiated water molecule per 10^{18} non-tritiated water molecules (Clark and Fritz, 1997). In Utah, concentrations in precipitation measured since 1953 ranged from background levels of 3 to 13 TU to over 8000 TU in 1963 (Michel et al., 2018). Tritium concentrations in precipitation have been approximately constant in North America since 2000 (Stewart and Morgenstern, 2016; Lindsey et al., 2019). Tritium in the atmosphere is incorporated into water molecules and enters the groundwater system as recharge from precipitation. Because tritium is part of the water molecule, it is not affected by chemical reactions other than radioactive decay, and thus can be used as a tracer of groundwater on a time scale of less than 10 to about 70 years before present. Water that entered the groundwater system before 1953 and has remained isolated from younger water contains negligible tritium. Therefore, tritium can be used to distinguish between water that entered an aquifer before 1953 and water that entered the aquifer after 1953. Location-specific thresholds for a groundwater sample can be calculated for defining modern and premodern groundwater, using measured or estimated time-series records of tritium for a given location (Lindsey et al., 2019). Using the tritium record in precipitation for a grid cell defined by 37°–39° N. latitude and 105°–110° W. longitude and groundwater samples collected in 2024, we define a premodern threshold as 0.15 TU and a modern threshold as 1.47 TU. Samples falling within this range between premodern and modern are considered mixed, including both modern and premodern fractions. For tritium concentrations above the modern threshold, a minimum recharge age can be calculated using the sample concentration and modern annual average tritium concentration in precipitation (Solomon and Gilmore, 2024).

A subset of water samples from wells and springs were analyzed for tritium (Table 6). All tritium samples were collected in two 0.5-liter high density polyethylene (HDPE) bottles and sealed with minimal head space. Tritium concentration was measured at the University of Utah Department of Geology and Geophysics Dissolved and Noble Gas Laboratory in Salt Lake City, Utah, via the tritium-^{3}He ingrowth method (Solomon and Cook, 2000), which measures the concentration of ^{3}He, a radioactive decay product of tritium.

Radiocarbon

Carbon-14 (^{14}C) is a naturally occurring radioactive isotope of carbon that has a half-life of about 5730 years, which can allow the determination of groundwater residence times of up to 40,000 years (Kalin, 2000). Carbon-14 data are expressed as percent modern carbon (pmC) relative to A.D. 1950 levels, based on the National Bureau of Standards oxalic acid standard. Carbon-13 (^{13}C) is a naturally occurring stable isotope of carbon that is used to evaluate chemical reactions involving carbon (Clark and Fritz, 1997). Carbon-13 is expressed as an isotopic ratio (^{13}C/^{12}C), reported as delta (δ) values in units of parts per thousand (per mill or ‰) relative to the Vienna Pee Dee Belemnite (VPDB) standard. The δ^{13}C ratio in groundwater depends upon numerous factors, which include the type of vegetation in the recharge area, whether carbonate (and the δ^{13}C compositions of those minerals) is dissolved or precipitated during recharge, and whether the system is open or closed.

Carbon-14 is produced naturally in the upper atmosphere by a cosmic ray reaction with nitrogen, and is added to fluids via incorporation of CO_2 gas and dissolution of carbonate minerals. ^{14}C activities are affected by chemical reactions between the aquifer material and the dissolved constituents in the water. Chemical reactions can either add or remove carbon and estimates of chemical reactions that occur during recharge and flow through the aquifer are necessary for estimating the initial activity (A_o) of ^{14}C. Age calculations therefore require estimates of some chemical parameters during recharge and model calculations of reactions during groundwater transport.

A_o is the initial, non-decayed ^{14}C composition of the groundwater and must be determined to calculate ^{14}C ages. In the absence of subsurface reactions, A_o is assumed to be 100 pmC. However, this assumption is rarely valid due to the common presence of carbonate minerals and elevated CO_2 concentrations in the soil. Many models account for geochemical reactions and gas exchanges to determine A_o (Ingerson and Pearson, 1964; Mook, 1972; Tamers, 1975; Fontes and Garnier, 1979; Han and Plummer, 2013). We estimated Ao using the graphical method devised by Han et al. (2012), which helps

Table 6. *Tritium and radiocarbon isotope results.*

Site Name	Type	Tritium concentration (TU)	Concentration error (TU)	Minimum tritium recharge age (yrs)	Radiocarbon concentration (pmC)	Concentration error (pmC)	δ^{13}C (‰)	^{13}C error (‰)
CV2	Well	1.40	0.14	33	75.6	0.28	-8.77	0.03
CV27	Well	1.46	0.07	32	5.63	0.04	-1.02	0.01
CV4	Well	2.05	0.21	26	54.5	0.18	-8.97	0.06
CV24	Well	2.17	0.23	25	64.8	0.23	-9.49	0.04
CV9	Well	1.81	0.08	28	--	--	--	--

conceptualize isotopic exchange and geochemical reactions controlled by soil gas CO_2 in the unsaturated zone and carbonate minerals in the saturated zone. We assumed end members of radiocarbon activity and $\delta^{13}C$ ratios to be 100 pmC and -17.5 ± 0.8‰, respectively for soil gas CO_2 (Hart, 2009), and 0 pmC and 0‰ for carbonate minerals, respectively.

A subset of water samples from wells and springs were analyzed for carbon-14 and carbon-13 (Table 6). All radiocarbon samples were collected in 1-liter HDPE bottles sealed with minimal head space and analyzed by accelerator mass spectrometer at the University of Georgia Center for Applied Isotope Studies in Athens, Georgia.

Isotopes of Sulfate

Sulfur-34 (^{34}S) and oxygen-18 (^{18}O) are naturally occurring stable isotopes of sulfur and oxygen that are found in sulfate molecules. These isotopes fractionate preferentially during processes like dissolution and precipitation of sulfate minerals, reduction of sulfate to HS^-, and oxidation of HS^-, sulfide minerals, organic sulfur, and SO_2. Isotopic composition of sulfate in groundwater is driven primarily by both the isotopic composition of primary and secondary sulfate sources and isotopic exchange reactions defined above. Values for ^{34}S and ^{18}O are expressed as ratios in delta notation (δ) per mill (‰) relative to a reference standard. The reference standard for ^{34}S is the Vienna Canyon Diablo Troilite (VCDT) (Beaudoin et al., 1994).

A subset of water samples from wells and springs were analyzed for sulfate isotopes. All sulfate isotope samples were field-filtered with disposable 0.45-µm disc filters into 1-liter HDPE bottles. Isotopic analysis of $\delta^{34}S$ and $\delta^{18}O$-$_{SO4}$ was conducted using a Costech Elemental Analyzer (EA) and Thermo-Finnigan High Temperature Conversion/ Elemental Analyzer (TC/EA) coupled to a Thermo-Finnigan Isotope Ratio Mass Spectrometer (IRMS) at the Stable Isotope Laboratory, University of Tennessee, Knoxville.

Results

Stable Isotopes of Water

We collected stable isotope samples from 32 wells, 15 springs, 10 surface water sites, and a vertical snow profile to represent water sources from groundwater (both valley-fill and bedrock aquifers), surface water, and precipitation (Figure 26; Appendix A Tables A-1 and A-5). Sampling occurred from October 2023 to May 2024. To capture a comprehensive representation of precipitation accumulated during the October–May snow accumulation period, eight snow samples were taken in the La Sal Mountains south of the study area boundary in late April 2024 (Figure 26). A 47-inch (118 cm) deep pit was excavated down to the ground surface, and eight vertical profile samples were collected in the snow column.

Precipitation: To expand our precipitation dataset, we leveraged preexisting precipitation stable isotope data from two sites in the greater Moab area: Island in the Sky within Canyonlands National Park, and a site near La Sal Junction (Scholl et al., 2023; National Ecological Observatory Network [NEON], 2025). Precipitation isotope compositions for $\delta^{18}O$ ranged from -29.29‰ to 0.46‰ (mean ≈ -9.31‰) and $\delta^{2}H$ ranged from -226.9‰ to 2.4‰ (mean ≈ -67.62‰). We calculated a linear regression using these data to create a LMWL shown on Figure 27.

Wells and Springs: Well samples demonstrate a clear evaporative signature, plotting along a regression line with a slope of 4.3, notably shallower than the LMWL (Figure 27). Evaporation prior to recharge can occur in both surface water and soil water, yielding regression line slopes ranging from 2.5 to 6 (Gibson et al., 2008). The isotopic composition of $\delta^{18}O$ in well water ranged from -16‰ to -13.5‰ (mean ≈ -14.8‰) and $\delta^{2}H$ ranged from -115‰ to -105‰ (mean ≈ -110‰). These values suggest significant modification of the original precipitation signal through soil-water interaction and evaporative processes, including snowpack sublimation. Spring waters exhibit intermediate isotopic compositions, with $\delta^{18}O$ values between -15.5‰ and -14.5‰ (mean ≈ -15.0‰) and $\delta^{2}H$ values from -112‰ to -108‰ (mean ≈ -110‰).

Surface Water: Surface water samples were collected along Castle Creek from southeast of La Sal Loop Road and in Willow Basin near the headwaters to USGS gage 09182400 near the Colorado River confluence (Figure 26). Surface water samples show similar values to groundwater and springs, with $\delta^{18}O$ ranging from -15.5‰ to -14.5‰ (mean ≈ -15.0‰) and $\delta^{2}H$ from -112‰ to -107‰ (mean ≈ -109.5‰). The dominant evaporative signature reinforces the similarity to groundwater and the connection between surface water and groundwater in the valley-fill aquifer.

Tritium

We collected water samples for tritium analysis from five wells in the study area (Figure 28, Table 6). Tritium concentrations measured in groundwater range from 1.40 to 2.17 TU with a mean of 1.78 TU and a mean measurement uncertainty of 0.15 TU. Three samples have tritium concentrations greater than the established modern threshold of 1.47 TU and are considered modern recharge. The remaining two samples have tritium concentrations slightly below the established modern threshold (1.46 and 1.40 TU) and can be considered mixed recharge age. Using a modern annual average tritium concentration in precipitation of 8.79 TU (Michel et al., 2018), we calculated minimum recharge ages for all tritium samples, yielding a range of 25 to 33 years (Table 6).

Radiocarbon

We collected water samples for radiocarbon analysis from four wells in the study area (Figure 28, Table 6). Carbon-14 activities

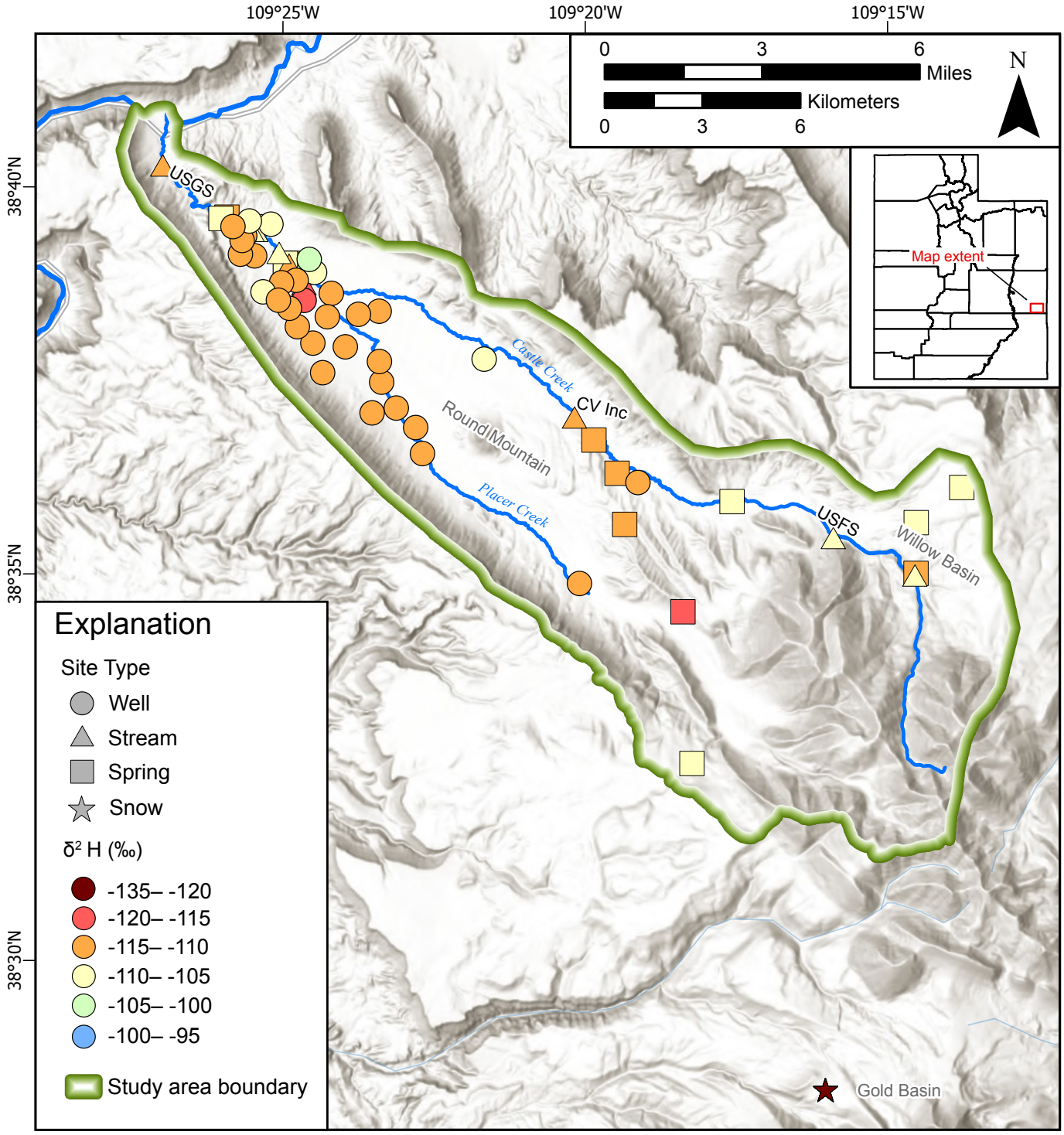

Figure 26. *Locations of stable isotope sampling sites classified by type shown by their deuterium (δ^2H) distributions in Castle Valley.*

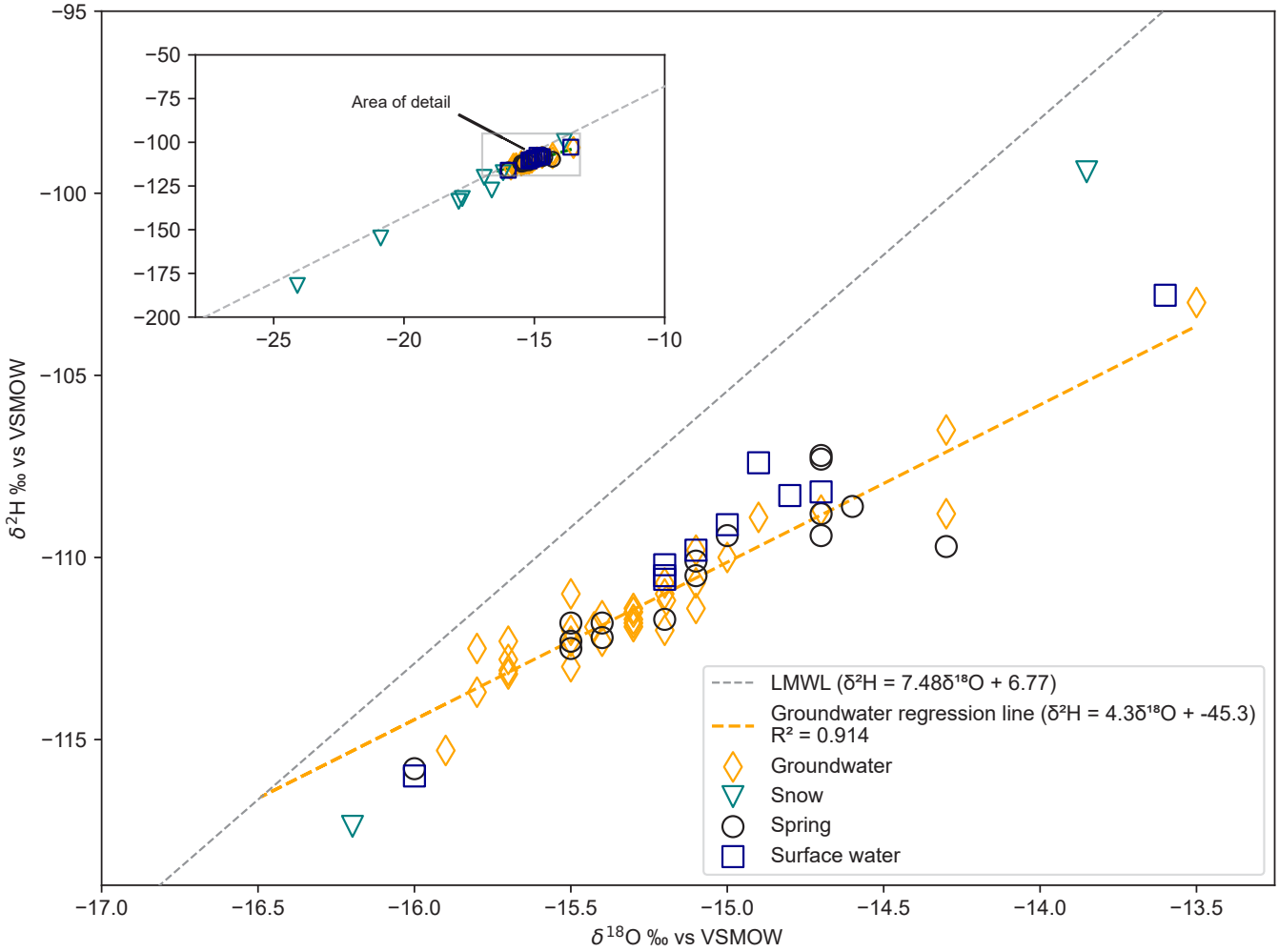

Figure 27. *Stable isotope ratios for groundwater, springs, surface water, and snow sampled in the Castle Valley region.*

ranged from 5.63 to 75.6 pmC, with a mean measurement uncertainty of 0.18 pmC. $\delta^{13}C$ ratios ranged from -9.49‰ to -1.02‰. Three of the samples have carbon-14 and $\delta^{13}C$ values consistent with modern recharge (Figure 29). The remaining sample (from site CV27) has carbon-14 and $\delta^{13}C$ values close to that of carbonate rocks, indicating significant post-recharge water-rock interaction. This sample, from a well completed in the Cutler Formation, likely has a longer residence time than valley-fill aquifer samples. However, the recharge age cannot be constrained by radiocarbon data.

Isotopes of Sulfate

We collected samples for sulfate isotope analysis from 13 wells, 6 springs, and 1 stream location (Figure 30, Table 7). Values for $\delta^{34}S$ ranged from -14.699 to 13.853‰ and $\delta^{18}O_{SO4}$ values ranged from -1.204 to 11.854‰ (Figure 31). Two spring samples sourced from the Jurassic Morrison Formation on the southeast margin of the study area have $\delta^{34}S$ and $\delta^{18}O_{SO4}$ values consistent with the established field of sulfide oxidation (Krouse and Mayer, 1999) (Figures 30 and 31a). Values of $\delta^{34}S$ and $\delta^{18}O_{SO4}$ from wells and the remaining spring samples in Castle Valley plot along a linear mixing trend between the established fields of soil sulfate and evaporites. Data from brine pumping wells in Paradox Valley to the southeast are included for comparison (Kim et al., 2022) (Figure 31a). The $\delta^{34}S$ and $\delta^{18}O_{SO4}$ value of Castle Creek above the Colorado River confluence also plots in the established fields of evaporites (Figure 31a). Groundwater sulfate concentrations in Castle Valley and Paradox Valley brines plot along an exponential mixing trend between soil sulfate and evaporite $\delta^{34}S$ signatures, although the highest Castle Valley sulfate concentration (15.2 mmol/L) is still a factor of 4 to 5 lower than Paradox Valley brine concentrations (Figure 31b).

WATER BUDGET

Water Budget Methods

Water Budget Development

We used the USGS Soil-Water-Balance (SWB) model (Westenbroek et al., 2018) to simulate the watershed for water years 2005 to 2022 (October 1 to September 30) and

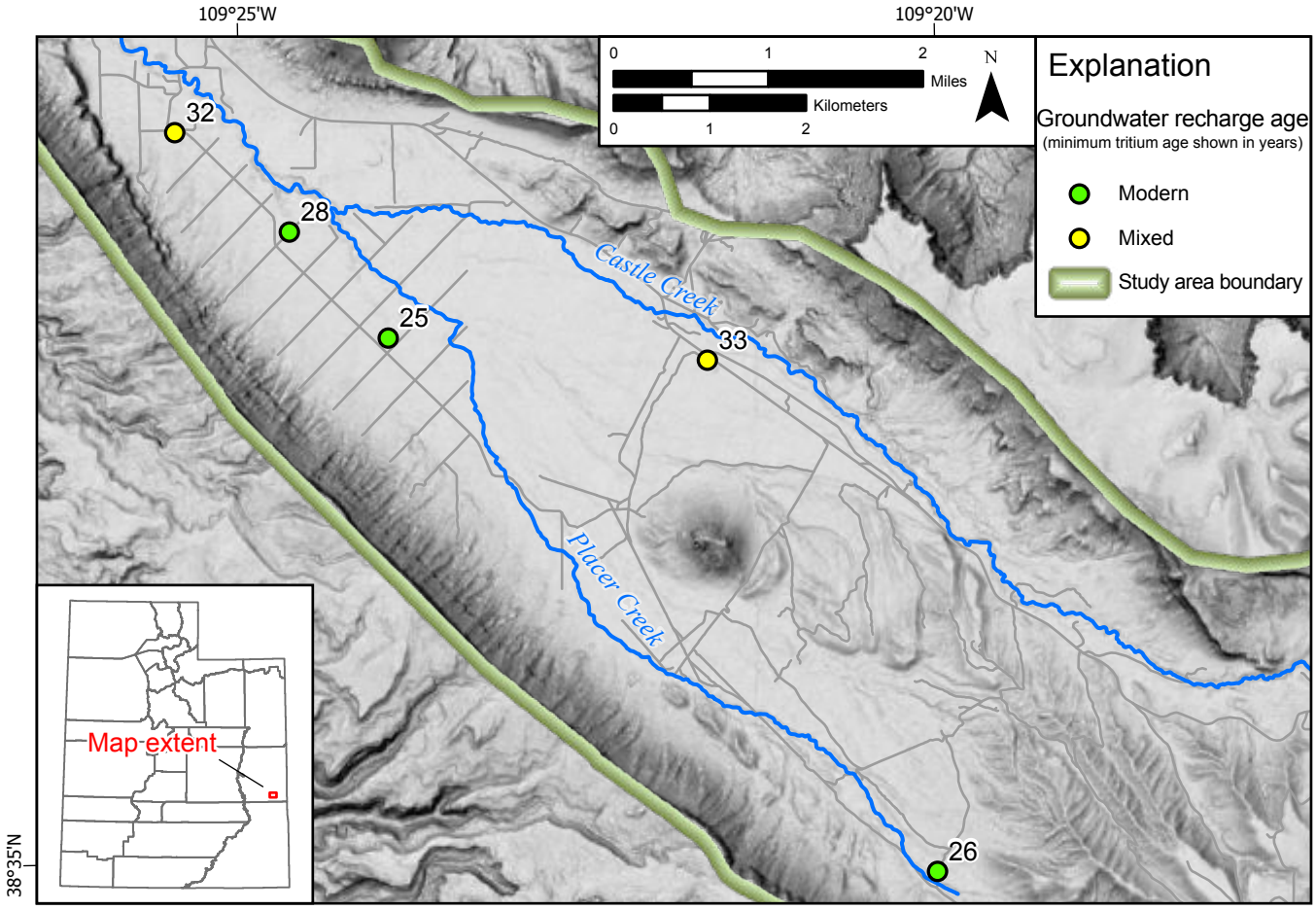

Figure 28. *Groundwater recharge age based on tritium and radiocarbon data.*

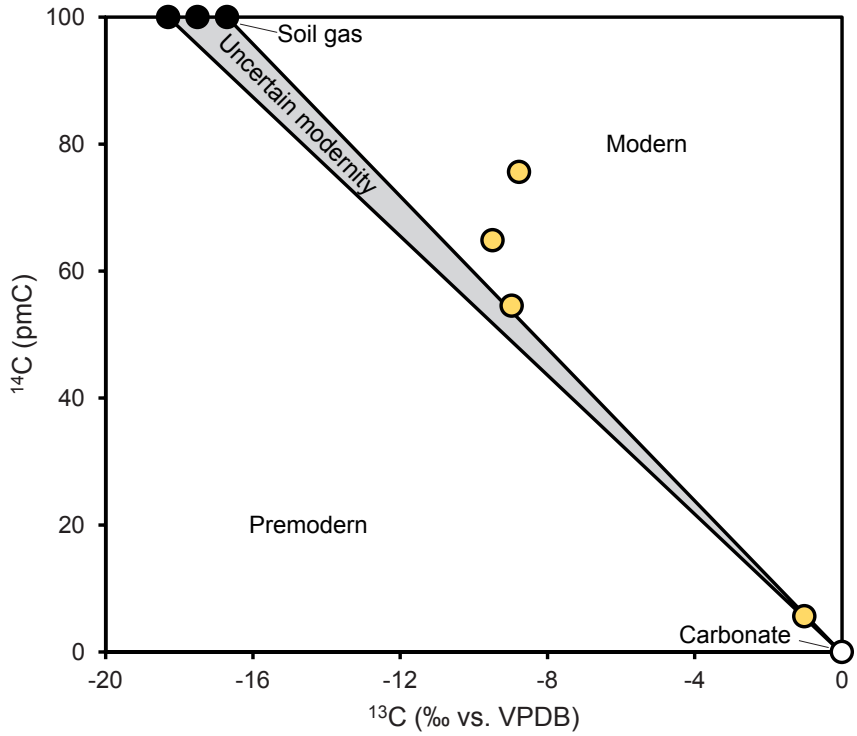

Figure 29. *Carbon isotopes in groundwater samples and mixing lines between soil gas and subsurface carbonate end members.*

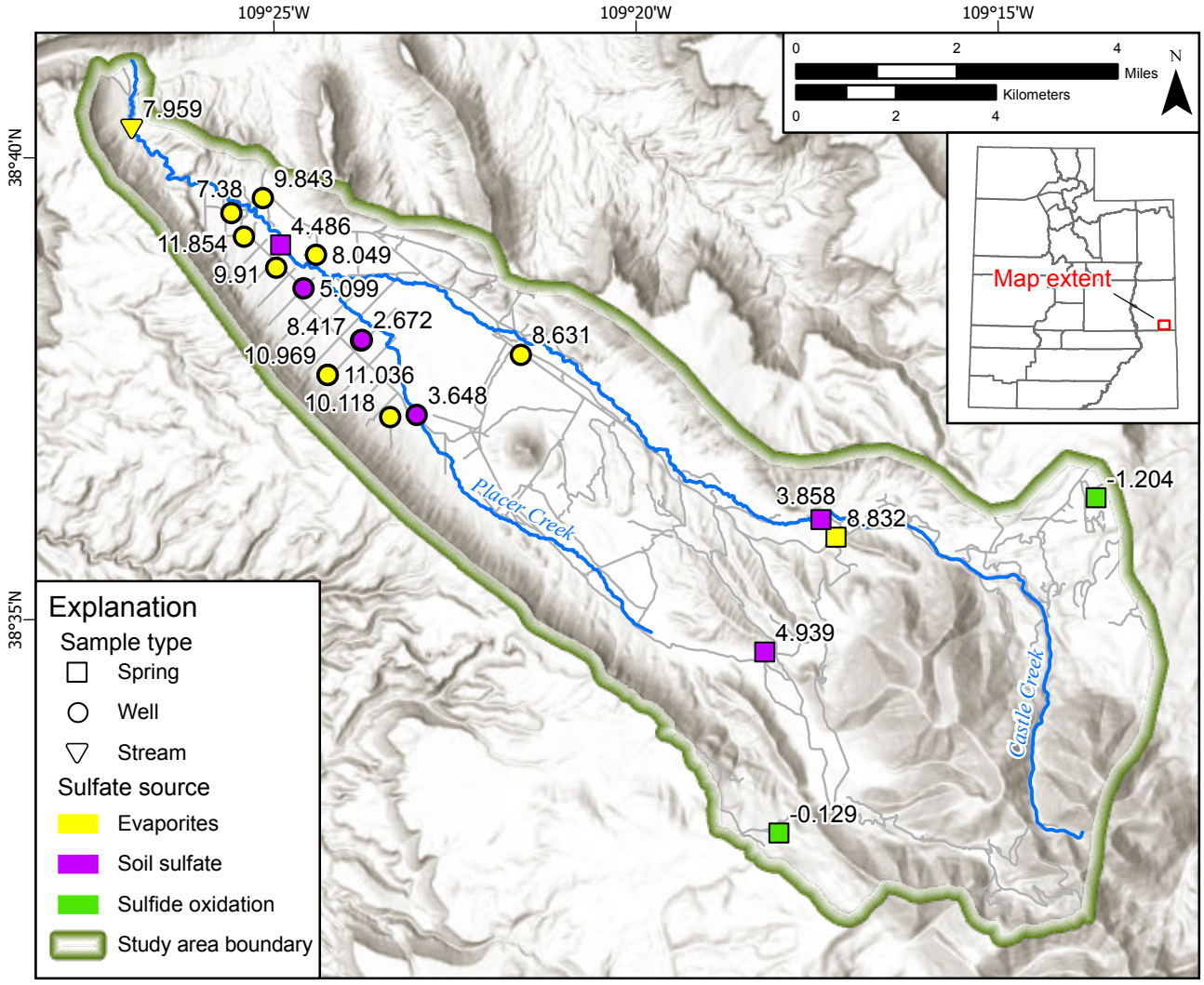

Figure 30. *Sulfur and oxygen isotopes of SO_4 sample locations. Samples are colored by primary sulfate source and labeled with $\delta^{34}S$ ‰.*

Table 7. *Isotopes of sulfate and sulfate concentration results.*

Site Name	Site Type	$\delta^{34}S$ (‰)	$\delta^{18}O$ (‰)	SO_4 (mg/L)	SO_4 (mmol/L)
CV5	Spring	7.6100	4.486	66.0	0.69
CV15	Spring	9.7850	8.832	--	--
CV43	Spring	-14.6990	-1.204	--	--
CV53	Spring	-9.9300	-0.129	--	--
CV54	Spring	6.7500	4.939	--	--
CV300	Spring	2.8720	3.858	--	--
CV17	Stream	10.7230	7.959	--	--
CV1	Well	9.9110	8.631	209.0	2.18
CV7	Well	9.7950	7.38	187.0	1.95
CV8	Well	10.9150	8.049	532.0	5.54
CV9	Well	7.9470	5.099	60.2	0.63
CV11	Well	6.0840	3.648	47.0	0.49
CV19	Well	12.8720	10.118	736.0	7.66
CV23	Well	12.4350	11.036	1460.0	15.20
CV25	Well	5.5620	2.672	--	--
CV26	Well	10.1080	8.417	215.0	2.24
CV27	Well	13.8530	11.854	1450.0	15.09
CV31	Well	12.9010	10.969	1290.0	13.43
CV35	Well	12.4840	9.91	501.0	5.22
CV38	Well	11.7160	9.843	1090.0	11.35

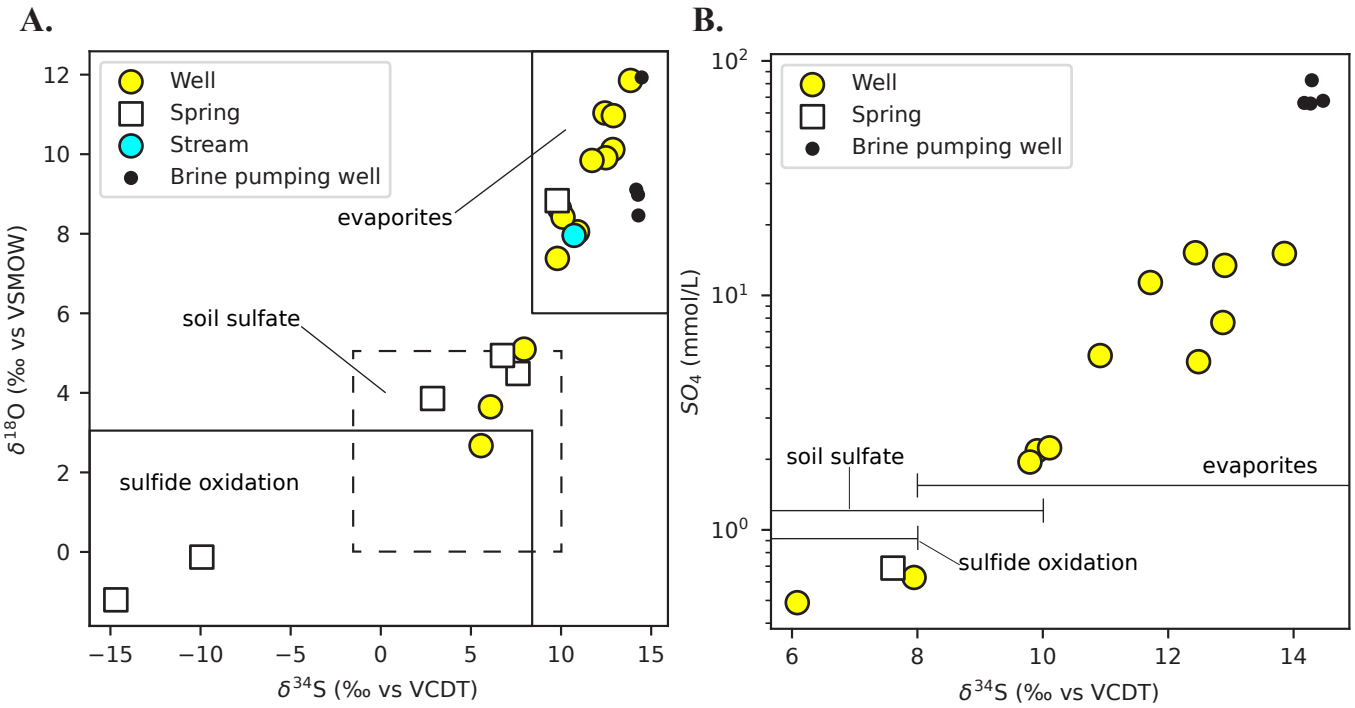

Figure 31. A) *Sulfur and oxygen isotopes of SO_4 and* ***B)*** *sulfur isotopes of SO_4 versus SO_4 concentrations of Castle Valley waters to distinguish SO_4 sources. Brine pumping well and oil and gas well data from Kim et al. (2022).*

quantify annual inflow and outflow. The results were then used to estimate and verify results used in our water budget for 2024. Alongside the SWB, historical and current USGS streamflow data were used in addition to streamflow and water-level measurements by UGS staff. The principal SWB inputs are Daymet V4 (Thornton et al., 2021) precipitation, air temperature, soil, and elevation data, while the main outputs are ET and Castle Creek streamflow. We compared SWB model results to the well-established climate datasets of PRISM (Parameter-elevation Regressions on Independent Slopes Model; Daly et al., 2008, 2015) and OpenET (Melton et al., 2021). The discussion below details methods of how we measured or estimated all water budget inputs and outputs.

Soil-Water-Balance Model

The SWB model calculates how water from precipitation moves through the landscape and potentially reaches aquifers. This modified Thornthwaite-Mather (Thornthwaite, 1948; Mather, 1978, 1979) approach tracks water movement on a daily basis, providing detailed estimates of net infiltration that closely approximate actual groundwater recharge rates.

The model requires several types of spatial data prepared in Albers Equal Area projection (EPSG:5070) and converted to ASCII raster format. To ensure complete coverage of water movement patterns, we extended the analysis area 2 kilometers (1.2 mi) beyond the primary study boundaries. The input precipitation datasets are derived from Daymet climate information (Thornton et al., 2021), elevation data for tracking water flow paths, detailed soil characteristics (SSURGO), and land cover and land use patterns (Dewitz and U.S. Geological Survey, 2021).

For soil properties, we drew from the USDA's comprehensive SSURGO database (Natural Resources Conservation Service, 2022), specifically incorporating two critical layers: the Soil Hydrologic Group classification and Available Water Storage measurements extending to 150 centimeters (59 in) deep. These soil characteristics help determine whether rainfall tends to soak into the ground or flow across the surface. The Available Water Storage metric reveals how much water the soil can hold in a form accessible to plants, whereas the hydrologic groupings reflect fundamental soil properties that influence water movement. We connected these soil attributes to specific curve numbers, following the Natural Resources Conservation Service rainfall-runoff methodology (U.S. Department of Agriculture, 1986). The curve numbers were adjusted based on local soil conditions and land cover types in Castle Valley. These adjustments considered the specific soil textures identified in the SSURGO database and were validated against observed runoff events during 2005 through 2022. For our curve number values, we referenced Tillman's (2015) work in the Upper Colorado River basin, which includes our study area.

To account for water loss through evaporation and plant uptake, we implemented the Hargreaves-Samani (1985) method in the SWB. This approach generates spatially-detailed estimates of potential ET using daily maximum and minimum temperature data obtained from Daymet's climate database.

The model also incorporates 2021 National Land Cover Database information from the Multi-Resolution Land

Characteristics Consortium, which provides essential details about surface characteristics that influence water movement. Both the land cover and soil data are connected to lookup tables that the model uses to determine the balance between surface runoff and ground infiltration.

To track how water moves across the landscape, we utilized 30-meter elevation data from the Utah Geospatial Resource Center, originally produced by the USGS 3DEP program. We processed this elevation data by first filling major depressions, then applying an eight-direction flow analysis to map potential water movement pathways across the terrain.

Evapotranspiration

To estimate evapotranspiration, we divided the study area into six distinct regions based on their unique geological, geomorphic, and topographic characteristics. These regions include three valley-fill areas: Placer Creek, Castle Creek, and the lower valley, along with areas dominated by sedimentary and intrusive bedrock units (Figure 32). This division allowed us to conduct detailed remote analysis while accounting for the diverse landscape features that influence water movement patterns.

To estimate ET for the entire watershed and its subregions we employed the Open-ET SSEBop model (Operational Simplified Surface Energy Balance Model) developed by Senay et al. (2013, 2017). This approach combines data from Landsat satellites with Daymet climate information to calculate how water moves from the ground into the atmosphere. For our reference ET calculations, we incorporated data from the University of Idaho's Gridded Surface Meteorological Dataset (gridMET; Abatzoglou, 2011). This comprehensive modeling approach enabled us to quantify ET across the entire basin.

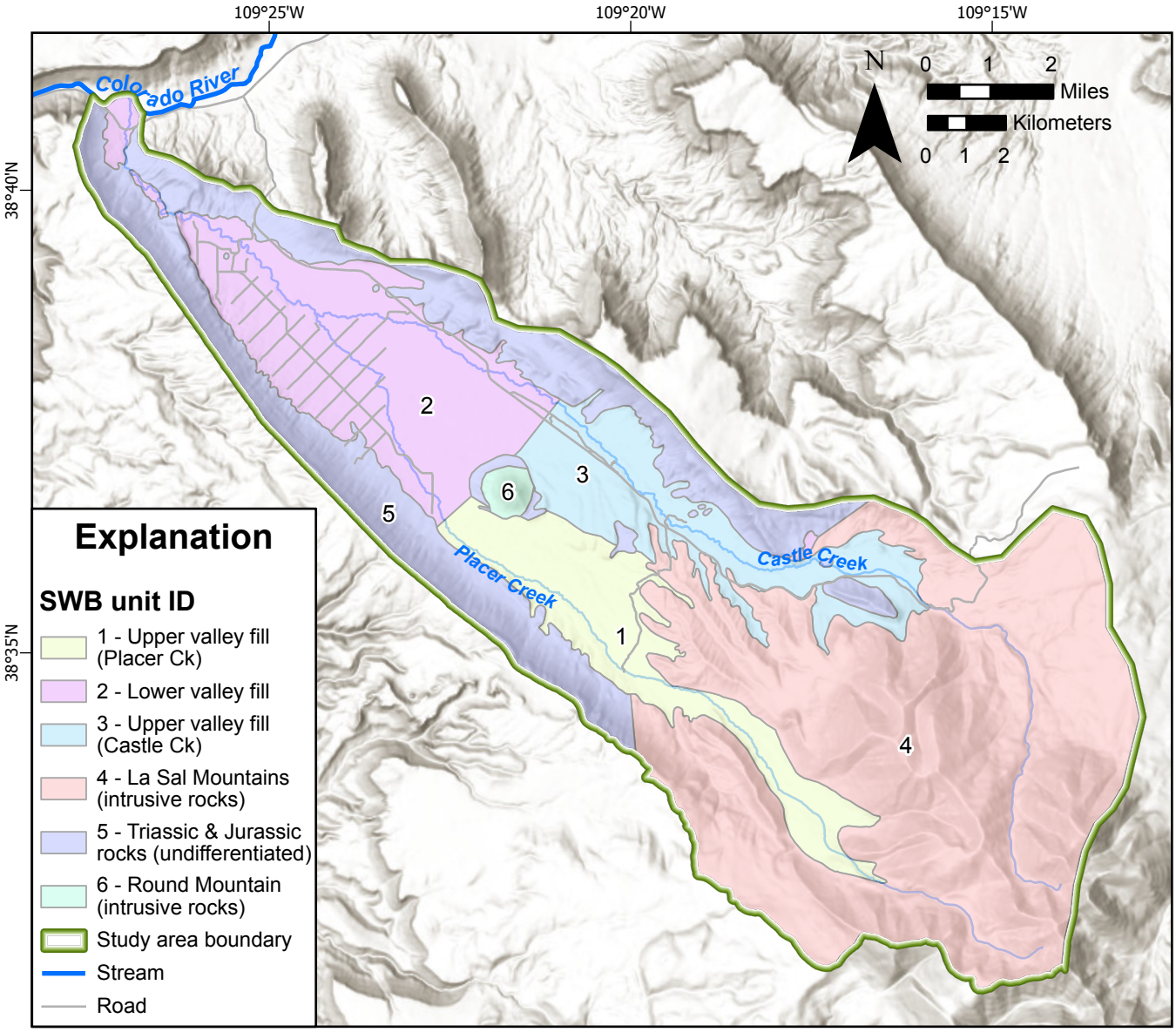

Figure 32. *Regions created for SWB modeling based on geologic units from Doelling (2002) and topographic and hydrogeologic boundaries.*

The OpenET gridMET ensemble combines rainfall data from a network of weather stations with measurements of how temperature changes with elevation to model precipitation patterns across the landscape. The model then uses information about the types of plants present, their seasonal growth patterns, and how densely they cover the ground to calculate water loss through ET across different parts of the study area.

The OpenET Intercomparison Summary (Huntington et al., 2022) shows that the SSEBop model performs relatively well in arid and semi-arid regions like Castle Valley. SSEBop estimates compare favorably to eddy covariance flux stations in the Upper Colorado River Basin (UCRB), We compared the ET estimate of the SSEBop model to an eddy covariance flux station in Vernal, Utah, the closest representative station to Castle Valley.

The comparison showed that the SSEBop had a slope of 1.08 with Root Mean Squared Error (RMSE) values of 0.72 inches per month. The R-squared value was 0.92, indicating good skill in predicting ET variability, and the bias metrics indicated SSEBop results were within 8% of in-situ closed energy balance ET estimates.

Huntington et al. (2022) note that for 2020, the SSEBop model estimated higher ET values compared to other models in the ensemble for most Utah locations. Differences in cloud screening thresholds and reference ET used for time integration affected SSEBop results, with a higher scene average cloud cover threshold (70% in OpenET vs 40% in United States Bureau of Reclamation implementations) potentially causing some bias in surface temperature estimates in high elevation areas (Huntington et al., 2022). For Castle Valley specifically, which shares similar arid/semi-arid characteristics with other parts of the UCRB, SSEBop appears to be a reliable dataset for ET estimates, though users should be aware of its tendency to estimate slightly higher ET values compared to some other models in the OpenET ensemble.

Castle Creek is subject to yearly surface water distribution reporting by the Utah Division of Water Rights (Utah Division of Water Rights, 2025). We leveraged this reporting to determine total surface water diversions and combine that with the reported usage data for the two irrigation companies in Castle Valley. To better understand the relationship between applied irrigation water, irrigation seepage to the valley-fill aquifer, and consumptive use by plants, we utilized Google Earth Engine to run and analyze ET metrics. We performed an analysis of annual ET using the OpenET SSEBop model on irrigated areas from 2005 through the 2022 water year. These data were calculated using the Utah Division of Water Resources (2024) water-related land use (WRLU) layer, which consists of polygons of irrigated crop types and extents, phreatophyte coverage, wet or open water areas, dryland agriculture, and residential/industrial zones. The WRLU data used for this study is based on the latest 2023 field survey.

Streamflow

We validated streamflow estimates from the SWB model through multiple approaches that include measuring monthly flow along the main stem of Castle Creek from November 2023 to November 2024, analyzing historical data from USGS gage 09182400, and analyzing precipitation-runoff relationships derived from PRISM data and discharge measurements provided by the Grand County Watershed Coordinator (A. Hultquist, written communication, January 2024). Additionally, we conducted a year-long continuous streamflow monitoring campaign at three locations along Castle Creek (Figure 33), with quarterly measurements to capture seasonal variations in groundwater–surface-water interactions. The mean gain/loss values between monitoring points were calculated by averaging the differences between upstream and downstream measurements, while accounting for tributary inputs and diversions. The basin's streamflow ultimately drains into the Colorado River via Castle Creek.

Placer Creek is an ungaged ephemeral stream that typically flows during spring runoff and summer monsoonal storms. Due to the sporadic nature of the flow regime, Placer Creek's flow is not well constrained. Because of the ephemeral nature of Placer Creek we assume its flow to be a negligible portion of the total sum of streamflow and excluded its flow from our streamflow analysis.

We measured streamflow along Castle Creek to estimate seepage between surface water and groundwater systems. Seepage runs quantify streamflow gains or losses over a measured reach at specific points in time. We conducted measurements along Castle Creek at the USFS boundary, above the Castle Valley Inc. (CV Inc, formerly Daystar Academy) diversion, and at State Route 128 (near reinstalled USGS gage 09182400) (Figure 33). Using spring and fall seepage run data, we estimated seasonal patterns of groundwater exchange throughout the year.

To assess baseflow conditions in Castle Creek we looked at daily mean flow during the month of January. The month of January is used as representative of baseflow conditions due to (1) the lack of uptake of water by vegetation, (2) lower evaporation rates, and (3) low mean daily temperatures causing precipitation to be retained as snowfall near the headwaters of the watershed rather than contributing to stream flow (Wolf et al., 2022). These factors contribute as evidence that any streamflow measured during this period represents antecedent groundwater storage, and can be analyzed to determine storage changes over time.

USGS Data

We conducted fieldwork from fall 2023 through fall 2024 and no active USGS gage operated within the study area during this time. In October 2024, USGS personnel reinstalled gage

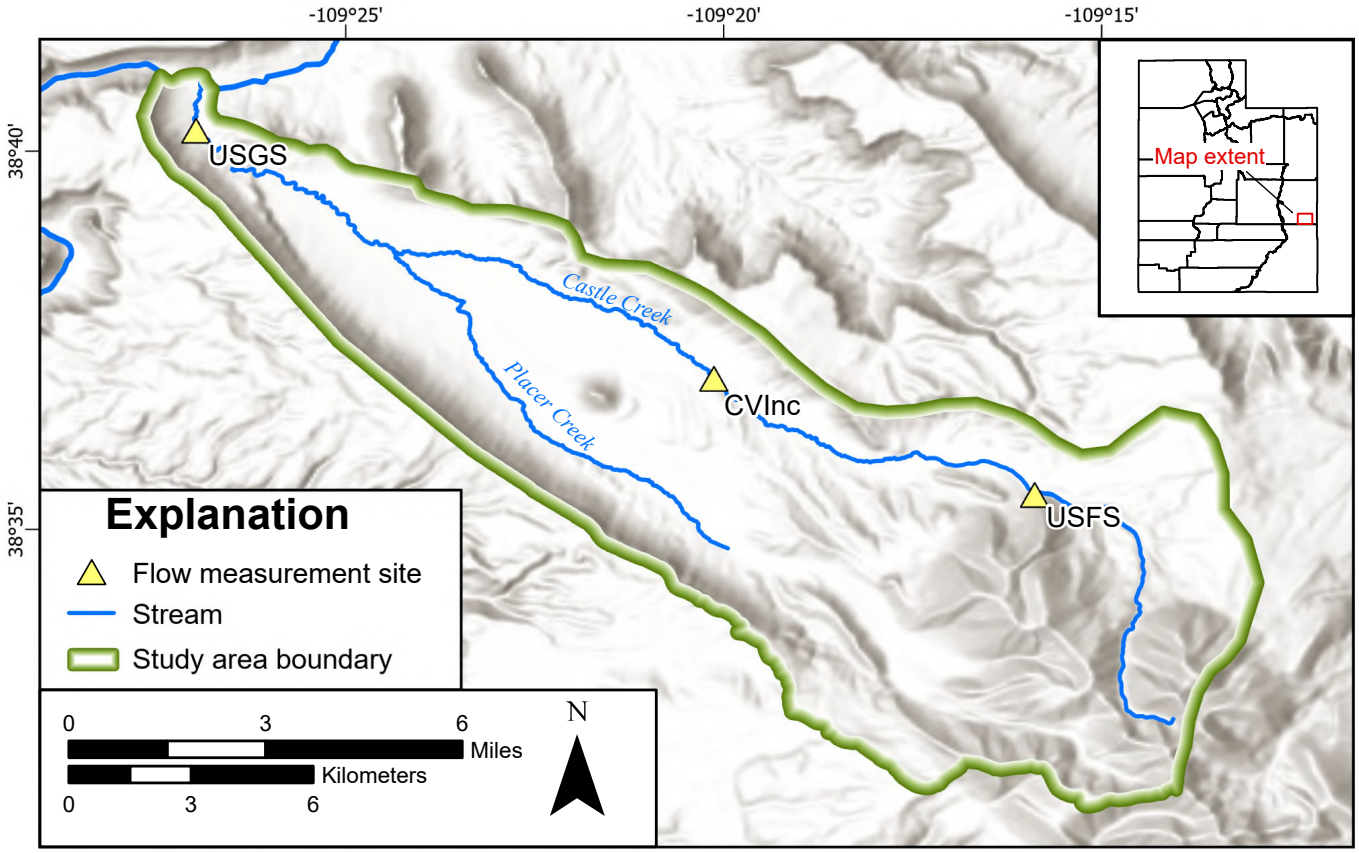

Figure 33. *Flow monitoring locations along Castle Creek at the U.S. Forest Service boundary (USFS), Castle Valley Inc. diversion (CVInc), and USGS gage 09182400 (USGS).*

09182400 on Castle Creek near State Route 128. This gage recorded data from April 1992 to October 2016. We used historical data from this gage to compare with newly measured data at that exact location, allowing us to statistically analyze both observed and modeled streamflow.

Wells

Castle Valley has a population of approximately 347, with most homes supplied by individual wells. Discharge estimates were based on totalizers installed on nine actively used wells (Ford and Grandy, 1997), which remained in place for two years. The recorded volumes showed that actual pumping was less than the amounts permitted by the associated water rights. Based on these findings, the Town estimated that users typically pump about 50% of their allocated water right. To account for variability, a 10% safety buffer was applied, resulting in an estimated use of 60% of the water right per well.

Subsurface Groundwater Outflow

We calculated the flow of groundwater exiting the study area into the Colorado River using the Darcy flux equation. We established a cross sectional area at the midpoint between the Colorado River's southern edge mean elevation and our northernmost groundwater monitoring well. The Moenkopi Formation is exposed across the width of the watershed north of the Town of Castle Valley (Figure 32). The cross section incorporated the Moenkopi Formation's measured thickness of 1400 feet (Doelling, 2002) for the region where no valley fill is present. For hydraulic conductivity (K), we applied the range of geometric mean values from 0.0023 ft/day to 0.016 ft/day as published by Belcher et al. (2001) for the Moenkopi.

$$Q = -KA\frac{dh}{dx} \quad (6)$$

Where:

Q = total discharge rate (ft^3/day),
K = hydraulic conductivity (ft/day),
A = cross sectional area (ft^2),
$\frac{dh}{dx}$ = hydraulic gradient (dimensionless).

Septic-Tank Drainfield Seepage

We estimated the volume of groundwater recharge from septic-tank drainfield leachate by multiplying the Castle Valley town population of 347 by the estimated per capita indoor usage of 60 gallons (227 L) per day (Utah Division of Water Resources, 2010). We obtained the number of septic-tank

systems from data provided by the Southeastern Health Department and Grand County (Jonathan Dutrow, Southeastern Utah Health Department, written communication, December 2024). Many homes in Castle Valley are utilized as vacation or secondary residences. Currently, about 313 households utilize septic-tank systems for primary wastewater disposal in the valley. We used septic-tank location information from Lowe et al. (2004) and the Town of Castle Valley lot map to identify structures served by these systems.

Error Analysis and Uncertainty

Uncertainty estimates were assigned to each component of the Castle Valley groundwater budget to reflect variability in data sources and modeling approaches. Streamflow measurements, used to estimate stream gain and stream loss, were assigned a ±10% uncertainty based on published accuracy ranges for USGS stream gaging (Rantz et al., 1982). Irrigation return flow uncertainty (±20%) accounts for compounding errors from both streamflow measurements and ET estimates. The latter was derived from remote sensing products, with phreatophytic ET assigned a ±17% uncertainty based on Anderson et al. (2023), who found mean absolute error values of ~17% for cropland across western U.S. eddy covariance sites. Infiltration from precipitation derived from the SWB model was assigned a ±20% uncertainty, consistent with values reported in SWB-based regional modeling applications (Niswonger and Prudic, 2023). Water well pumping uncertainty (±15%) accounts for variability in reported and unmetered usage, particularly for self-supplied systems, and aligns with typical estimates for municipal and rural withdrawals (U.S. Geological Survey, 2021). Septic effluent was assigned a ±10% uncertainty based on standardized per capita wastewater generation rates and household density (U.S. Environmental Protection Agency, 2002). Flow from bedrock was treated as a residual term and assigned a higher uncertainty of ±30%, reflecting its derivation as the difference between measured and modeled components and the absence of direct observation (Pope and Burbey, 2019). Finally, seepage to the Colorado River was assigned the highest uncertainty (±50%) due to its small magnitude and the use of Darcy's Law with estimated values for hydraulic conductivity and gradient (Healy, 2007). These uncertainty estimates were used to support error propagation and provide confidence intervals for the overall water budget.

Groundwater Inflow

A major unknown contributor to Castle Valley's water budget is the inflow of groundwater from upland bedrock aquifers, including Oligocene-age igneous intrusive rocks of the La Sal Mountains and Triassic/Jurassic-age sedimentary rocks. To calculate bedrock inflow we assumed no change in storage and used the residual volume remaining from the known inputs and outputs of the water budget calculations:

$$(Sg + ET + Qw + Cs) - (IF + Irr + Sl + Se) = Qbed \quad (5)$$

where:

- Sg = stream gain
- ET = evapotranspiration
- Qw = water well pumping
- Cs = seepage to the Colorado River
- IF = infiltration of precipitation
- Irr = infiltration of unconsumed irrigation water
- Sl = stream loss
- Se = septic effluent
- $Qbed$ = groundwater flow from bedrock

Water Budget Results

Precipitation

Between 2005 and 2022, the Castle Valley watershed received an average of 48,717 acre-feet per year of gross precipitation (Appendix B). Of this amount, approximately 2708 acre-feet (~6%) is estimated to infiltrate to groundwater. This relatively low infiltration rate reflects the semi-arid climate and geologic conditions of the watershed, where most precipitation is lost to ET or becomes surface runoff. Precipitation is unevenly distributed across the watershed. Approximately 58% of the mean annual total falls on SWB Unit 4, which encompasses the La Sal Mountains intrusive rocks (Figure 32). However, additional uncertainty of infiltration and recharge estimates in SWB Unit 4 is introduced due to variability in secondary porosity of fracture networks, fracture connectivity, and aperture with depth of these intrusives.

We compared precipitation patterns between the Daymet dataset (our SWB model input) and the PRISM dataset. The comparison showed strong agreement (R^2 correlation coefficient exceeded 0.84) in precipitation patterns, indicating that our input precipitation data sources are reliable and provide a solid foundation for the water budget calculations (Figure 34, Table 8).

Analysis of snow water equivalent (SWE) in the La Sal Mountains reveals a decreasing trend in SWE over the period of record at the Lasal Mountain SNOTEL site (station #572), located at an elevation of 9580 feet. The linear regression indicates a slope of -0.15 inches per year (Figure 35). The R^2 value of 0.091 suggests that only 9.1% of the variation in SWE is explained by the regression model, indicating that while the downward trend is evident, other climatic or hydrologic factors likely influence SWE variability. Despite the low R^2, the trend is statistically significant ($p < 0.05$), suggesting a persistent, though modest, decline in snowpack over time. These findings may point to regional shifts in precipitation patterns or temperature-driven changes affecting snow retention.

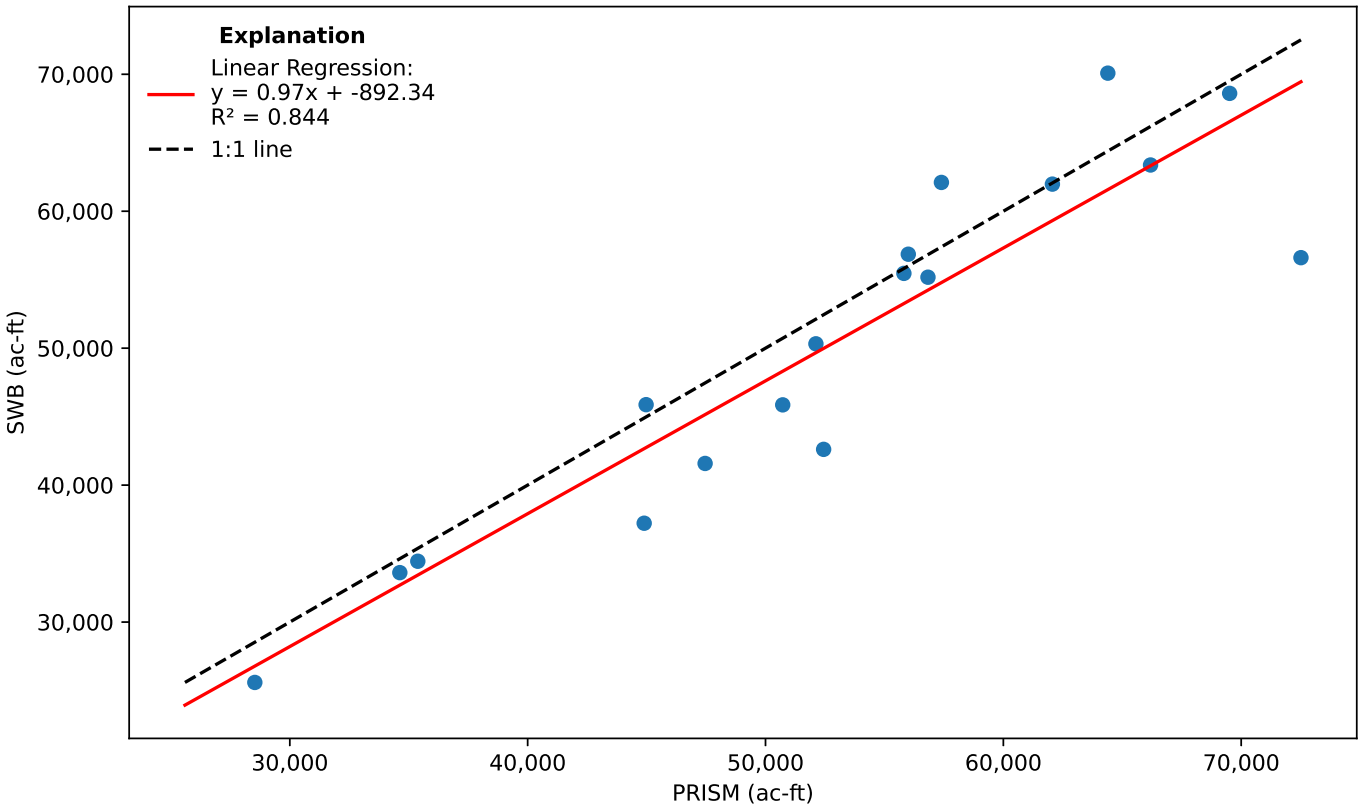

Figure 34. *Regression analysis comparing precipitation data of the SWB (Daymet) and PRISM models.*

Table 8. *Statistical comparison of PRISM and SWB precipitation data for water years 2005 through 2022.*

Statistic	PRISM (ac-ft)	SWB (ac-ft)
Mean	52,882	50,409
Standard Deviation	12,136	12,816
Minimum	28,529	25,591
Maximum	72,513	70,082
Correlation	0.92	
RMSE	5519.01	
Mean Absolute Error	3822.94	
R-squared	0.84	

Groundwater Inflow

Groundwater inflow from upland bedrock aquifers represents a significant component of Castle Valley's water budget, contributing an estimated 1235 acre-feet per year. This value was derived as a residual calculation, assuming a balanced groundwater budget with no net change in storage. The estimate accounts for measured inputs such as infiltration (2700 acre-feet), irrigation return flow (722 acre-feet), stream loss (0 acre-feet), and septic effluent (23 acre-feet), alongside outputs including stream gain (3788 acre-feet), phreatophyte evapotranspiration (147 acre-feet), water well pumping (741 acre-feet), and seepage to the Colorado River (5 acre-feet). Given the lack of direct measurement, this residual method highlights the importance of groundwater contributions from the La Sal Mountains intrusive rocks and underlying Triassic/Jurassic sedimentary formations, underscoring their role in sustaining the valley's aquifer system.

Streamflow

Peak streamflow measured during monsoonal precipitation was up to 42 cfs in July 2013. The lowest measured flow was 2.56 cfs in July 2006. These data show the highly variable flow regime of Castle Creek. Streamflow data from USGS gage 09182400 illustrates both seasonality and direct influence from major precipitation events (Figure 36). Mean annual streamflow was calculated based on daily mean values. Mean annual streamflow ranged from 4.4 cfs measured in 2014 to 8.8 cfs in 1993 (Table 9). The standard deviation of flows in Castle Creek averaged 1.8 cfs from 1993 through 2016.

January mean baseflow showed variability from 1993 through 1998. From 1999 through 2016 monthly mean baseflow fluctuations ranged from approximately 4.5 cfs to 7.8 cfs. The 2024 UGS estimate of annual mean streamflow for Castle Creek was 6.1 cfs (Figure 37).

Comparison with data from the Lasal Mountain SNOTEL site (station #572), located at La Sal Pass, indicated a weak relationship (Figure 38) between January baseflow and the prior water year's total SWE. This relationship may be

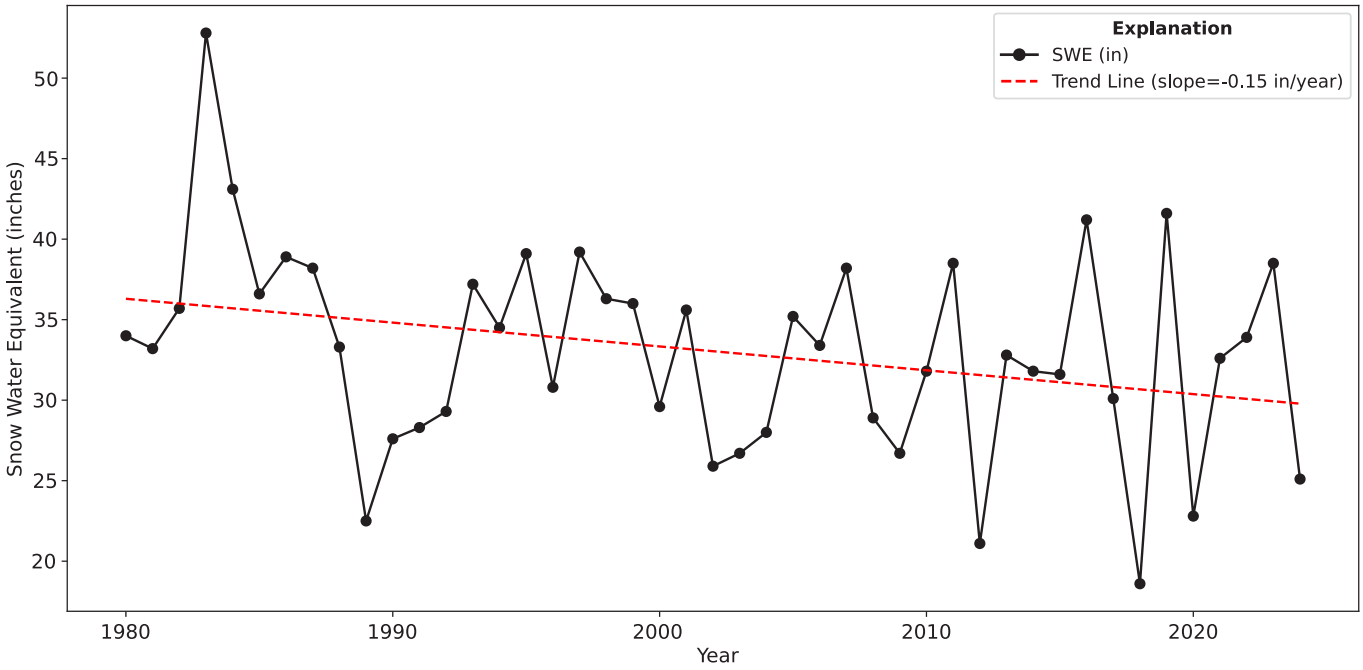

Figure 35. *Snow water equivalent (SWE) at the Lasal Mountain SNOTEL site #572 (9580 ft) for the period of record (1980–2024) with an observed decreasing trend of approximately 0.15 inches per year (dashed red line). SWE values are displayed as annual water year averages.*

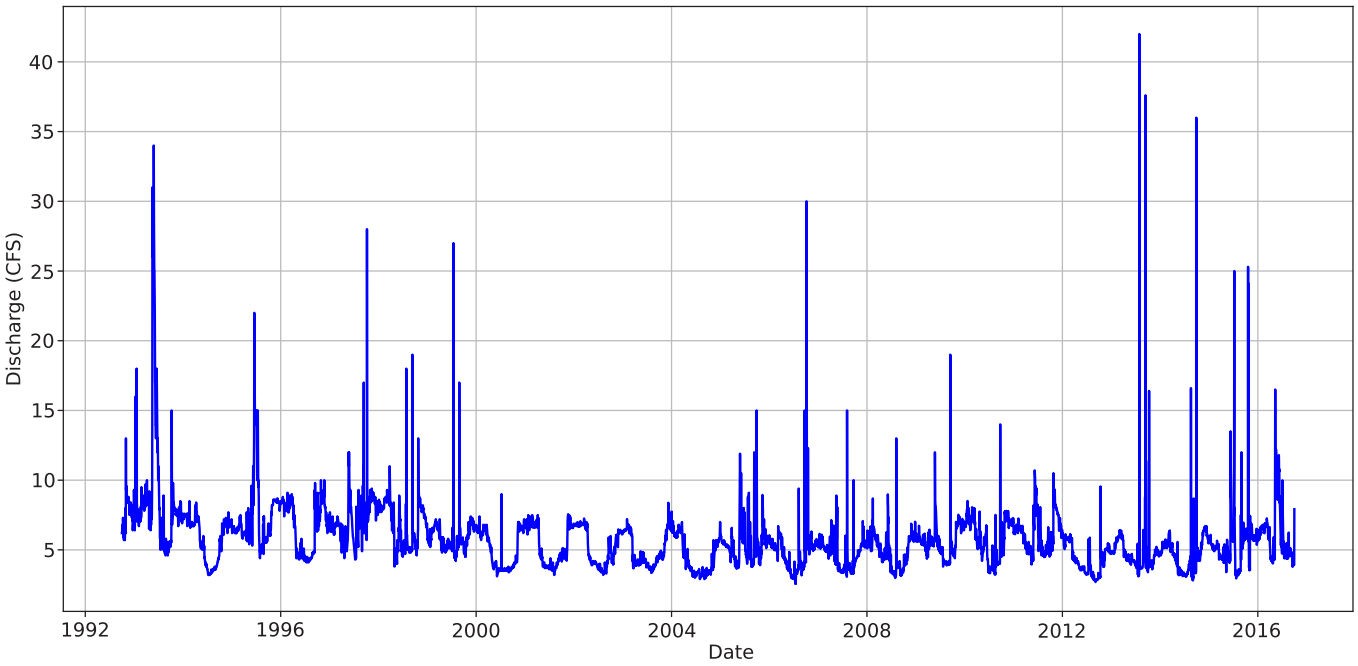

Figure 36. *USGS gage 09182400 daily data hydrograph from beginning (1993) to end (2016) of period of record.*

Table 9. *Annual water year flow statistics for USGS gage 09182400, Castle Creek.*

Year	Minimum (cfs)	Maximum (cfs)	Mean (cfs)	Standard deviation (cfs)
1993	4.6	34	8.8	4.8
1994	3.2	15	6.1	1.8
1995	4.4	22	7.1	2.5
1996	4.1	9.8	6.6	1.8
1997	4.3	17	6.9	1.4
1998	3.8	28	7.1	2.1
1999	4.2	27	6.1	1.7
2000	3.1	9	5.1	1.4
2001	3.2	7.5	5.2	1.4
2002	3.2	7.6	5.3	1.4
2003	3.4	7.2	4.9	1.1
2004	2.9	8.4	4.7	1.4
2005	3.2	15	5.2	1.5
2006	2.6	15	4.8	1.3
2007	3.1	30	5.1	2.1
2008	3	13	4.8	1.1
2009	3.6	19	5.3	1.2
2010	3.2	14	5.7	1.4
2011	4	10.7	6.1	1.2
2012	2.7	10.5	4.9	1.6
2013	3	42	4.9	2.8
2014	2.8	36	4.4	2.1
2015	3	25	5.2	1.7
2016	3.5	25.3	6.2	2.3

explained by the relatively limited area of the upper Castle Creek watershed. The highest peak in the watershed, Mount Waas, rises to 12,331 ft above sea level, but it is bounded by steep ridgelines that limit only a portion of its runoff to the north into Castle Valley. Precipitation falling onto the upper reaches of the watershed infiltrates into the fractured bedrock composed of igneous intrusive rocks, resulting in moderate transit times from mountain recharge to discharge into Castle Valley (Gardner et al., 2020).

The La Sal Mountain SNOTEL station (9580 ft) is located approximately 4.7 miles southwest of Mount Waas (12,331 ft) and may not accurately reflect the precipitation received at Mount Waas or within the headwaters of Castle Creek. Although the SNOTEL station provides reliable precipitation measurements, spatial variability introduces an unquantified degree of uncertainty. Additional factors such as soil moisture, net radiation, vegetation, and mean annual temperature also influence runoff availability, but these variables cannot be directly measured or reliably extrapolated to the Mount Waas catchment.

Mann-Kendall test results for Castle Creek indicate a statistically significant decreasing trend in annual average streamflow ($p = 0.0445$) from 1993 through 2024 (Figure 39). The average annual streamflow at USGS gage 09182400 measured by the USGS or UGS throughout that period declined at a rate of approximately 0.058 cfs per year, suggesting a consistent reduction in water availability over the period of record. Combining measured streamflow and our modeled streamflow, annual streamflow volume in Castle Creek shows a distinct decreasing trend of approximately 38 acre-feet per year over the same period. The early water years (1993–1999) consistently yielded higher volumes compared to subsequent years, with 1993 producing the maximum volume at over 6000 acre-feet (Figure 40). Since around 2000, annual volumes have generally remained below the geometric mean of 3849 acre-feet, with only occasional years approaching or exceeding this long-term average. The SWB model tends to agree well with USGS and UGS measurements, but does show an anomalously high volume of runoff in 2019. While precipitation for 2019 was above average we believe the runoff value to be over estimated. Our 2024 volumetric estimate of 3788 acre-feet falls just below this long-term average.

Septic-Tank Drainfield Seepage

We assumed that all indoor water use is discharged to septic tanks, and water is conserved in the septic tank and leach field.

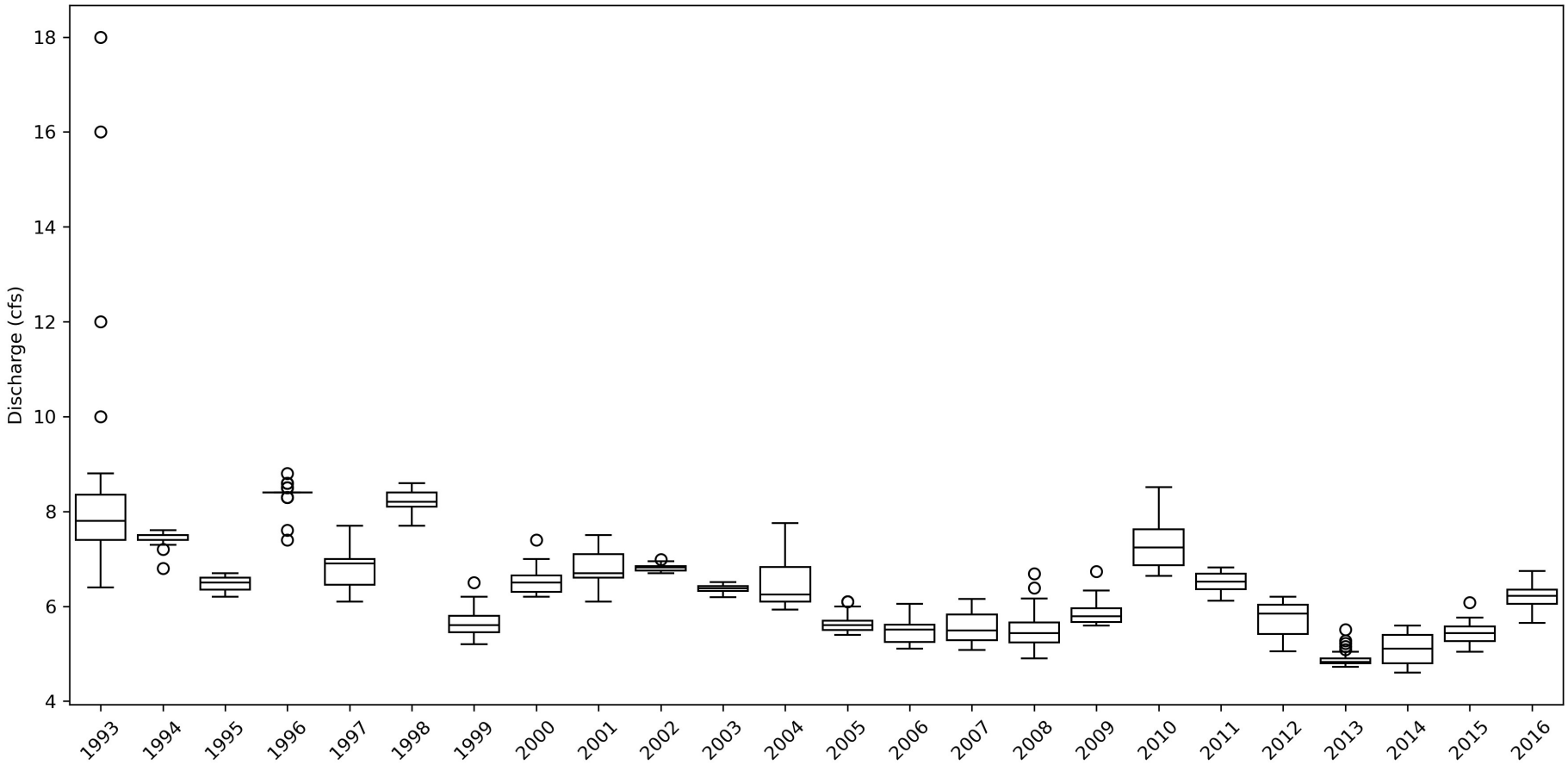

Figure 37. *Box plot showing January baseflow at USGS gage 09182400.*

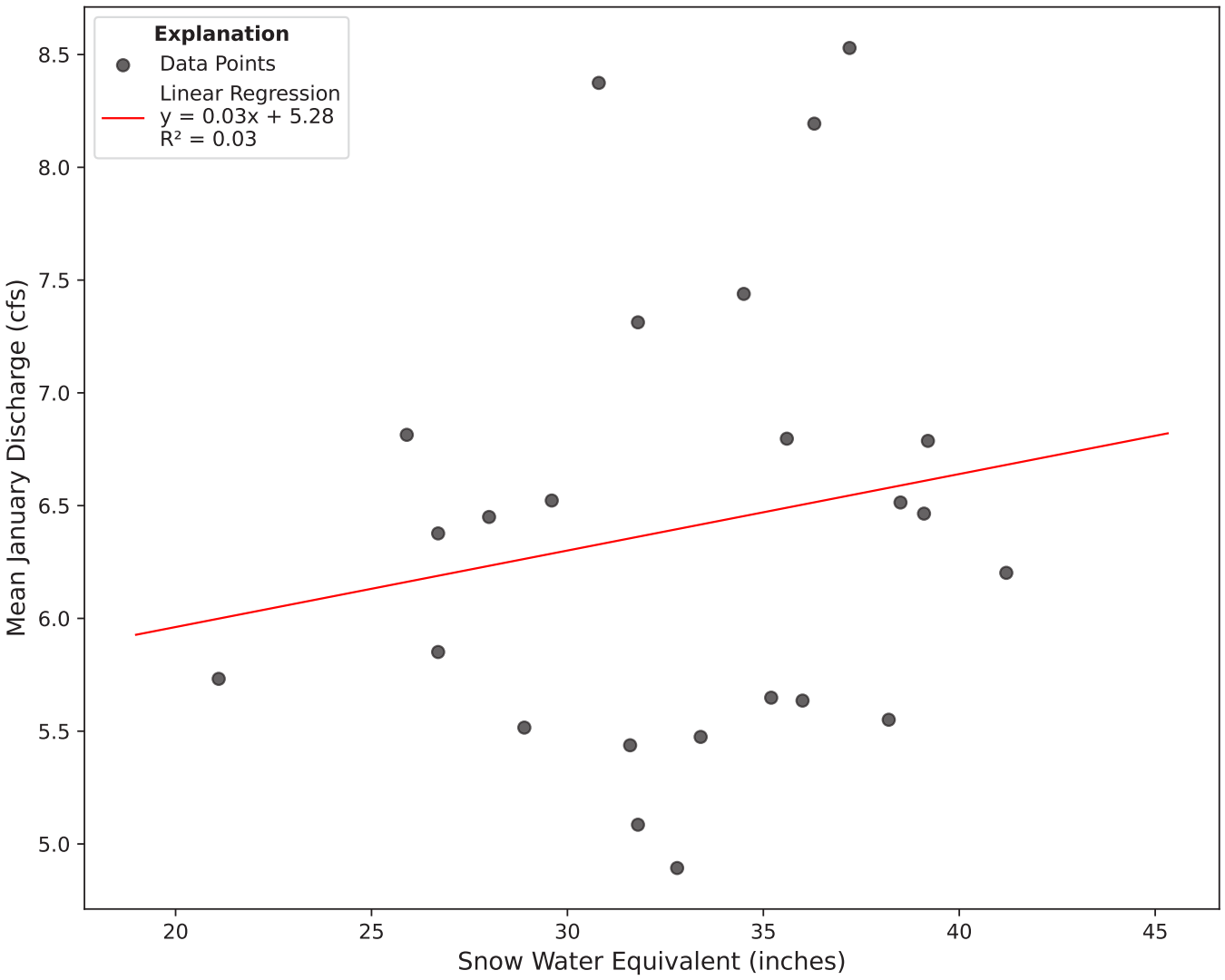

Figure 38. *Mean January baseflow of Castle Creek at USGS gage 09182400 compared to the prior year's total snow water equivalent at Lasal Mountain SNOTEL site (station #527) for water years 1993–2016.*

We calculated that about 0.032 cfs (23 acre-feet per year) is discharged from septic tanks into the valley-fill aquifer. We applied the current water use sum of 741 acre-feet per year. Assuming the estimated maximum well water diversion volume of 741 acre-feet (Ford and Grandy, 1997), septic effluent represents about 3.1% of the total volume of well water discharged.

Soil-Water-Balance Model

The SWB results provide us with modeled annual values of precip, ET, storage, and recharge and the spatial distribution of each. The hydrologic data for the watershed spanning water years 2005–2022 exhibits significant temporal variability in water balance components. Mean annual gross precipitation was 48,717 acre-feet (standard deviation of 12,129 acre-feet) (Table 10), with ET constituting the primary water loss pathway (mean of 43,927 acre-feet, standard deviation of 8982 acre-feet). Streamflow measurements from both the SWB model and USGS gage 09182400 demonstrate reasonable agreement during their overlapping period (2005–2016), with means of 3485 acre-feet and 3756 acre-feet, respectively. Nash-Sutcliffe efficiency coefficients, which indicate model performance and range from 1.0 (perfect agreement between predicted and observed values) to -∞ (negative values indicate observed mean is a better predictor than model), display marked year-to-year fluctuations, with values ranging from 1.00 to -1050.27. This range indicates substantial variation in model performance across different hydrological conditions. Storage flux calculations reveal significant annual variations, alternating between maximum accumulation of 7462 acre-feet in 2016, and a depletion of -3353 acre-feet in 2008. An unusually high streamflow year in 2019 (10,360 acre-feet) represents nearly three times the long-term average and may represent an anomalous model value. These data highlight the dynamic nature of watershed processes and the complex relationship between precipitation inputs, ET demands, and resulting streamflow and storage responses.

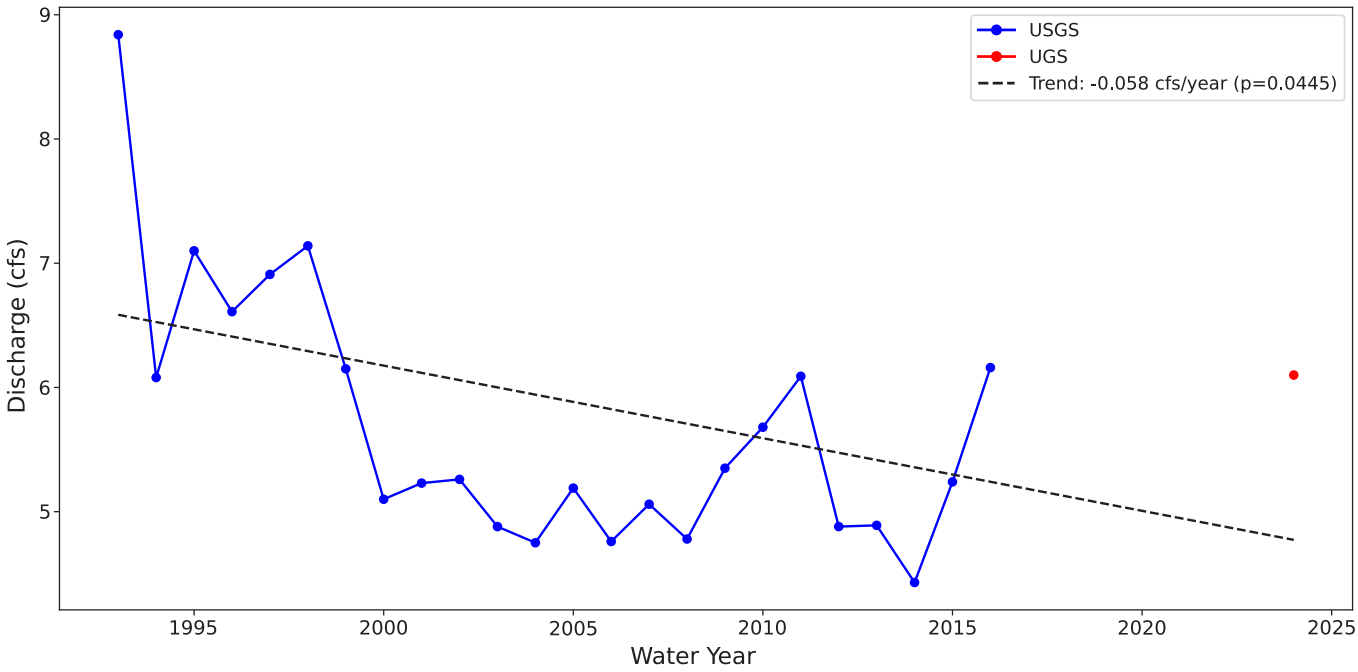

Figure 39. *Annual average streamflow in Castle Creek at USGS gage 09182400 from 1993–2016 water years showed a statistically significant decreasing trend of 0.058 cfs per year (p = 0.0445).*

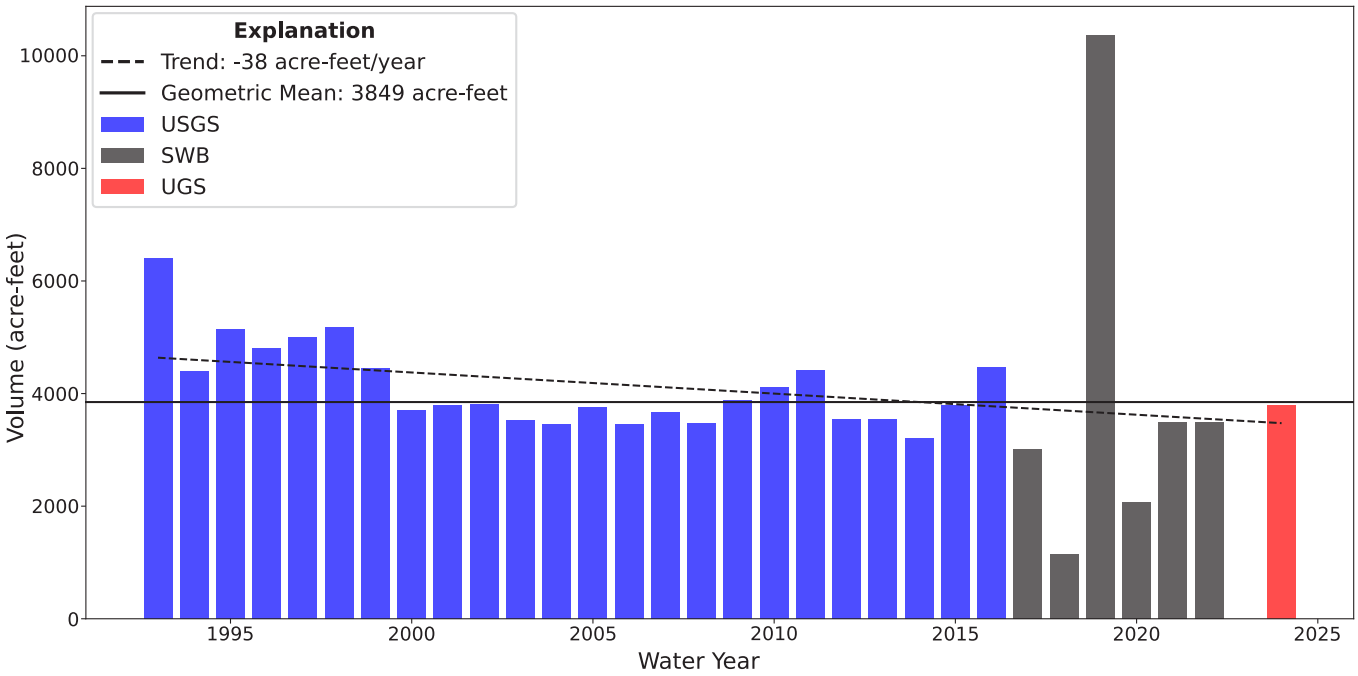

Figure 40. *Annual streamflow volume for Castle Creek from 1993 to 2024, showing measurements from the USGS, the SWB model, and the UGS with a declining trend of 38 acre-feet per year and geometric mean of 3849 acre-feet.*

Table 10. *Annual water balance components (2005–2022) showing precipitation, ET, streamflow measurements, Nash-Sutcliffe efficiency, and storage changes in acre-feet (ac-ft). Mean values and standard deviations are provided at bottom. Note that * denotes mean runoff value for the 2022 water year as runoff was not included in the SWB output for that year.*

Water year	Gross precipitation (acre-feet)	Evapotranspiration (acre-feet)	SWB streamflow (acre-feet)	USGS 09182400 streamflow (acre-feet)	Nash-Sutcliffe efficiency	Change in storage (acre-feet)
2005	56,609	51,825	3852	3761	-1.39	932
2006	42,611	39,067	2159	3449	-23.37	1384
2007	61,979	53,372	7054	3661	-884.61	1552
2008	41,582	41,453	3482	3470	1.00	-3353
2009	37,217	34,656	2290	3873	-1050.27	271
2010	55,461	46,684	7436	4113	-183.71	1342
2011	63,375	55,973	3564	4407	-1.44	3839
2012	33,610	32,514	1624	3543	-44.69	-528
2013	50,318	43,288	3678	3537	0.34	3352
2014	56,860	49,705	3328	3209	0.95	3828
2015	62,102	61,186	4247	3791	0.53	-3331
2016	70,082	55,314	7306	4473	-3.27	7462
2017	45,875	41,102	3017	-	-	1756
2018	25,591	27,661	1150	-	-	-3220
2019	68,606	52,267	10,360	-	-	5979
2020	34,441	32,684	2069	-	-	-312
2021	45,860	39,146	2896	-	-	3817
2022	55,182	50,785	*3485	-	-	912
Mean	**48,717**	**43,927**	**3485**	**3756**	**-**	**1981**
St. Dev.	**12,129**	**8982**	**2355**	**388**	**-**	**3045**

Evapotranspiration

We calculated ET using the OpenET SSEBop model and the SWB model. Mean ET for the entire Castle Valley study area is 43,927 acre-feet for the years between 2005 and 2022 (Table 10), representing approximately 90% of the precipitation input. This high ET ratio is characteristic of semi-arid environments (Volk et. al, 2024) where water loss to the atmosphere dominates the water budget.

A small but important portion of ET within the region is the area along riparian zones that support phreatophytes. For this study, we mapped the riparian region on the north end of the valley fill adjacent to Castle Creek and several springs issuing from the valley fill. Approximately 50 acres of riparian area was mapped using OpenET's data explorer tool. Using this tool to estimate ET from phreatophytes, we calculated a geometric mean volume of 147 acre-feet per year from 2019 through 2024, representing a direct groundwater discharge component through plant respiration. ET for the entire study area shows clear patterns based on elevation, ranging from 10 to 20 inches (25–51 cm) per year in the valley floor to 46 inches (117 cm) per year in the higher elevations of the La Sal Mountains to the southeast (Figure 41).

The spatial variation in ET rates of 6.5 to 43.7 inches (16.5–111 cm) per water year correlates strongly with elevation, aspect, and vegetation density. Higher ET rates are observed in the irrigated agricultural areas with alfalfa rotation and high elevation north-facing slopes due to greater quantities of available water, whereas lower ET rates occur in areas with sparse vegetation and at lower elevations with lower amounts of available water and different soil moisture conditions.

We also examined historical ET data within the water related land use (WRLU) polygons to determine changes over time. The cumulative change in irrigated crop ET ranges between -16 and 14.5 inches (-41–10 cm) of water from 2016 to 2022 (Figure 42). Lesser or negative values represent fallowing of what was once arable and irrigated land. Positive values can represent a field that has either been brought back into rotation or a plot whose irrigation system has been improved, leading to denser, more vibrant crops.

The mean ET for irrigated fields from 2005 to 2022 ranges between 6.5 and about 44 inches (17–112 cm) per year (Figure 43). This range of values illustrates the variability of irrigation techniques, crop water usage, and crop rotation. Fields may be watered throughout the entire irrigation season—March 15th

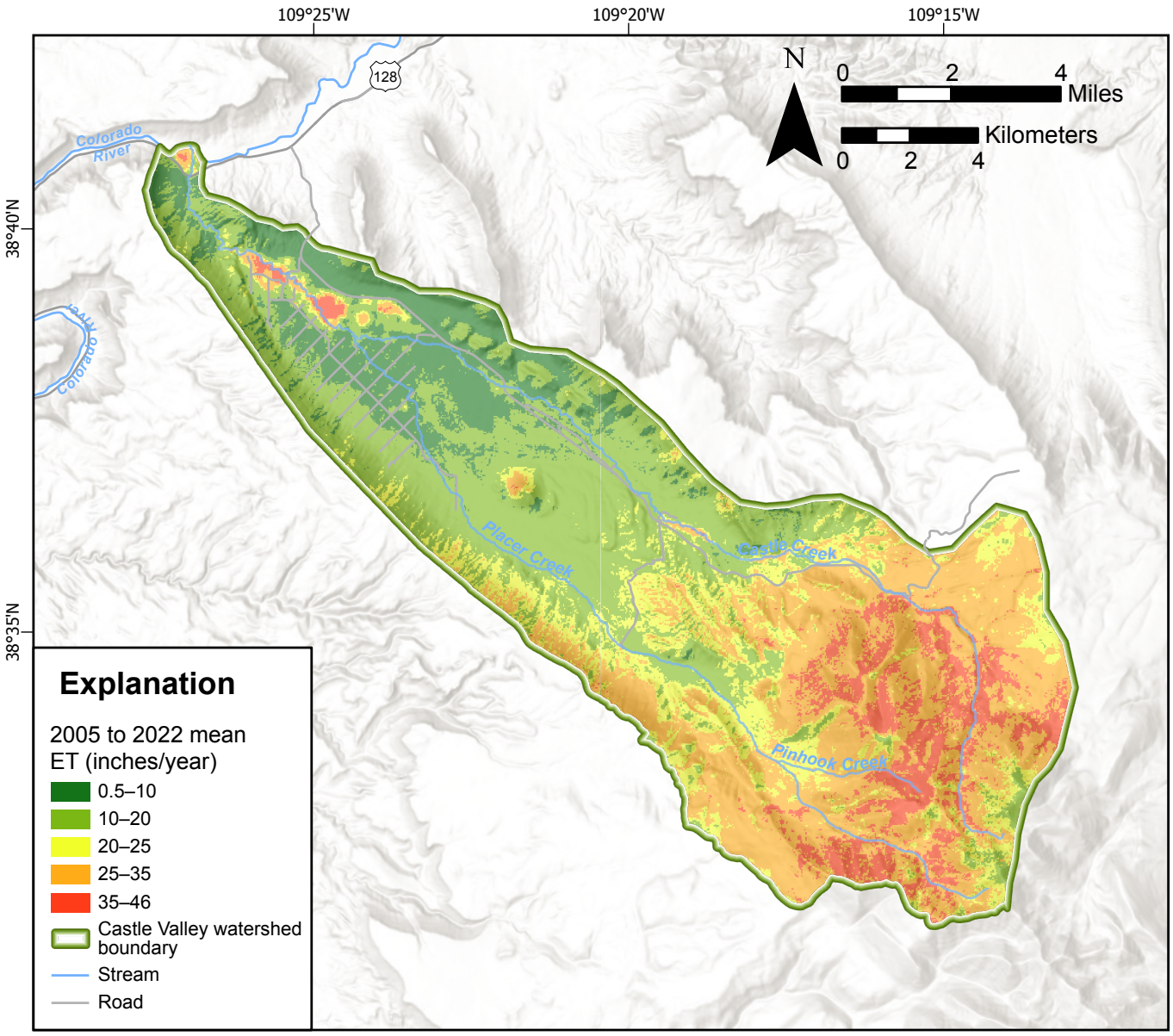

Figure 41. *Mean annual ET for the Castle Valley study area from 2005 through 2022.*

through November 15th—but durations may be shortened or extended based on growing season needs.

Irrigation Diversions and Efficiency

We analyzed irrigation system data reported by the Utah Division of Water Rights (2025) in Castle Valley between 2014 and 2024 to reveal variations in total surface water volumes diverted and system efficiency (Table 11). We then used this analysis to quantify potential groundwater recharge to the valley-fill aquifer through irrigation return flow. Total annual diversions demonstrate substantial fluctuation, ranging from 928 acre-feet in 2014 to 2481 acre-feet in 2023, with the two irrigation entities showing distinct usage patterns. Castle Valley Irrigation Company's diversions varied from 397 to 1565 acre-feet annually, while CV Inc. maintained slightly more consistent withdrawals, ranging from 531 to 1364 acre-feet per year. During the irrigation season this water is diverted from Castle Creek at the CV Inc. measurement site, and at times may constitute the entirety of the flow in Castle Creek.

ET values for irrigated land were tabulated from the OpenET SEEBop model and queried via WRLU map layer data, providing accurate estimates of crop water consumption and irrigation requirements.

The system's irrigation efficiency metrics, from 2016 through 2022, provide insights into operational effectiveness. Irrigation efficiency is calculated as the ratio of ET (consumptive use) to total water diverted, with higher percentages indicating more efficient water use. Peak efficiency was achieved in 2018 at 75%, corresponding with the lowest total diversions of 1095 acre-feet during the measured period. This relationship suggests optimal system performance under conditions

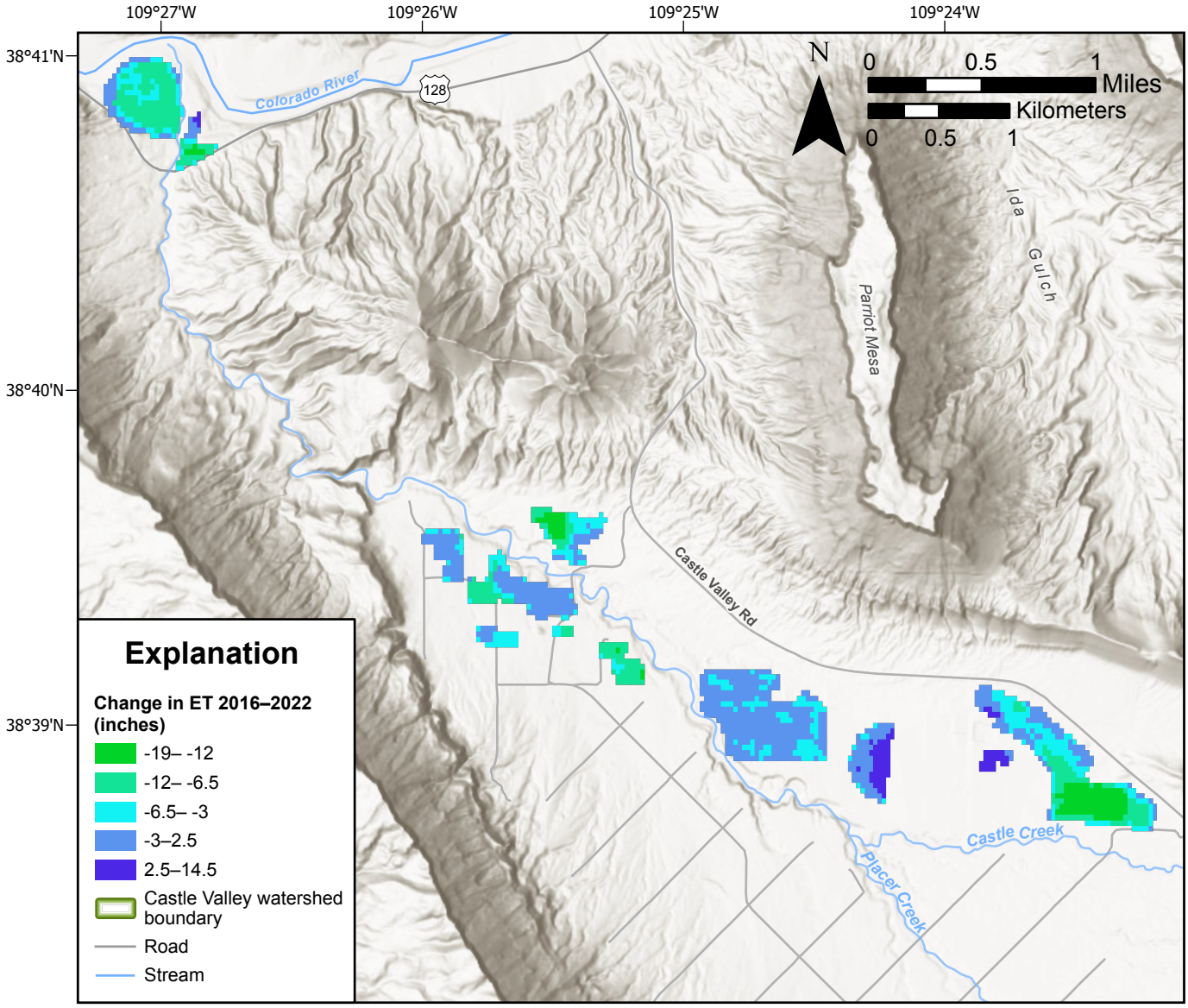

Figure 42. *Cumulative change in ET on irrigated land from 2016 through 2022 water years.*

of reduced water availability. In contrast, years with higher diversion volumes typically showed lower efficiency rates, as evidenced by the 39% efficiency recorded in 2016 when diversions reached 2224 acre-feet.

Unconsumed irrigation water that infiltrates into valley-fill sediments, representing aquifer recharge, similarly fluctuated from 273 acre-feet to 1351 acre-feet during this period. The geometric mean of return flow from unconsumed irrigation water is 722 acre-feet per year (2016 to 2022) (Table 11). This unconsumed irrigation water is a significant component of groundwater recharge in Castle Valley, particularly in low-efficiency years when more water percolates back to the aquifer. This relationship between irrigation efficiency and aquifer recharge represents an important water management consideration, as improvements in irrigation efficiency may reduce this beneficial recharge component.

Change in Storage

Data from the Castle Valley monitoring well network indicates relatively stable groundwater elevations from 2016 to 2024 (Table 2), despite the SWB model calculating an average annual change in storage of 1200 acre-feet for the same period (Table 10), ranging from -3353 acre-feet during the low-precipitation year of 2008 to 7462 acre-feet during the high snowfall year of 2016. We believe this offset is related to the SWB over estimating runoff. We calculated groundwater and soil-water change in storage using the period of record (2005–2022) and annual fluctuations (Table 10). Change in storage for the valley-wide water balance is the difference between input and output. We interpret the overall stability of water levels as indicating a negligible change in total storage for the valley-fill aquifer from 2016 through 2024, despite the annual variations in modeled storage.

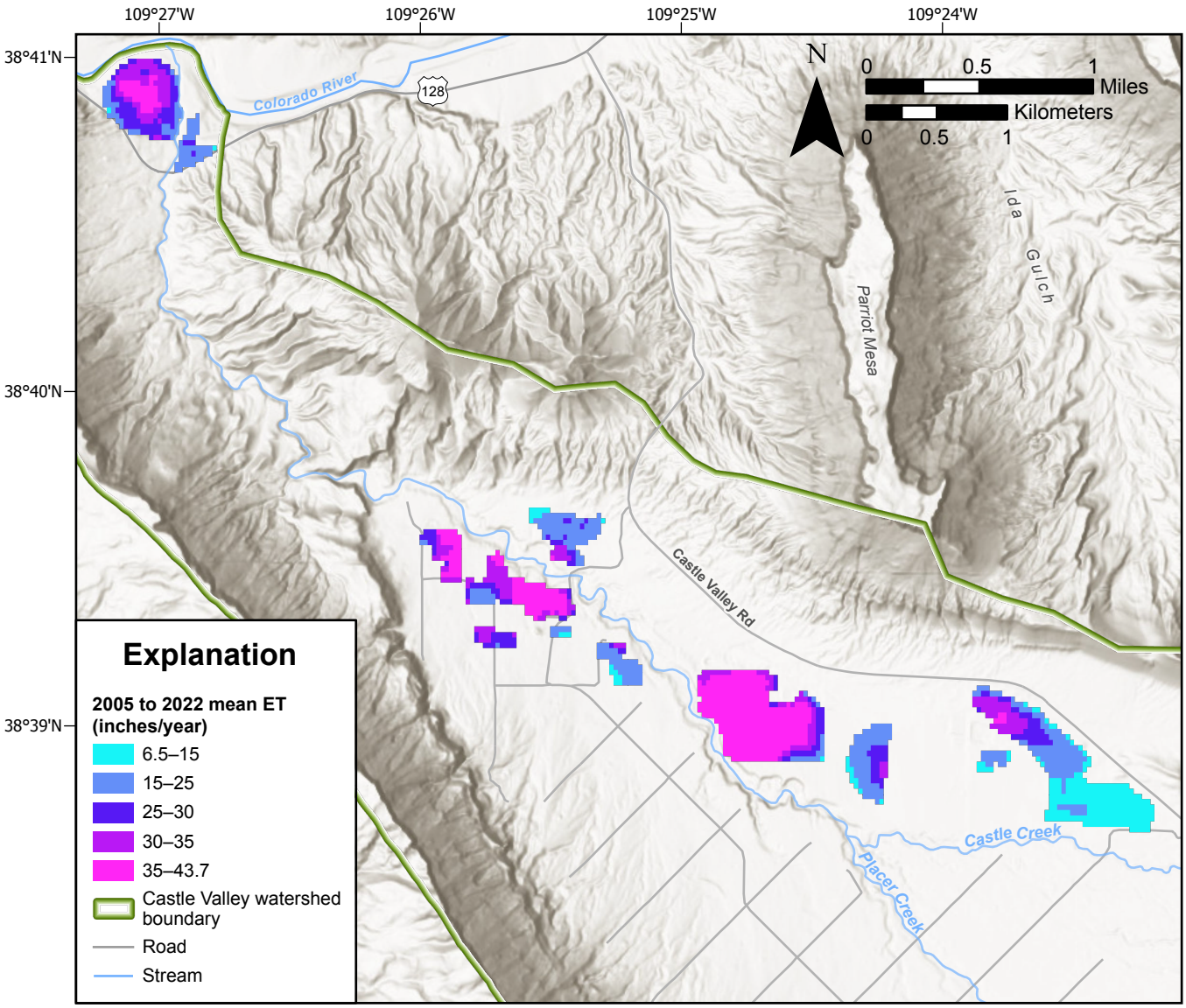

Figure 43. *Mean annual ET on irrigated land between 2005 and 2022.*

Table 11. *Annual water budget analysis for Castle Creek irrigation systems (2014–2024) comparing diversion records against ET estimates to determine system efficiency.*

Year	Castle Valley Irr. Co.	Castle Valley Inc.	Total diversions (ac-ft)	Evapotranspiration (ac-ft)	Return flow (ac-ft)	Irrigation efficiency
2014	397	531	928	-	-	-
2015	744	827	1571	-	-	-
2016	860	1364	2224	874	1351	39%
2017	745	807	1552	811	741	52%
2018	483	612	1095	822	273	75%
2019	1025	1086	2111	884	1227	42%
2020	605	827	1432	906	526	63%
2021	651	849	1500	801	699	53%
2022	751	824	1575	749	826	48%
2023	1565	916	2481	-	-	-
2024	850	772	1622	-	-	-

Groundwater Discharge

The Darcy flux calculated for groundwater leaving the study area at the Colorado River was estimated to range from 2 to 14 acre-feet per year with a geometric mean of 5 acre-feet per year (Table 12). This relatively small outflow component reflects the limited hydraulic gradient and cross sectional area at the valley outlet.

Groundwater Budget

The main components of the water budget for the groundwater system in Castle Valley for the 2024 water year are summarized in Table 13. This integrated budget accounts for all major inputs and outputs to the valley-fill aquifer system.

Long-term water-level stability observed in the monitoring well network suggests that the valley-fill aquifer is in equilibrium with its hydrological inputs and outputs, resulting in a balanced groundwater budget of 4681 acre-feet. Statistical trends in streamflow show a declining trend. This decline could be due to a few factors including reduction in snowfall, reduced soil moisture, or less frequent rainfall. Although annual fluctuations in groundwater elevations exist (Table 2), and annual stream flows are declining (Figure 39), the overall groundwater system appears to be in equilibrium when averaged over the study period.

Key components of the groundwater budget include:

1. **Inputs.** Infiltration from precipitation (2700 acre-feet) and flow from bedrock aquifers (1240 acre-feet) constitute the primary recharge sources (Table 13). Return flow from unconsumed irrigation water adds another 722 acre-feet. Infiltration represents approximately 6% of the total precipitation, which is consistent with recharge rates in similar semi-arid environments. The absence of stream loss (0 acre-feet) confirms that Castle Creek functions as a net gaining stream across Castle Valley.

Table 12. *Darcy flux calculation inputs and results for groundwater flow out of Castle Valley.*

Darcy Flux	
Hydraulic Gradient	0.031
Width	2400 ft
Depth	1400 ft
Hydraulic Conductivity (low end)	0.0023 ft/day
Hydraulic Conductivity (high end)	0.016 ft/day
Groundwater Flow (upper range)	14 ac-ft/year
Groundwater Flow (lower range)	2 ac-ft/year

2. **Outputs.** The largest discharge component is stream gain (3788 acre-feet), representing groundwater discharge to Castle Creek. This supports baseflow in the creek and downstream water users. Phreatophyte ET (147 acre-feet) and well pumping (741 acre-feet) represent smaller but significant discharge components. The minimal seepage to the Colorado River (5 acre-feet) indicates that most groundwater discharges within the valley before reaching the river.

The Castle Valley water budget indicates a hydrologically stable system with significant seasonal and annual variations related to precipitation patterns and irrigation practices. The groundwater system is broadly in balance with monitoring wells indicating stable water levels despite variations in annual precipitation and irrigation diversions. Streamflow is more responsive to yearly fluctuations in precipitation exhibiting long term declines in yearly streamflow volume, whereas groundwater as evidenced by consistent water levels shows little long term change. The high correlation between precipitation datasets validates the water budget approach, while the detailed analysis of irrigation efficiency provides valuable insights for water management.

Key findings include:

- Average annual precipitation is 48,717 acre-feet (2005–2022),
- Only about 6% (~2708 acre-feet) of precipitation becomes groundwater infiltration,
- Unconsumed irrigation water (return flow) averages 722 acre-feet/year, representing significant groundwater recharge,
- Lower irrigation efficiency corresponds with higher aquifer recharge,
- Decrease of 0.058 cfs per year (-37.51 acre-feet/yr) in streamflow from 1994 to 2024,
- Castle Creek functions as a gaining stream throughout most of Castle Valley,
- Monitoring well water levels indicate stable aquifer storage,
- Groundwater budget balances at 4685 acre-feet for inputs and outputs,
- Main inputs are precipitation infiltration (2700 acre-feet) and bedrock aquifer flow (1240 acre-feet),
- Main outputs are stream gain (3788 acre-feet), well pumping (741 acre-feet), and phreatophyte ET (147 acre-feet),
- Minimal groundwater seepage to Colorado River (only ~5 acre-feet/year), and
- The groundwater system shows resilience with stable water levels despite variations in precipitation, streamflow, and irrigation.

Table 13. *Groundwater budget for the Castle Valley valley-fill aquifer, 2024 water year.*

		Water Budget		Uncertainty	Uncertainty Estimate
		Acre-feet	Source	%	Acre-feet
Recharge	Infiltration	2700	SWB model	±20 %	540
	Flow from bedrock	1236	residual calculation	±30 %	371
	Irrigation return flow	722	DWRi - ET	±20 %	144
	Stream loss	0	UGS measurement	±10 %	0
	Septic effluent	23	Septic tank density	±10 %	2
	TOTAL RECHARGE	4681			±1058
Discharge	Stream Gain	3788	UGS measurement	±10 %	379
	Phreatophytes (ET)	147	OpenET	±17 %	25
	Water well pumping	741	Town of Castle Valley	±15 %	111
	Seepage to Colorado River	5	Darcy flux	±50 %	3
	TOTAL DISCHARGE	4681			±517
Groundwater Storage Change		**0**			

SUMMARY AND CONCLUSIONS

Groundwater resource development and the threat of future drought in Castle Valley prompted this study. Water quality and quantity, and the potential for water-quality degradation, are critical elements determining the extent and nature of future development in the valley. Most development is focused along the north-central corridor of the valley, though the potential for development in unincorporated areas of the valley also exists.

Our major findings show that (1) water-level trends in the valley-fill aquifer are stable, with little to no long-term decline; (2) valley-fill aquifer transmissivity exceeds that of bedrock aquifers in the study area, with geometric means of 379 ft^2/day and 119 ft^2/day, respectively; (3) Castle Creek is a net gaining stream and the primary pathway for groundwater discharge from the valley-fill aquifer; (4) high TDS and sulfate concentrations in groundwater located on the valley margins coupled with the sulfate isotope signature of evaporite deposits reinforces the Paradox Formation as the primary source of water quality issues; (5) based on radiogenic isotope data, valley-fill groundwater is primarily modern-age recharge from at least two decades ago, except where influenced by flow through adjacent bedrock on valley margins; (6) the valley-fill aquifer receives recharge primarily from direct infiltration of precipitation (2700 acre-feet/yr) and from bedrock recharge (1240 acre-feet/yr); (7) snow water equivalent (SWE) at the Lasal Mountain SNOTEL site shows a decreasing trend of 0.15 inches per year from 1980 through 2024, suggesting a gradual decline in mountain snowpack that likely influences streamflow; and (8) groundwater discharge from the valley-fill aquifer is primarily from stream gain (3788 acre-feet/yr) and well water withdrawal (745 acre-feet/yr).

Groundwater levels in select wells measured in 1994 and 2024 show an average increase of 1.45 feet (0.4 m) over that time period. However, based on monitoring well data from 2016 through 2024, groundwater elevations in the valley-fill aquifer have fluctuated little; monitoring wells show no statistically significant trends in groundwater elevations, indicating that the valley-fill aquifer is at equilibrium with recharge and discharge.

The valley-fill aquifer is the most productive aquifer in the study area. Valley-fill aquifer transmissivities ranged from 42 to 12,900 ft^2/day, compared to bedrock aquifer transmissivities of 3.5 to 1838 ft^2/day. Valley-fill aquifer thickness varies from less than 50 feet (15 m) on the valley margins to 410 feet (125 m) in the valley center.

The Paradox Basin's complex fault and fold structures constrain Castle Valley's groundwater movement. The cross sections prepared in this study reveal the possibility of additional concealed normal faults associated with the collapse of the salt-core anticline in the nose and eastern margin of Castle Valley. However, the role of these faults is still poorly understood, partially due to their concealed nature, and partially due to the lack of sufficient water wells situated on the eastern margin of the valley.

We measured discharge on Castle Creek to understand the groundwater-surface water connection better. Flow measured at three locations along Castle Creek shows the stream is gaining from groundwater, averaging 3788 acre-feet/yr. Over the course of the year, streamflow at the USGS monitoring site averaged six times greater than that measured at the upstream USFS site. This substantial increase in discharge represents the largest discharge component from the valley-fill aquifer system. These measurements verify Castle Creek's role as a

significant groundwater discharge zone, receiving consistent groundwater contributions along its course. In contrast, Placer Creek functions as an ephemeral stream that flows only during significant precipitation events and snowmelt periods. When flowing, it primarily contributes to groundwater recharge rather than receiving groundwater discharge.

Groundwater chemistry maintains consistent quality, which has been documented over decades, with high TDS and sulfate concentrated in the northwestern and western regions, and lower TDS and sulfate in the central and southern margins of the valley. This spatial pattern reflects the variable influence of different geologic units on water quality, particularly where groundwater influenced by Paradox Formation evaporites occurs.

Environmental tracer analysis allowed us to make several distinctions regarding the aquifers in Castle Valley. Groundwater stable isotope samples have an evaporative signature, indicative of evaporation occurring prior to recharge, likely from sublimation of the snowpack prior to spring runoff or longer vadose zone residence times. Spring waters closer to the La Sal Mountains exhibit isotopic composition closer to that of the original precipitation composition. Stable isotope ratios also provide evidence of the connection between groundwater and surface water. Surface water samples show similar isotopic values to wells and springs, which aligns with seepage data indicating substantial groundwater contributions to streamflow.

Sulfate isotope analysis in Castle Valley reveals three distinct sources affecting groundwater sulfate composition. Soil sulfate minerals primarily influence groundwater sulfate in the center of the valley-fill aquifer, whereas evaporite minerals are the predominant source of sulfate on the valley-fill margins adjacent to bedrock. Groundwater sulfate from some springs high in the recharge zone is influenced by sulfate oxidation. Higher sulfate concentrations correlate with evaporite sulfate isotope signatures, and together these data are indicative of Paradox Formation dissolution as the source of elevated TDS in Castle Valley.

The groundwater in the valley-fill aquifer is young. The predominance of modern groundwater suggests the aquifer relies on active recharge with relatively short flow paths and thus is sensitive to fluctuations in snowpack levels and shifts in climatic conditions. Groundwater with mixed-age recharge is influenced by recharge from bedrock sources.

A basin-wide SWB model for 2005 to 2022 coupled with historical and current USGS streamflow data and new streamflow and water-level measurements from this study shows the principal water balance input is precipitation, while the main outputs are ET and Castle Creek streamflow. The average recharge to the watershed is 4685 acre-feet/yr from infiltration of precipitation (58%), flow from bedrock (26%), irrigation return flow (15%), and septic-system effluent (1%). Average discharge from the valley-fill aquifer balances at 4685 acre-feet/yr from stream gain (81%), well withdrawal (16%), phreatophytic ET (3%), and seepage to the Colorado River (<1%) (Figure 44). Additionally, the SWB model estimates an average annual storage change of 1167 acre-feet/yr, despite monitoring well water-level data from 2016 through 2024 suggesting stable aquifer storage over the time period. Our recharge and discharge estimates fall below the estimated inflow calculated by Kolm and van der Heidje (2016) and Ford (2006) of 5527 acre-feet per year and 6819 acre-feet per year, respectively.

Although Castle Valley is currently sparsely inhabited, potential development may result in increased demand on water resources. The demonstrated interconnection between surface and groundwater has important management implications for Castle Valley. Understanding these groundwater-surface water interactions is essential for long-term water supply continuity.

The water levels in the valley-fill aquifer may decline if long term precipitation trends decline, groundwater withdrawals in the valley increase, or if irrigation diversion from Castle Creek increases. Given the stability of water-level trends and recharge inputs, an increase in groundwater withdrawal could impact the relationship between high TDS groundwater on the valley margins and low TDS groundwater in the valley center. Depending on the location and magnitude, increased groundwater withdrawal could capture water from Castle Creek, further reducing its flow, and/or impact the phreatophytic vegetation along its banks. Careful water management planning is recommended to preserve the current Pristine and Drinking Water status of the classified sole source aquifer.

Future studies could focus on five key areas to build on the current understanding of the system. (1) High-frequency water-level observations (transducers) in wells could help reveal short-term and long-term variability and improve understanding of recharge and discharge (2) Modeling groundwater inflows from bedrock in response to valley-fill groundwater elevation and pumping changes would allow for better quantifying bedrock contributions. (3) Further geophysics and geochemistry exploration could help delineate the boundaries between valley-fill and bedrock units and clarify the hydraulic connection between the valley-fill aquifer and evaporite-derived, high-sulfate groundwater sources. (4) Incorporating predicted future climate scenarios into the SWB model could produce estimates of potential changes in recharge under varying temperature and precipitation regimes. (5) Depending on available water rights and permitting, Managed Aquifer Recharge (MAR) could help mitigate any future declines in groundwater storage. This report provides much of the data needed for a MAR feasibility analysis including water quality distribution, groundwater flow directions, groundwater depth below land surface, and aquifer transmissivity.

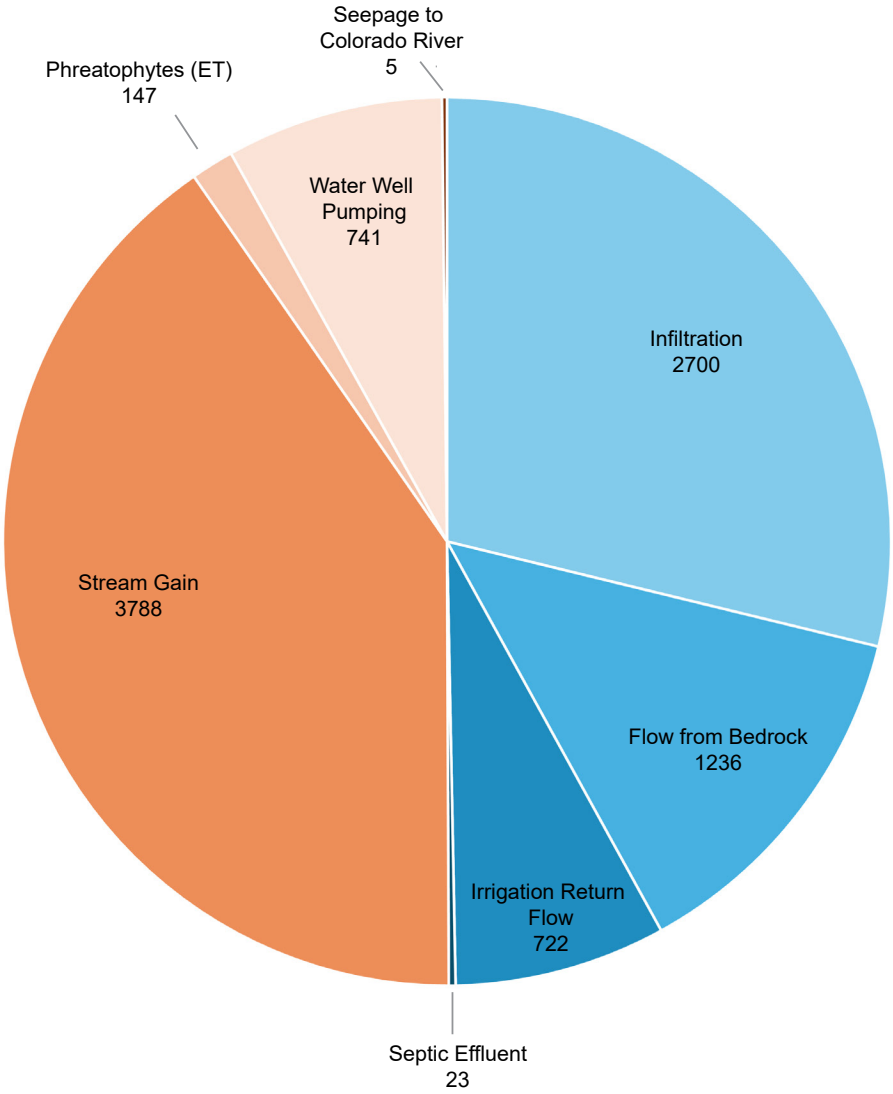

Figure 44. *Ground water budget for Castle Valley using values from Table 13. Inflows shown in blue and outflows shown in orange.*

ACKNOWLEDGMENTS

This project was funded by the Town of Castle Valley and the Utah Geological Survey. We thank landowners for allowing access to their land and wells. We thank Town of Castle Valley Water Rights Agent John Groo for contacting well owners and assisting with field investigations. Pam Hackley provided valuable surface water diversion information. Special thanks to UGS colleagues Kate Baustian, Paul Inkenbrandt, Emily Jainarain, Claire Spangenberg-Kellner and Grand County Watershed Coordinator Arne Hultquist for helping with field work. Thanks to UGS colleague Lauren Reeher for insights on geologic structure. We also thank UGS colleagues Stephanie Carney, Hugh Hurlow, Lucy Jordan; Cash Stallings (Utah Division of Water Rights); Arne Hultquist (Grand County Watershed Coordinator); and Sam Taylor (Utah Division of Water Quality) for reviewing the manuscript.

We would also like to express our gratitude to Janae Wallace for her dedication to the Castle Valley area over her three decades of service at the UGS. She has contributed valuable information and historical insights about the region while fostering lasting connections within the community. Her previous research has provided both the Town of Castle Valley and the UGS with a solid foundation for this report and future initiatives.

REFERENCES

Abatzoglou, J.T., 2011, Development of gridded surface meteorological data for ecological applications and modelling: International Journal of Climatology, v. 33, no. 1, p. 121–131, https://doi.org/10.1002/joc.3413.

Anderson, M.C., Huntington, J.L., Kilic, A., Allen, R.G., Melton, F.S., Erickson, T.A., and Morton, C.G., 2024, OpenET model intercomparison and accuracy assessment report—Supplementary material to OpenET: A satellite-

based ensemble framework for operational evapotranspiration estimation in the western United States: Nature Water, v. 2, p. 193–205, https://doi.org/10.1038/s44221-023-00181-7.

Beaudoin, G., Taylor, B.E., Rumble, D., Thiemens, M., 1994, Variations in the sulfur isotope composition of troilite from the Cañon Diablo iron meteorite: Geochimica et Cosmochimica Acta, v. 58, p. 4253–4255.

Belcher, W.R., Elliott, P.E., and Geldon, A.L., 2001, Hydraulic-property estimates for use with a transient ground-water flow model of the Death Valley regional ground-water flow system, Nevada and California: U.S. Geological Survey Water-Resources Investigations Report 01-4210, 28 p., https://doi.org/10.3133/wri014210.

Blanchard, P.J., 1990, Ground-water conditions in the Grand County area, Utah, with emphasis on the Mill Creek-Spanish Valley area: Utah Department of Natural Resources Technical Publication 100, 69 p.

Bradbury, K.R., and Rothschild, E.R., 1985, A computerized technique for estimating the hydraulic conductivity of aquifers from specific capacity data: Groundwater, v. 23, no. 2, p. 240–246.

Buchanan, T.J., and Somers, W.P., 1969, Discharge measurements at gaging stations: U.S. Geological Survey Techniques of Water-Resources Investigations, book 3, chap A8, p. 32–33.

Clark, I., and Fritz, P., 1997, Environmental isotopes in hydrogeology: Boca Raton, CRC Press, 328 p.

Cooper, H.H., and Jacob, C.E., 1946, A generalized graphical method for evaluating formation constants and summarizing wellfield history: Eos, Transactions American Geophysical Union, v. 27, no. 4, p. 526–534.

Craig, H., 1961, Isotopic variations in meteoric waters: Science, v. 133, no. 3465, p. 1702–1703.

Cunningham, W.L., and Schalk, C.W., compilers, 2011, Groundwater technical procedures of the U.S. Geological Survey: U.S. Geological Survey Techniques and Methods 1–A1, 151 p., https://pubs.usgs.gov/tm/1a1/.

Daly, C., Halbleib, M., Smith, J.I., Gibson, W.P., Doggett, M.K., Taylor, G.H., Curtis, J., and Pasteris, P.A., 2008, Physiographically-sensitive mapping of temperature and precipitation across the conterminous United States: International Journal of Climatology, v. 28, p. 2031–2064.

Daly, C., Smith, J.I., and Olson, K.V., 2015, Mapping atmospheric moisture climatologies across the conterminous United States: PloS ONE, v. 10, no. 10, https://doi.org/10.1371/journal.pone.0141140.

Dewitz, J., and U.S. Geological Survey, 2021, National land cover database (NLCD) 2019 products (ver. 2.0): U.S. Geological Survey data release, https://doi.org/10.5066/P9KZCM54.

Doelling, H.H., 2001, Geologic map of the Moab and eastern part of the San Rafael Desert 30' x 60' quadrangles, Grand and Emery Counties, Utah, and Mesa County, Colorado: Utah Geological Survey Map 180, 3 plates, scale 1:100,000, https://doi.org/10.34191/M-180.

Doelling, H.H., 2002, Geologic map of the Fisher Towers quadrangle, Grand County, Utah: Utah Geological Survey Map 183, 22 p., scale 1:24,000, https://doi.org/10.34191/M-183.

Doelling, H.H., and Ross, M.L., 1998, Geologic map of the Big Bend quadrangle, Grand County, Utah: Utah Geological Survey Map 171, 29 p., scale 1:24,000, https://doi.org/10.34191/M-171.

Domenico, P.A., 1972, Concepts and models in groundwater hydrology: New York, McGraw Hill, 416 p.

Escosa, F.O., Rowan, M.G., Giles, K.A., Deatrick, K.T., Mast, A.M., Langford, R.P., Hearon, T.E., and Roca R., 2019, Lateral terminations of salt walls and megaflaps—an example from Gypsum Valley Diapir, Paradox Basin, Colorado, USA: Basin Research, v. 31, p. 191–212, https://doi.org/10.1111/bre.12316.

Fontes, J.C., and Garnier, J.M., 1979, Determination of the initial 14C activity of the total dissolved carbon—a review of the existing models and a new approach: Water Resources Research, v. 15, p. 399–413.

Ford, C.E., 2006, Water resources of the Castle Valley area: unpublished Utah Division of Water Rights Hydrologic Data Report No. 3, 13 p., https://waterrights.utah.gov/docsys/v910/x910/x91003mt.pdf.

Ford, C., and Grandy, A., 1997, Records of well water levels and water quality in alluvial and bedrock aquifers, Castle Creek seepage study, precipitation, and water uses for Castle Valley, Grand County, Utah: Utah Division of Water Rights Hydrologic Data Report No. 1, 53 p.

Gardner, P.M., Nelson, N.C., Heilweil, V.M., Solder, J.E., and Solomon, D.K., 2020, Rethinking a groundwater flow system using a multiple-tracer geochemical approach—A case study in Moab–Spanish Valley, Utah: U.S. Geological Survey Scientific Investigations Report 2020–5089, 72 p., https://doi.org/10.1016/j.jhydrol.2020.125512.

Gibson, J.J., Birks, S.J., and Edwards, T.W.D., 2008, Global prediction of δA and δ2H-δ18O evaporation slopes for lakes and soil water accounting for seasonality: Global Biogeochemical Cycles, v. 22, no. 2, p. GB2031.

Giles, K.A., Hearon, T.E., Rowan, M.G., and Langford, R.P., 2017, The Paradox Salt Basin, Utah and Colorado—Recognition of new types of salt features and their impact on salt-related traps: Adapted presentation given at the Association of American Petroleum Geologists 2017 Annual Convention and Exhibition, Houston, Texas, April 2–5, 2017.

Gonfiantini, R., 1978, Standards for stable isotope measurements in natural compounds: Nature, v. 271, no. 5645, p. 534–536.

Hargreaves, G.H., and Samani, Z.A., 1985, Reference crop evapotranspiration from temperature: Applied Engineering in Agriculture, v. 1, no. 2, p. 96–99, https://doi.org/10.13031/2013.26773.

Han, L.F., Plummer, L.N., and Aggarwal, P., 2012, A graphical method to evaluate predominant geochemical processes occurring in groundwater systems for radiocarbon dating, Chemical Geology, v. 318–319, p. 88–112, https://doi.org/10.1016/j.chemgeo.2012.05.004.

Han, L.F., and Plummer, L.N., 2013, Revision of Fontes & Garnier's model for the initial 14C content of dissolved inorganic carbon used in groundwater dating: Chemical Geology, v. 351, p. 105–114.

Hart, R., 2009, Isotopic evaluation of carbon dioxide in soil gas in Utah for a more accurate input variable in groundwater age models: Provo, Utah, Brigham Young University, M.S. thesis, 62 p.

Healy, R.W., 2007, Water budgets-foundations for effective water-resources and environmental management: U.S. Geological Survey Circular 1308, 90 p., https://doi.org/10.3133/cir1308.

Hem, J.D., 1985, Study and interpretation of the chemical characteristics of natural water: U.S. Geological Survey Water-Supply Paper 2254, 263 p.

Huntoon, P.W., Billingsley, G.H., and Breed, W.J., 1982, Geologic map of Canyonlands National Park and vicinity, Utah: Canyonlands Natural History Association, scale 1:62,500.

Huntington, J. L., Pearson, C., Minor, B., Volk, J., Morton, C., Melton, F., and Allen, R., 2022, Upper Colorado River basin OpenET intercomparison summary technical report: Reno, Nevada, Desert Research Institute, https://doi.org/10.13140/RG.2.2.21605.88808.

Hussain, M.M., and Mahmud, I., 2019, pyMannKendall: a python package for non parametric Mann Kendall family of trend tests, Journal of Open Source Software, v. 4, no. 39, 1556, https://doi.org/10.21105/joss.01556.

Ingerson, E., and Pearson, F.J., 1964, Estimation of age and rate of motion of ground water by the 14C method, *in* Miyake, Y., and Koyama, T., editors, Recent researches in the fields of hydrosphere, atmosphere and nuclear chemistry: Editorial Committee for Sugawara Volume, Water Research Laboratory, Nagoya University, Tokyo, p. 263–283.

Jelinski, J., Clayton, C.S., and Fulford, J.M., 2015, Accuracy testing of electric groundwater-level measurement tapes: U.S. Geological Survey Open-File Report 2014-1236, 27 p., https://doi.org/10.3133/ofr20141236.

Johnson, A.I., 1967, Specific yield—compilation of specific yield for various materials: U.S. Geological Survey Water-Supply Paper 1662-D, 74 p.

Kalin, R.M., 2000, Radiocarbon dating of groundwater systems, *in* Cook, P.G., and Herczeg, A.L., editors, Environmental tracers in subsurface hydrology: Boston, Springer, p. 111–144.

Kim, J.H., Bailey, L., Noyes, C., Tyne, R.L., Ballentine, C.J., Person, M., Ma, L., Barton, M., Barton, I., Reiners, P.W., Ferguson, G., and McIntosh, J., 2022, Hydrogeochemical evolution of formation waters responsible for sandstone bleaching and ore mineralization in the Paradox Basin, Colorado Plateau, USA: Geological Society of America Bulletin, v. 134, no. 9–10, p. 2589–2610, https://doi.org/10.1130/B36078.1.

Kolm, K.E., and van der Heijde, P.K., 2016, Hydrologic assessment of the surface water and groundwater resources of Castle Valley, Utah—Part 1 hydrologic and environmental analysis (HESA) and preliminary water budget: Unpublished consultants report for Town of Castle Valley, 60 p.

Kolm, K.E., and van der Heijde, P.K., 2020, Hydrologic assessment of the surface water and groundwater resources of Castle Valley, Utah—Part 2 hydrologic and environmental system analysis (HESA) – based aquifer storage: Unpublished consultants report for Town of Castle Valley, 14 p.

Krouse, H. and Mayer, B., 1999, Sulphur and oxygen isotopes in sulphate, *in* Cook, P., and Herczeg, A.L., editors, Environmental tracers in subsurface hydrology: Boston, Kluwer Academic Publishers, p. 195–231.

Lindsey, B.D., Jurgens, B.C., and Belitz, K., 2019, Tritium as an indicator of modern, mixed, and premodern groundwater age: U.S. Geological Survey Scientific Investigations Report 2019–5090, 18 p., https://doi.org/10.3133/sir20195090.

Lowe, M., Wallace, J., Bishop, C.E., and Hurlow, H.A., 2004, Ground-water quality classification and recommended septic tank soil-absorption-system density maps, Castle Valley, Grand County, Utah: Utah Geological Survey Special Study 113, 65 p., https://doi.org/10.34191/SS-113.

Masbruch, M.D., and Shope, C.L., 2014, Groundwater and surface-water resources in the Bureau of Land Management Moab master leasing plan area and adjacent area, Grand and San Juan counties, Utah, and Mesa and Montrose counties, Colorado: U.S. Geological Survey Open-File Report 2014-1062, 12 p.

Mather, J.R., 1978, The climatic water balance in environmental analysis: Lexington, Mass., D.C. Heath and Company, 239 p.

Mather, J.R., 1979, Use of the climatic water budget to estimate streamflow, in Mather, J.R., editor, Use of the climatic water budget in selected environmental water problems: Elmer, New Jersey, C.W. Thornthwaite Associates, Laboratory of Climatology, Publications in Climatology, v. 32, no. 1, p. 1–52.

Melton, F.S., Huntington, J., Allen, R.G., Hain, C., Anderson, M., Erickson, T., and Morton, C., 2021, OpenET—Filling a critical data gap in water management for the western United States: Journal of the American Water Resources Association, v. 57, no. 6, p. 837–857, https://doi.org/10.1111/1752-1688.12956.

Michel, R. L., Jurgens, B. C., and Young, M. B., 2018, Tritium deposition in precipitation in the United States, 1953–2012: U.S. Geological Survey Scientific Investigations Report, https://doi.org/10.3133/sir20185086.

Mook, W.G., 1972, On the reconstruction of the initial 14C content of groundwater from the chemical and isotopic composition, in Proceedings of the 8th International Conference on Radiocarbon Dating:Wellington, New Zealand, Royal Society of New Zealand, v. 1, p. 342–352.

National Ecological Observatory Network (NEON), 2025, Bundled data products—eddy covariance (DP4.00200.001), RELEASE-2025, https://doi.org/10.48443/r7zp-y487. Dataset accessed from https://data.neonscience.org/data-products/DP4.00200.001/RELEASE-2025.

Natural Resources Conservation Service, 2022, Soil survey geographic (SSURGO) database: United States Department of Agriculture, https://sdmdataaccess.sc.egov.usda.gov, accessed May 2024.

Niswonger, R.G., and Prudic, D.E., 2023, Simulation of groundwater flow in the Mississippi Embayment using the Soil-Water-Balance model and MODFLOW: U.S. Geological Survey Scientific Investigations Report 2023–5080, 58 p., https://doi.org/10.3133/sir20235080.

Pope, J.P., and Burbey, T.J., 2019, Water-budget analysis of groundwater and surface-water interaction in the Ridge and Valley physiographic province, eastern United States: U.S. Geological Survey Scientific Investigations Report 2019–5056, 82 p., https://doi.org/10.3133/sir20195056.

Rozanski, K., Araguás-Araguás, L., and Gonfiantini, R., 1993, Isotopic patterns in modern global precipitation, *in* Swart, P.K., Lohmann, K.C., McKenzie, J., and Savin, S., editors, Climate change in continental isotopic records: American Geophysical Union Monograph 78, p. 1–36.

Rantz, S.E., and others, 1982, Measurement and computation of streamflow—Volume 1, Measurement of stage and discharge: U.S. Geological Survey Water-Supply Paper 2175, 284 p., https://pubs.usgs.gov/wsp/wsp2175/.

Scholl, M.A., Anderson, L., Bern, C., Clow, D.W., Reid, L.T., and Coplen, T.B., 2023, Stable hydrogen and oxygen isotopic compositions of precipitation samples from selected Colorado and Utah National Atmospheric Deposition Program (NADP) sites: U.S. Geological Survey data release, https://doi.org/10.5066/P9S5ZTS0.

Senay, G., Bohms, S., Singh, R., Gowda, P., Velpuri, N., Alemu, H., and Verdin, J., 2013, Operational evapotranspiration mapping using remote sensing and weather datasets—A new parameterization for the SSEB approach: Journal of the American Water Resources Association, v. 49, https://doi.org/10.1111/jawr.12057.

Senay, G., Schauer, M., Friedrichs, M., Manohar, V., and Singh, R., 2017, Satellite-based water use dynamics using historical Landsat data (1984–2014) in the southwestern United States: Remote Sensing of Environment, v. 202, https://doi.org/10.1016/j.rse.2017.05.005.

Solomon, D.K., and Cook, P.G., 2000, ^{3}H and ^{3}He, *in* Cook, P., and Herczeg, A.L., editors, Environmental tracers in subsurface hydrology: Boston, Kluwer Academic Publishers, p. 397–424.

Solomon, D. K., and Gilmore, T, 2024, Age dating young groundwater—How to determine groundwater age from environmental tracer data: The Groundwater Project, https://gw-project.org/books/age-dating-young-groundwater/.

Snyder, N.P., 1996a, Recharge area and water quality of the valley-fill aquifer, Castle Valley, Grand County, Utah: Utah Geological Survey Report of Investigation 229, p. 17–22, https://doi.org/10.34191/RI-229.

Snyder, N.P., 1996b, Recharge area and water quality of the valley-fill aquifer, Castle Valley, Grand County, Utah, *in* Huffman, A.C., Jr., Lund, W.R., and Godwin, L.H., editors, Geology and resources of the Paradox Basin: Utah Geological Association Guidebook 25, p. 395–404.

Stewart, M. K., and Morgenstern, U., 2016, Importance of tritium-based transit times in hydrological systems: Wiley Interdisciplinary Reviews Water, v. 3, p. 145–154

Stokes, W.L., 1977, Subdivisions of the major physiographic provinces in Utah: Utah Geology, v. 4, no. 1, p. 1–17.

Tamers, M.A., 1975, Validity of radiocarbon dates on groundwater: Geophysical Surveys, v. 2, no. 2, p. 217–239.

Theis, C.V., 1935, The relation between the lowering of the piezometric surface and the rate and duration of discharge of a well using ground-water storage: EOS, Transactions American Geophysical Union, v. 16, no. 2, p. 519–524.

Thornton, M.M., Shrestha, R., Wei, Y., Thornton, P.E., Kao, S., and Wilson, B.E., 2021, Daymet—daily surface weather data on a 1-km grid for North America, version 4: ORNL DAAC, Oak Ridge, Tennessee.

Thornthwaite, C.W., 1948, An approach toward a rational classification of climate: Geographical Review, v. 38, p. 55–94.

Tillman, F.D., 2015, Documentation of input datasets for the soil-water balance groundwater recharge model of the Upper Colorado River Basin: U.S. Geological Survey Open-File Report 2015–1160, 26 p., https://doi.org/10.3133/ofr20151160.

Trudgill, B.D., 2011, Evolution of salt structures in the northern Paradox Basin—controls on evaporite deposition, salt wall growth and supra-salt stratigraphic architecture: Basin Research, v. 23, p. 208–238.

U.S. Census Bureau, 2020, Decennial Census, Castle Valley town, Grand County, Utah, https://data.census.gov/profile/Castle_Valley_town,_Utah?g=160XX00US4911000, accessed November 4, 2024.

U.S. Department of Agriculture, 1986, Urban hydrology for small watersheds: Natural Resources Conservation Service Technical Release 55 (TR-55), 164 p.

U.S. Environmental Protection Agency, 2002, Onsite wastewater treatment systems manual: U.S. Environmental Protection Agency EPA/625/R-00/008, 367 p., https://www.epa.gov/septic.

U.S. Geological Survey, 2021, Estimated use of water in the United States in 2015: U.S. Geological Survey Circular 1441, 65 p., https://doi.org/10.3133/cir1441.

Utah Division of Water Resources, 2010, 2009 residential water use—survey results and analysis of residential water use for seventeen communities in Utah: Salt Lake City, Utah Department of Natural Resources, 37 p.

Utah Division of Water Resources, 2024, Water Related Land Use (2010 to 2015): https://utahdnr.maps.arcgis.com/apps/webappviewer/index.html?id=e03fd241be0149059d4f402aea90b4f3, accessed August 8, 2024.

Utah Division of Water Rights, 2024, Public Water Supplier Information: https://www.waterrights.utah.gov/asp_apps/viewEditPWS/pwsView.asp?SYSTEM_ID=11094&inactive=show, accessed August 8, 2024.

Utah Division of Water Rights, 2025, 2024 Annual Report—Castle Creek Distribution System, Castle Valley, Utah: Office of the State Engineer, prepared January 3, 2025.

Volk, J.M., Huntington, J.L., Melton, F.S., and others, 2024, Assessing the accuracy of OpenET satellite-based evapotranspiration data to support water resource and land management applications: Nature Water, v. 2, p. 193–205. https://doi.org/10.1038/s44221-023-00181-7.

Wallace, J., and Lowe, M., 2007, Petition for ground-water quality classification, Castle Valley, Grand County, Utah: Salt Lake City, unpublished petition submitted to the Utah Division of Water Quality, 23 p.

Wallace, J., and Lowe, M., 2012, Groundwater quality classification/reclassification, Castle Valley, Grand County, Utah, *in* Hylland, M.D., and Harty, K.M., editors, Selected topics in engineering and environmental geology in Utah: Utah Geological Association Publication 41, p. 135–154.

Westenbroek, S.M., Engott, J.A., Kelson, V.A., and Hunt, R.J., 2018, SWB Version 2.0—a soil-water-balance code for estimating net infiltration and other water-budget components: U.S. Geological Survey USGS Numbered Series 6-A59, https://doi.org/10.3133/tm6A59.

Winter, T.C., Harvey, J.W., Franke, O.L., and Alley, W.M., 1998, Ground water and surface water—a single resource: U.S. Geological Survey Circular 1139, 79 p.

Wolf, M.A., Jamison, L.R., Solomon, D.K., Strong, C., and Brooks, P.D., 2022, Multi-year controls on groundwater storage in seasonally snow-covered headwater catchments: Water Resources Research, v. 58, no. 3, https://doi.org/10.1029/2022WR033394.

APPENDICES

APPENDIX A

Sample Location and Chemistry Data (2023–2024)

Table A1.

Site ID	Lot #	Site Type	Date	Latitude	Longitude	Water Level	Discharge	Chemistry	Field Parameters	Stable Isotopes	^{14}C Isotope	Tritium Isotope	Sulfate Isotopes	Nitrate + nitrite
CV1		well	11/15/2023	38.629584	-109.361183	X		X	X	X			X	
CV11		well	11/15/2023	38.619063	-109.385358	X		X	X	X			X	X
CV12	447	well	10/24/2023	38.65801	-109.42567				X					
CV13	447	well	10/24/2023	38.65776	-109.42381				X	X				
CV18	365	well	10/24/2023	38.609253	-109.378196			X	X	X				X
CV19	338	well	11/15/2023	38.618814	-109.391545	X		X	X	X			X	X
CV20	328	well	10/24/2023	38.62462	-109.38944			X	X	X				X
CV21	307	well	11/15/2023	38.629105	-109.39005	X		X	X	X				
CV23	219	well	10/24/2023	38.62663	-109.40574			X	X	X			X	
CV24	227	well	10/24/2023	38.63216	-109.39933			X	X		X	X		
CV25	228	well	11/15/2023	38.632827	-109.397717	X			X	X			X	
CV26	238	well	10/24/2023	38.639918	-109.389682			X	X	X			X	
CV27	2	well	11/15/2023	38.651813	-109.424406	X		X	X	X	X	X	X	X
CV28	187	well	10/24/2023	38.6394753	-109.3960653				X	X				
CV29	110	well	11/15/2023	38.643731	-109.403238	X			X	X				
CV30	140	well	10/24/2023	38.63871	-109.40441				X	X				
CV31	164	well	10/24/2023	38.633068	-109.408445			X	X	X			X	
CV32	100	well	10/24/2023	38.63657	-109.41268				X	X				
CV33	74	well	10/24/2023	38.64053	-109.41486				X	X				
CV34	53	well	10/24/2023	38.6466331	-109.4129661				X	X				
CV35	35	well	10/24/2023	38.64605	-109.41709			X	X	X			X	
CV36	24	well	10/24/2023	38.6440451	-109.4222027				X	X				
CV38	439	well	11/15/2023	38.658709	-109.419908	X		X	X	X			X	
CV4		well	11/15/2023	38.581343	-109.334835	X		X	X	X	X	X		X
CV41	419	well	10/24/2023	38.6551857	-109.4278443				X	X				
CV42	430	well	11/15/2023	38.659325	-109.425868	X			X	X				
CV47	390	well	10/24/2023	38.65811	-109.43041				X	X				
CV51		well	10/24/2023	38.651053	-109.409402					X				
CV56	46	well	11/16/2023	38.642268	-109.41789	X								
CV57	158	well	11/16/2023	38.63691	-109.403862	X				X				
CV58	225	well	11/16/2023	38.6308	-109.400085	X								
CV59	415	well	11/16/2023	38.652134	-109.428371	X			X	X				
CV60	435	well	11/16/2023	38.661084	-109.423164	X								
CV61		well	11/16/2023	38.584178	-109.291093	X								
CV62	8	well	11/16/2023	38.649702	-109.421526	X								
CV63	433	well	11/16/2023	38.661283	-109.423914	X								
CV65	432	well	11/16/2023	38.661073	-109.424819	X								
CV66	13	well	11/15/2023	38.648993	-109.419208	X								
CV67		well	11/15/2023	38.644568	-109.385193	X								
CV68	401	well	11/15/2023	38.651846	-109.430003	X								
CV69	179	well	11/15/2023	38.633729	-109.402765	X								
CV7		well	11/15/2023	38.656126	-109.427159	X		X	X				X	X
CV70	194	well	11/15/2023	38.642298	-109.390117	X								
CV71	287	well	11/15/2023	38.625073	-109.398019	X								
CV72	352	well	11/15/2023	38.614851	-109.380073	X				X				
CV73	356	well	11/15/2023	38.613487	-109.379216	X								
CV74		well	11/16/2023	38.603009	-109.318816	X								
CV75	311	well	4/1/2024	38.624665	-109.392011	X								
CV76	111	well	4/2/2024	38.64327	-109.402299	X				X				
CV77	433	well	4/2/2024	38.661615	-109.424539	X								
CV8		well	11/15/2023	38.648259	-109.407923	X		X	X	X			X	X
CV9		well	11/15/2023	38.642343	-109.410911	X		X	X	X		X	X	X
CV100		stream	11/14/2023	38.662157	-109.434581		X							
CV101		stream	11/14/2023	38.6624	-109.4342		X							
CV102		stream	11/14/2023	38.6622	-109.4333		X							
CV103		stream	11/14/2023	38.659992	-109.430413		X							
CV104		stream	11/14/2023	38.65834	-109.42613		X							
CV105		stream	11/14/2023	38.658003	-109.425417		X							
CV106		stream	11/14/2023	38.657131	-109.425151		X							
CV107		stream	11/14/2023	38.6567	-109.4232		X							
CV108		stream	11/14/2023	38.61699	-109.33555		X							
CV109		stream	11/14/2023	38.6172228	-109.3360562					X				
CV110		Stream	5/14/2024	38.633711	-109.367113		X		X					
CV14		stream	11/14/2023	38.65777	-109.42381		X	X	X	X				
CV16		stream	11/14/2023	38.591416	-109.265083		X	X	X	X				
CV17		stream	11/14/2023	38.671551	-109.449724		X		X	X			X	
CV2		stream	11/14/2023	38.65025	-109.41499		X		X	X	X	X		
CV201		stream	11/14/2023	38.645343	-109.406764		X							
CV203		stream	11/14/2023	38.646	-109.4108					X				
CV204		stream	11/14/2023	38.617332	-109.336317		X			X				
CV301		stream	11/14/2023	38.60011	-109.29169		X			X				
CV303		stream	11/14/2023	38.59896	-109.29479		X							
CV304		stream	11/14/2023	38.60763	-109.32484		X							
CV302		stream	11/14/2023	38.59902	-109.29413		X							

Table A1 Continued.

Site ID	Lot #	Site Type	Date	Latitude	Longitude	Water Level	Discharge	Chemistry	Field Parameters	Stable Isotopes	^{14}C Isotope	Tritium Isotope	Sulfate Isotopes	Nitrate + nitrite
CV45		stream	11/14/2023	38.5833	-109.24251				X	X				
CV6		stream	11/14/2023	38.6575	-109.4241				X	X				
CV10		spring	11/14/2023	38.65762	-109.42381				X	X				
CV15		spring	11/14/2023	38.61216	-109.33094				X	X			X	
CV3		spring	11/14/2023	38.65019	-109.41492				X	X				
CV300		spring	11/15/2023	38.5989	-109.29289				X	X			X	
CV39		spring	11/14/2023	38.65161	-109.39845				X					
CV40		spring	11/14/2023	38.60501	-109.32458				X	X				
CV43		spring	11/14/2023	38.60194	-109.22958				X	X			X	
CV44		spring	11/14/2023	38.58344	-109.2422		X		X	X				
CV46		spring	11/14/2023	38.59437	-109.24214				X	X				
CV49		spring	11/14/2023	38.660146	-109.43209			X	X	X				
CV5		spring	11/14/2023	38.6502	-109.41596			X	X	X				
CV50		spring	11/14/2023	38.65986	-109.43371				X	X				
CV52		spring	11/14/2023	38.651482	-109.40975				X	X				
CV53		spring	11/14/2023	38.542474	-109.30394				X	X			X	
CV54		spring	11/14/2023	38.575164	-109.30642				X	X			X	
CV78		snow	4/13/2024	38.47218	-109.26686					X				
CV79		snow	4/13/2024	38.47218	-109.26686					X				
CV80		snow	4/13/2024	38.47218	-109.26686					X				
CV81		snow	4/13/2024	38.47218	-109.26686					X				
CV82		snow	4/13/2024	38.47218	-109.26686					X				
CV83		snow	4/13/2024	38.47218	-109.26686					X				
CV84		snow	4/13/2024	38.47218	-109.26686					X				
CV85		snow	4/13/2024	38.47218	-109.26686					X				

Table A2.

			Fall 2023			Spring 2024			Fall 2024			Water-level change		
Site ID	**Land elev. (ft)**	**Land elev. Source**	**Date**	**Water-level BGS (ft)**	**Water-level elev. (ft)**	**Date**	**Water-level BGS (ft)**	**Water-level elev. (ft)**	**Date**	**Water-level BGS (ft)**	**Water-level elev. (ft)**	**Fall 2023 - Spring 2024 (ft)**	**Spring 2024 - Fall 2024 (ft)**	**Fall 2023 - Fall 2024 (ft)**
CV1	5141.85	RTK	11/15/2023	218.99	4922.86	4/2/2024	219.10	4922.75	11/18/2024	217.75	4924.10	-0.11	-1.35	1.24
CV4	6064.92	RTK	11/15/2023	93.00	5971.92	4/2/2024	89.68	5975.24	11/18/2024	88.51	5976.41	3.32	-1.17	4.49
CV7	4613.97	RTK	11/15/2023	7.77	4606.20	4/2/2024	7.94	4606.03	11/18/2024	8.93	4605.04	-0.17	0.99	-1.16
CV8	4434.03	RTK	11/15/2023	43.65	4390.38	4/2/2024	42.66	4391.37	11/18/2024	45.33	4388.70	0.99	2.67	-1.68
CV9	4643.65	RTK	11/15/2023	54.95	4588.70	4/2/2024	53.56	4590.09	11/18/2024	55.15	4588.50	1.39	1.59	-0.20
CV11	4952.96	RTK	11/15/2023	74.14	4878.82	4/2/2024	74.52	4878.44	11/18/2024	74.06	4878.90	-0.38	-0.46	0.08
CV19	4995.14	RTK	11/15/2023	192.41	4802.73	4/1/2024	191.32	4803.82	11/18/2024	191.46	4803.68	1.09	0.14	0.95
CV21	4839.16	RTK	11/15/2023	97.33	4741.83	4/1/2024	97.37	4741.79	11/18/2024	96.66	4742.50	-0.04	-0.71	0.67
CV25	4764.83	RTK	11/15/2023	92.02	4672.81	4/1/2024	90.79	4674.04	11/18/2024	92.52	4672.31	1.23	1.73	-0.50
CV27	4504.44	RTK	11/15/2023	57.46	4446.98	4/2/2024	63.27	4441.17	11/18/2024	63.65	4440.79	-5.81	0.38	-6.19
CV29	4664.90	RTK	11/15/2023	52.98	4611.92	4/2/2024	51.63	4613.27	11/18/2024	--	--	1.35	--	--
CV38	4474.31	RTK	11/15/2023	44.93	4429.38	4/2/2024	44.39	4429.92	11/18/2024	45.23	4429.08	0.54	0.84	-0.30
CV42	4407.81	RTK	11/15/2023	34.25	4373.56	4/2/2024	35.21	4372.60	11/18/2024	35.85	4371.96	-0.96	0.64	-1.60
CV56	4651.99	RTK	11/16/2023	89.59	4562.40	4/2/2024	88.69	4563.30	11/18/2024	89.11	4562.88	0.90	0.42	0.48
CV57	4711.25	RTK	11/16/2023	74.50	4636.75	4/2/2024	76.52	4634.73	11/18/2024	78.47	4632.78	-2.02	1.95	-3.97
CV58	4781.87	RTK	11/16/2023	97.98	4683.89	4/2/2024	97.17	4684.70	11/18/2024	98.85	4683.02	0.81	1.68	-0.87
CV59	4513.62	RTK	11/16/2023	86.15	4427.47	4/2/2024	89.97	4423.65	11/18/2024	--	--	-3.82	--	--
CV60	4451.62	RTK	11/16/2023	88.33	4363.29	4/2/2024	--	--	11/18/2024	89.45	4362.17	--	--	-1.12
CV61	7181.37	RTK	11/16/2023	203.33	6978.04	4/2/2024	202.39	6978.98	11/18/2024	--	--	0.94	--	--
CV62	4524.14	RTK	11/16/2023	41.48	4482.66	4/1/2024	45.19	4478.95	11/18/2024	41.72	4482.42	-3.71	-3.47	-0.24
CV63	4442.96	RTK	11/16/2023	81.98	4360.98	4/2/2024	82.54	4360.42	11/18/2024	82.16	4360.80	-0.56	-0.38	-0.18
CV65	4435.43	RTK	11/16/2023	71.42	4364.01	4/2/2024	71.97	4363.46	11/18/2024	71.62	4363.81	-0.55	-0.35	-0.20
CV66	4539.81	RTK	11/15/2023	30.93	4508.88	4/1/2024	30.31	4509.50	11/18/2024	31.23	4508.58	0.62	0.92	-0.30
CV67	4821.07	RTK	11/15/2023	98.69	4722.38	4/2/0204	100.64	4720.43	11/18/2024	99.81	4721.26	-1.95	-0.83	-1.12
CV68	4520.92	RTK	11/15/2023	100.58	4420.34	4/2/2024	101.14	4419.78	11/18/2024	102.71	4418.21	-0.56	1.57	-2.13
CV69	4747.53	RTK	11/15/2023	96.66	4650.87	4/1/2024	95.44	4652.09	11/18/2024	97.24	4650.29	1.22	1.80	-0.58
CV70	4779.49	RTK	11/15/2023	109.70	4669.79	4/1/2024	108.96	4670.53	11/18/2024	109.51	4669.98	0.74	0.55	0.19
CV71	4863.48	RTK	11/15/2023	98.28	4765.20	4/1/2024	97.95	4765.53	11/18/2024	99.08	4764.40	0.33	1.13	-0.80
CV72	5034.12	RTK	11/15/2023	83.21	4950.91	4/1/2024	83.87	4950.25	11/18/2024	82.85	4951.27	-0.66	-1.02	0.36
CV73	5051.79	RTK	11/15/2023	79.72	4972.07	4/1/2024	80.20	4971.59	11/18/2024	79.19	4972.60	-0.48	-1.01	0.53
CV74	5909.49	RTK	11/16/2023	28.32	5881.17	4/2/2024	27.27	5882.22	11/18/2024	28.38	5881.11	1.05	1.11	-0.06
CV75	4871.46	RTK	--	--	--	4/1/2024	95.26	4776.20	11/18/2024	95.36	4776.10	--	0.10	--
CV76	4671.69	RTK	--	--	--	4/2/2024	52.16	4619.53	11/18/2024	54.30	4617.39	--	2.14	--
CV77	4445.39	RTK	--	--	--	4/2/2024	86.17	4359.22	11/18/2024	85.90	4359.49	--	-0.27	--

Abbreviations: Elev. = elevation, BGS = below ground surface
Land elev. source: RTK = Trimble GNSS RTK GPS
Global datum: WGS 1984, GEOID18 (CONUS)

Table A3.

Site ID	Seepage Run	Date	Time	Discharge (cfs)	Rating (%)	Discharge error (cfs)
CV44	Fall 2023	11/14/2023	10:00	0.12	10	0.0
CV16	Fall 2023	11/14/2023	11:15	0.96	8	0.1
CV301	Fall 2023	11/14/2023	12:00	0.08	8	0.0
CV302	Fall 2023	11/14/2023	12:52	1.28	8	0.1
CV303	Fall 2023	11/14/2023	12:34	2.46	8	0.2
CV304	Fall 2023	11/14/2023	16:37	2.54	8	0.2
CV108	Fall 2023	11/14/2023	13:44	2.10	8	0.2
CV204	Fall 2023	11/14/2023	16:15	2.60	8	0.2
CV201	Fall 2023	11/14/2023	10:15	1.30	8	0.1
CV2	Fall 2023	11/14/2023	14:10	2.45	10	0.2
CV107	Fall 2023	11/14/2023	16:01	2.60	8	0.2
CV14	Fall 2023	11/14/2023	15:07	2.90	10	0.3
CV106	Fall 2023	11/14/2023	15:26	2.60	8	0.2
CV105	Fall 2023	11/14/2023	14:43	3.10	8	0.2
CV104	Fall 2023	11/14/2023	14:28	3.90	8	0.3
CV103	Fall 2023	11/14/2023	13:53	4.50	8	0.4
CV102	Fall 2023	11/14/2023	11:08	1.20	10	0.1
CV101	Fall 2023	11/14/2023	10:54	8.50	8	0.2
CV100	Fall 2023	11/14/2023	10:20	7.20	10	0.7
CV17	Fall 2023	11/14/2023	9:20	7.46	10	0.7
CV44	Spring 2024	5/14/2024	7:25	0.118	10	0.0
CV16	Spring 2024	5/14/2024	7:59	1.677	8	0.2
CV301	Spring 2024	5/14/2024	8:44	1.574	10	0.2
CV303	Spring 2024	5/14/2024	8:53	1.614	10	0.2
CV304	Spring 2024	5/14/2024	9:36	3.455	8	0.3
CV108	Spring 2024	5/14/2024	10:03	2.904	10	0.3
CV109	Spring 2024	5/14/2024	10:19	3.276	10	0.3
CV110	Spring 2024	5/14/2024	10:46	2.140	8	0.2
CV201	Spring 2024	5/14/2024	11:51	1.017	8	0.1
CV2	Spring 2024	5/14/2024	13:40	0.215	10	0.0
CV14	Spring 2024	5/16/2024	14:00	0.200	10	0.0
CV104	Spring 2024	5/14/2024	14:23	0.733	10	0.1
CV102	Spring 2024	5/14/2024	15:24	1.950	8	0.2
CV100	Spring 2024	5/14/2024	15:10	4.747	8	0.4
CV17	Spring 2024	5/14/2024	16:06	5.502	8	0.4

Table A4.

Site ID	Site ID full name	Site type	Owner/ LOT	Sample date	pH	Temp (°C)	Specific conductance (µS/cm)	TDS (mg/L)*	Sodium (mg/L)	Potassium (mg/L)	Calcium (mg/L)	Magnesium (mg/L)	Chloride (mg/L)	Bicarbonate (mg/L)	Sulfate (mg/L)	Nitrate + nitrite as nitrogen (mg/L)
CV4	WL-CV4-PORCUPINE	well	town of cv	10/23/23	7.47	12.8	383	210	14.4	1.45	42.2	13.4	14.4	145	42	0.249
CV11	WL-CV11-PLACER	well	town of cv	10/24/23	7.8	13.7	420	232	16.3	1.37	47.3	13.6	17	154	47	0.233
CV20	WL-CV20-328	well	328	10/25/23	7.9	13.7	425	234	17.4	1.53	47.5	14.2	16.2	152	50.2	0.255
CV18	WL-CV18-365	well	365 (Pam and Bob)	10/25/23	7.71	14.3	605	360	17.8	1.87	77.1	20.7	18	172	134	0.209
CV9	WL-CV9-BAILEY	well	town of cv	10/24/23	7.79	15	477	242	19.5	1.41	54	15.9	17.4	157	60.2	0.335
CV21	WL-CV21-307	well	307	10/25/23	7.97	12.8	405	218	19.8	1.38	44.2	13	20.1	139	45.8	-
CV24	WL-CV24-227	well	227	5/16/24	7.59	14.5	612	362	25.6	1.79	72.4	22.5	19.7	193	121	-
CV7	WL-CV7-CL	well	town of cv	10/24/23	7.56	15	827	518	40.2	2.13	91.3	25.6	43.7	182	187	0.429
CV35	WL-CV35-035	well	35	10/25/23	7.46	15.7	1366	1010	52.6	2.83	200	43.2	61.6	156	501	-
CV1	WL-CV1-LOOP ROAD	well	town of cv	10/25/23	7.6	14.1	968	596	63.5	2.64	99.5	21.8	72.2	183	209	-
CV26	WL-CV26-238	well	238	10/25/23	7.63	16.1	969	620	69.1	2.74	90.9	28.1	70.4	188	215	-
CV19	WL-CV19-338	well	338	10/25/23	7.48	17.2	1800	1410	94.1	4.1	239	64.9	99.9	168	736	<0.1
CV8	WL-CV8-CREEKSIDE	well	town of cv	10/23/23	7.27	15.5	1888	1310	126	6.74	222	47.9	160	288	532	2.16
CV31	WL-CV31-164	well	164	10/25/23	7.91	17	2840	2410	144	8.48	381	104	174	152	1290	-
CV38	WL-CV38-439	well	439	10/25/23	7.3	17.9	2530	2040	152	8.09	291	114	149	207	1090	-
CV23	WL-CV23-219	well	219	10/25/23	7.51	16.1	3310	2720	223	18.3	393	121	262	157	1460	-
CV27	WL-CV27-002	well	2	10/25/23	7.49	17.1	3560	2820	292	19.6	364	125	345	101	1450	<0.1
CV1	WL-CV1-LOOP ROAD	well	town of cv	5/16/24	7.5	15	933	*644*	-	-	-	-	-	-	-	-
CV13	WL-CV13-447	well	447 merrill domestic	10/24/23	7.6	14	1544	*1065*	-	-	-	-	-	-	-	-
CV23	WL-CV23-219	well	219	5/16/24	7.69	14.5	3340	*2305*	-	-	-	-	-	-	-	-
CV24	WL-CV24-227	well	227	10/25/23	7.77	15.9	720	*497*	-	-	-	-	-	-	-	-
CV25	WL-CV25-228	well	228	10/25/23	7.92	14	414	*286*	-	-	-	-	-	-	-	-
CV27	WL-CV27-002	well	2	5/16/24	7.52	16.6	3100	*2139*	-	-	-	-	-	-	-	-
CV28	WL-CV28-187	well	187	10/25/23	7.95	17.6	471	*325*	-	-	-	-	-	-	-	-
CV29	WL-CV29-110	well	110	10/25/23	8.06	20.7	848	*585*	-	-	-	-	-	-	-	-
CV30	WL-CV30-140	well	140	10/25/23	8.01	14.8	517	*357*	-	-	-	-	-	-	-	-
CV32	WL-CV32-100	well	100	10/25/23	7.46	17.5	2980	*2056*	-	-	-	-	-	-	-	-
CV33	WL-CV33-074	well	74	10/25/23	7.77	16.1	2390	*1649*	-	-	-	-	-	-	-	-
CV34	WL-CV34-053	well	53	10/25/23	7.86	19	444	*306*	-	-	-	-	-	-	-	-
CV36	WL-CV36-024	well	24	10/25/23	7.42	16.4	3750	*2588*	-	-	-	-	-	-	-	-
CV59	WL-CV59-415	well	415	10/25/23	7.41	17.5	2880	*1987*	-	-	-	-	-	-	-	-
CV41	WL-CV41-419	well	419	10/26/23	7.77	21.7	830	*573*	-	-	-	-	-	-	-	-
CV42	WL-CV42-430	well	430	10/26/23	7.16	14.3	2640	*1822*	-	-	-	-	-	-	-	-
CV47	WL-CV47-390	well	390	11/1/23	7.15	13.6	1124	*776*	-	-	-	-	-	-	-	-
CV51	WL-CV51-CFI	well	cfi pond	11/1/23	7.34	14.3	2040	*1408*	-	-	-	-	-	-	-	-
CV57	WL-CV57-158	well	158	4/2/24	7.86	13.6	634	*437*	-	-	-	-	-	-	-	-
CV70	WL-CV70-194	well	194	11/15/23	7.8	14.8	1092	*753*	-	-	-	-	-	-	-	-
CV72	WL-CV72-352	well	352	11/15/23	8.05	11.5	385	*266*	-	-	-	-	-	-	-	-
CV76	WL-CV76-111	well	111	4/2/24	8.16	14.9	694	*479*	-	-	-	-	-	-	-	-
CV9	WL-CV9-BAILEY	well	town of cv	5/16/24	7.72	15.2	484	*334*	-	-	-	-	-	-	-	-
CV16	ST-CV16-USFS	stream	castle creek	5/14/24	8.03	6.1	200	112	3.29	1.08	31.9	4.21	1.34	98.4	14.2	-
CV14	ST-CV14-CC2	stream	castle creek	5/16/24	8.24	15.8	1054	684	62.6	2.17	112	31.7	69.7	215	261	-
CV14	ST-CV14-CC2	stream	castle creek	10/24/23	8.4	12	770	*531*	-	-	-	-	-	-	-	-
CV16	ST-CV16-USFS	stream	castle creek	10/24/23	8.2	7.5	229	*158*	-	-	-	-	-	-	-	-
CV17	ST-CV17-X128	stream	castle creek	10/24/23	8.42	14.3	2440	*1684*	-	-	-	-	-	-	-	-
CV2	ST-CV2-CC1	stream	castle creek	10/24/23	8.02	13.5	691	*477*	-	-	-	-	-	-	-	-
CV45	ST-CV45-WB3	stream	willow basin	11/1/23	7.8	2.2	148.6	*103*	-	-	-	-	-	-	-	-
CV6	ST-CV6-CCM	stream	castle creek	10/24/23	8.2	13	1900	*1311*	-	-	-	-	-	-	-	-
CV5	SP-CV5-CCSP2	spring	castle creek	10/24/23	7.68	13.8	489	282	23.3	1.59	52.5	15	25.2	187	66	-
CV49	SP-CV49-373	spring	jorgen	5/16/24	7.4	14.9	1295	914	73.1	3.45	147	46.1	82.8	229	371	-
CV203	SE-CV203	spring	seep in CC near BAsil	11/15/23	7.8	9.5	491	*339*	-	-	-	-	-	-	-	-
CV10	SP-CV10-CCMSP3	spring	castle creek Merrill	10/24/23	7.58	14	888	*613*	-	-	-	-	-	-	-	-
CV15	SP-CV15-LASAL	spring	spring LaSals	10/24/23	8.13	14	1310	*904*	-	-	-	-	-	-	-	-
CV3	SP-CV3-CCSP1	spring	castle creek	10/24/23	7.98	13.2	792	*546*	-	-	-	-	-	-	-	-
CV300	SP-CV300 RCCG	spring	rock castle CG	5/15/24	7.18	10.1	440	*304*	-	-	-	-	-	-	-	-
CV39	SP-CV39-DSA	spring		10/26/23	7.64	15.3	1348	*930*	-	-	-	-	-	-	-	-
CV40	SP-CV40-530	spring	schwartz spring	10/26/23	7.4	13.4	1650	*1139*	-	-	-	-	-	-	-	-
CV43	SP-CV43-WB1	spring	willow basin	11/1/23	7.08	3	451	*311*	-	-	-	-	-	-	-	-
CV43	SP-CV43-WB1	spring	willow basin	5/14/24	7.37	4.1	460	*317*	-	-	-	-	-	-	-	-
CV44	SP-CV44-WB2	spring	willow basin	11/1/23	7.48	4.8	274	*189*	-	-	-	-	-	-	-	-
CV46	SP-CV46-WB4	spring	willow basin	11/1/23	7.34	6.4	572	*395*	-	-	-	-	-	-	-	-
CV49	SP-CV49-373	spring	jorgen	11/1/23	7.32	14.6	1162	*802*	-	-	-	-	-	-	-	-
CV50	SP-CV50-374	spring	zuckerman	11/1/23	7.45	11.6	1595	*1101*	-	-	-	-	-	-	-	-
CV52	SP-CV52-CFI	spring	cfi pond	11/1/23	7.87	9.1	1233	*851*	-	-	-	-	-	-	-	-
CV53	SP-CV53-MASON	spring	mason draw	5/14/24	7.26	7.8	340	*235*	-	-	-	-	-	-	-	-
CV53	SP-CV53-MASON	spring	mason draw	11/4/23	8.15	5.9	453	*313*	-	-	-	-	-	-	-	-
CV54	SP-CV54-PINHOOK	spring	pinhook spring	5/14/24	6.95	20	307	*212*	-	-	-	-	-	-	-	-
CV54	SP-CV54-PINHOOK	spring	pinhook spring	11/4/23	8.19	11.3	477	*329*	-	-	-	-	-	-	-	-
CV100	ST-CV100	stream	Castle Creek	5/14/2024	8.14	17.9	2230	*1539*	-	-	-	-	-	-	-	-
CV102	ST-CV102	stream	Castle Creek	5/14/2024	8.02	17.7	2410	*1663*	-	-	-	-	-	-	-	-
CV3	ST-CV3	stream	Castle Creek	5/14/2024	8.41	19.4	1114	*769*	-	-	-	-	-	-	-	-
CV201	ST-CV201	stream	Castle Creek	5/14/2024	8.57	20	681	*470*	-	-	-	-	-	-	-	-

*Italicized numbers represent values calculated using a conversion factor of 0.69 multiplied by specific conductance.

Table A5.

Site Name	Type	$\delta^{2}H$(‰)	$\delta^{18}O$(‰)
CV1	well	-108.9	-14.90
CV11	well	-111.0	-15.50
CV18	well	-112.3	-15.70
CV19	well	-111.8	-15.30
CV20	well	-112.0	-15.50
CV206	well	-111.6	-15.40
CV21	well	-112.8	-15.70
CV23	well	-112.0	-15.20
CV25	well	-112.5	-15.80
CV26	well	-110.7	-15.20
CV27	well	-113.7	-15.80
CV28	well	-113.2	-15.70
CV29	well	-110.7	-15.10
CV30	well	-113.1	-15.70
CV31	well	-111.9	-15.30
CV32	well	-111.7	-15.30
CV33	well	-113.0	-15.50
CV34	well	-112.3	-15.50
CV35	well	-112.3	-15.40
CV36	well	-108.8	-14.30
CV37	well	-111.4	-15.10
CV38	well	-108.7	-14.70
CV4	well	-111.0	-15.20
CV41	well	-111.5	-15.30
CV42	well	-109.8	-15.10
CV47	well	-110.0	-15.00
CV51	well	-103.0	-13.50
CV57	well	-111.9	-15.43
CV76	well	-111.2	-15.19
CV76	well	-111.4	-15.30
CV8	well	-106.5	-14.30
CV9	well	-115.3	-15.90
CV78	snow	-127.3	-16.63
CV79	snow	-99.4	-13.85
CV80	snow	-132.2	-17.76
CV81	snow	-117.4	-16.20
CV82	snow	-133.8	-17.90
CV83	snow	-181.9	-24.09
CV84	snow	-154.7	-20.89
CV85	snow	-120.0	-16.92
CV10	spring	-110.1	-15.10
CV13	spring	-109.4	-15.00
CV15	spring	-111.8	-15.40
CV3	spring	-111.8	-15.50
CV300	spring	-107.2	-14.70
CV301	spring	-112.2	-15.40
CV40	spring	-112.5	-15.50
CV43	spring	-109.4	-14.70
CV44	spring	-111.7	-15.20
CV46	spring	-108.6	-14.60
CV49	spring	-110.5	-15.10
CV5	spring	-109.7	-14.30
CV5	spring	-112.3	-15.50
CV50	spring	-108.8	-14.70
CV53	spring	-107.3	-14.70
CV54	spring	-115.8	-16.00
CV109	stream	-109.8	-15.10
CV14	stream	-109.1	-15.00
CV16	stream	-108.3	-14.80
CV17	stream	-110.5	-15.20
CV2	stream	-110.6	-15.20
CV203	stream	-116.0	-16.00
CV204	stream	-110.2	-15.20
CV45	stream	-107.4	-14.90
CV52	stream	-102.8	-13.60
CV6	stream	-108.2	-14.70

APPENDIX B

Soil-Water-Balance Model Results (2005–2022)

Table B1.

Water Year	Gross Precipitation						Actual ET						Net Infiltration					
	Upper valley fill (Place Ck)	Lower valley fill	Upper valley fill (Castle Ck)	La Sal Mountains (intrusive rocks)	Triassic & Jurrasic rocks (undifferentiated)	Round Mountain (Intrusive rocks)	Upper valley fill (Place Ck)	Lower valley fill	Upper valley fill (Castle Ck)	La Sal Mountains (intrusive rocks)	Triassic & Jurrasic rocks (undifferentiated)	Round Mountain (Intrusive rocks)	Upper valley fill (Place Ck)	Lower valley fill	Upper valley fill (Castle Ck)	La Sal Mountains (intrusive rocks)	Triassic & Jurrasic rocks (undifferentiated)	Round Mountain (Intrusive rocks)
	1	2	3	4	5	6	1	2	3	4	5	6	1	2	3	4	5	6
2005	4812.63	6441.06	4536.95	31064.70	9527.95	225.45	4851.90	7015.33	4704.15	26300.10	8772.14	181.63	146.74	78.04	43.60	3833.62	547.00	28.18
2006	3545.90	4529.78	3313.58	24184.10	6877.46	160.21	3524.71	4957.45	3311.46	20725.78	6416.49	131.30	9.48	47.61	10.95	930.34	228.42	14.31
2007	5212.63	6965.41	4854.71	34312.45	10383.58	250.06	4983.24	7070.54	4742.83	27683.59	8709.91	182.28	102.09	177.73	67.21	2992.60	514.36	29.79
2008	3369.39	3890.16	3078.08	24829.92	6268.73	146.03	3738.24	4903.83	3499.90	23168.76	6020.96	121.60	50.69	40.82	22.28	2109.66	288.28	14.81
2009	3070.70	3488.28	2870.91	22022.99	5630.48	133.85	3115.12	4047.79	2956.27	19206.62	5221.80	108.31	11.65	33.45	11.77	1042.67	206.65	13.36
2010	4647.04	5732.63	4296.51	31755.82	8818.00	211.27	4231.20	6027.79	4111.98	24875.28	7285.25	152.36	204.31	113.02	109.93	3051.02	562.80	28.98
2011	5074.56	5993.01	4626.52	37761.33	9698.33	221.75	5051.43	6523.62	4723.09	30403.06	9089.09	182.75	114.57	53.30	32.34	4842.82	408.67	22.34
2012	2736.58	3208.62	2498.65	19836.14	5210.66	119.18	2883.07	3895.00	2657.21	18020.45	4960.51	98.05	7.85	31.16	9.09	1012.26	182.61	13.38
2013	4194.08	5188.52	3899.48	28825.64	8020.43	189.81	3971.95	5402.54	3732.94	22806.60	7224.87	148.88	20.20	50.52	19.13	1278.90	271.89	18.84
2014	4769.03	6308.14	4454.69	31655.71	9450.76	222.09	4495.91	6158.32	4188.31	26730.35	7971.42	160.49	30.05	72.45	21.50	1825.75	379.10	22.58
2015	5081.22	5942.05	4720.00	36662.01	9471.18	225.61	5669.29	7130.80	5326.72	33092.98	9765.54	200.81	26.54	47.81	19.69	3728.98	288.66	21.84
2016	5602.20	6207.61	5139.40	42669.35	10227.55	235.60	5179.64	6626.82	5042.82	29432.88	8854.38	177.91	275.18	67.04	88.10	8279.64	509.77	24.72
2017	3564.95	4814.45	3432.73	26676.41	7219.78	166.64	3495.49	5129.74	3422.29	22489.19	6435.19	129.95	62.03	48.35	20.13	2444.63	337.33	17.31
2018	1988.19	2607.59	1855.53	15065.09	3983.67	91.22	2348.18	3598.54	2212.54	15350.72	4071.28	80.15	3.95	28.41	6.45	689.55	150.36	9.51
2019	5624.45	7304.63	5351.12	38848.60	11214.83	261.95	5074.03	7336.07	5092.30	25844.65	8742.93	176.98	321.58	287.35	194.08	7882.50	808.88	37.17
2020	2846.01	3597.44	2651.89	19609.10	5606.43	129.84	2966.76	4218.91	2788.81	17602.01	5007.00	100.24	19.76	53.02	16.96	995.80	304.81	14.42
2021	3648.13	4365.16	3363.58	27334.70	6986.26	162.08	3422.02	4534.87	3166.58	21877.67	6025.82	119.50	10.11	42.15	12.52	1089.32	211.16	13.96
2022	4343.25	5084.08	3971.08	33409.64	8187.60	186.40	4549.29	5830.49	4261.07	28168.49	7821.67	154.09	75.31	45.29	22.77	3635.41	273.58	14.92

Table B1 Continued.

Water Year	Runoff						Runoff Outside					
	Upper valley fill (Place Ck)	Lower valley fill	Upper valley fill (Castle Ck)	La Sal Mountains (intrusive rocks)	Triassic & Jurrasic rocks (undifferentiated)	Round Mountain (Intrusive rocks)	Upper valley fill (Place Ck)	Lower valley fill	Upper valley fill (Castle Ck)	La Sal Mountains (intrusive rocks)	Triassic & Jurrasic rocks (undifferentiated)	Round Mountain (Intrusive rocks)
	1	2	3	4	5	6	1	2	3	4	5	6
2005	40.07	32.23	15.29	647.13	76.41	1.01	81.60	90.78	39.04	2342.57	466.68	19.04
2006	15.25	21.03	6.13	390.29	29.40	0.29	20.05	52.78	15.94	1373.55	222.03	12.72
2007	125.00	138.74	70.17	1299.31	398.17	6.10	177.33	241.80	106.44	3358.53	1096.94	35.80
2008	59.84	28.88	30.50	564.24	141.44	2.02	83.30	68.07	49.48	2020.04	415.69	18.02
2009	30.04	15.64	10.71	422.47	55.81	0.91	36.40	47.53	20.34	1411.91	227.09	11.14
2010	194.02	54.33	101.18	1624.73	397.37	5.68	278.51	115.66	137.58	3516.48	981.32	28.68
2011	23.31	21.39	8.51	476.32	31.47	0.39	56.37	46.42	34.08	2552.87	294.84	17.62
2012	6.32	11.97	3.26	261.58	21.13	0.33	9.45	34.23	10.71	1115.56	141.47	7.79
2013	52.29	72.39	24.95	669.28	159.15	2.24	62.81	114.60	40.23	2076.73	384.82	18.40
2014	31.61	52.95	20.50	405.91	114.57	1.49	47.15	136.88	39.82	1926.27	523.13	27.46
2015	48.40	23.08	17.07	817.41	68.84	0.87	59.40	64.29	36.95	2783.28	308.33	18.65
2016	71.60	30.55	30.24	1099.01	114.95	0.98	206.44	97.60	99.53	4699.53	823.85	31.29
2017	32.54	22.19	10.19	527.03	54.91	0.95	52.70	58.80	26.08	1895.57	320.66	15.18
2018	6.15	17.33	3.02	129.53	35.33	0.43	7.93	46.04	7.45	727.68	160.38	8.58
2019	204.07	155.92	102.90	1884.05	497.06	7.66	341.84	301.48	194.00	4918.56	1705.50	46.97
2020	15.44	28.06	8.35	239.33	64.36	0.85	23.66	80.58	21.67	1195.80	375.49	15.44
2021	26.16	35.04	14.21	423.10	85.95	1.55	32.45	90.68	27.95	1755.69	382.16	21.18
2022	32.88	22.76	14.71	859.89	61.89	0.63						